Master Thesis in Geosciences

The Gubbedalen Shear Zone; a terrane boundary in the EastGreenland Caledonides

A structural and geochronological study

Lars Eivind Augland

UNIVERSITY OF OSLO

FACULTY OF MATHEMATICS AND NATURAL SCIENCES

The Gubbedalen Shear Zone; a terrane boundary in the East Greenland Caledonides

A structural and geochronological study

Lars Eivind Augland

Master Thesis in Geosciences

Discipline: Tectonics, petrology and geochemistry
Department of Geosciences
Faculty of Mathematics and Natural Sciences

UNIVERSITY OF OSLO

[June 1, 2007]

Tutors: Professor Arild Andresen and Professor Fernando Corfu
This work is published digitally through DUO – Digitale Utgivelser ved UiO
http://www.duo.uio.no
It is also catalogued in BIBSYS (http://www.bibsys.no/english)

Cover photo: Tværdal, Southern Liverpool Land, NE Greenland. View towards the south.

Acknowledgements

Professor Arild Andresen was the main supervisor for this thesis. I thank him for proposing the study area and for supervising me in the field and throughout the writing of the thesis. He is always enthusiastic and available for answering questions and discussion of various topics related to this thesis. Many stimulating discussions have been carried out in his office throughout the work with this thesis. His thorough review is also highly appreciated.

Professor Fernando Corfu supervised me in the geochronology lab, and has patiently instructed me and taught me what "high precision geochronology" is all about. I want to thank him for this and all the discussions we have had concerning my data. His thorough review is highly appreciated.

MSc. Per Inge Myhre deserves special thanks for many fruitful discussions both in the field and at the office back home. Thanks also for helping me out with IT-related problems.

Thanks also go to Professor Mark Steltenpohl from the Univerisity of Auburn for helpful discussions during the first week of my field work.

Gunborg Bye Fjeld is thanked for teaching me crushing procedures and mineral separation. Cand. Scient Morten Schjoldager is thanked for crushing and separating some of my samples, when I was about to run out of time.

Dr. Muriel Erambert gave valuable help with electron micro probe analyses.

Thanks also to my office-mate, Lars Erik Haug, for discussions and helping me out with computer related challenges.

My fellow students at the Department of Geoscience, University of Oslo are thanked for hanging around and talking sense and nonsense during lunch, dinner and coffee breaks. And finally a salute also goes to all the friends I made at my time in the University of Bergen as an undergraduate student.

Contents

1 Introduction

1.1 Purpose of study

The focus of this study is the tectonometamorphic development of high pressure rocks, their exhumation and relation to large granitoid intrusives on southern Liverpool Land, North-East Greeland.

Eclogite lenses in a felsic gneiss were recognized on Liverpool Land already in the 1930's (Kranck, 1935; Sahlstein, 1935), but a modern study of these rocks was not undertaken before the "rediscovery" of these rocks by Hartz et al. (2005). The preliminary data by Hartz et al. (2005) indicated an age of c. 393-397 Ma for the ultra-high pressure metamorphism. A large granitoid pluton, the Hurry Inlet Granite, first recognised by Kranck (1935) was mapped by Coe and Cheeney in the early 1970's (Coe, 1975; Coe and Cheeney, 1972). These workers considered the contact between the undeformed Hurry Inlet Granite and the gneissic rocks containing the eclogite to be intrusive. The Hurry Inlet Granite was dated by the Rb-Sr method on biotite by Hansen and Steiger (1971), giving an imprecise age of c. 435 Ma. This apparent inconsistent relationship, with an older granite "intruding" a younger metamorphic complex, led Arild Andresen to do reconnaissance field work in the summer of 2005. This reconnaissance work indicated the presence of a shear zone between the Hurry Inlet Granite and gneisses with eclogite lenses.

The aim of this study is to:

1) Document the presence of a shear zone (Gubbedalen Shear Zone) between the Hurry Inlet Granite and the high grade gneisses containing eclogites to the south of it.
2) Understand the kinematic evolution of the Gubbedalen Shear Zone.
3) Constrain the age of the high grade metamorphism and related magmatism in the footwall block using the ID-TIMS method.
4) Date the inferred Caledonian intrusions in the hanging wall north of the shear zone.

As topographic maps at the scale of 1:100 000 maps have the highest resolution, detailed mapping of contacts etc. was almost impossible. The field work therefore had the character of mapping of a transect across the shear zone.

1.2 Study area and analytical methods

The study area for this thesis is the southern and central part of Liverpool Land situated at about 71˚ N (Figure 1) in North-East Greenland. Liverpool Land comprises the south-eastern part of the East Greenland Caledonides. Liverpool Land is an elevated peneplaned area, dipping shallowly to the west, cut by deep, glacially eroded valleys. In the south-eastern area, the topography is generally more rugged due to intense glacial erosion. The elevated central areas are partly covered by glaciers. To the west the peneplaned surface is cut by the Hurry Inlet (a N-S trending fjord) in the south, and goes under the Mesozoic sediments of Jameson Land in the north (Figure 1). To the north, south and east, Liverpool Land terminates in the sea. Fieldwork was conducted during 4 weeks in July and August 2006. As means of transportation, chartered airplane was used from Iceland to the airport Constable Pynt on Jameson Land, NE-Greenland. From the Constable Pynt to the respective field areas helicopter was used. The weather conditions in this part of Greenland in the summer are generally stable and dominated by high pressures and a lot of nice weather.

In the field, positions of the different localities visited were recorded with an Etrex hand-held GPS. Structural data were recorded using a Silva 360 ° compass. Declination is 27 ° to the west. Mapping was conducted on 1:100 000 topographic maps. The 1:100 000 map sheet Hurry Inlet 70 Ø. 1 NORD, Grønlands Geologiske Undersøgelse geological map was used to locate the main lithologic units. For the subsequent analytical work, the Isotope Dilution-Thermal Ionisation Mass Spectrometry (ID-TIMS) method for U-Pb dating of zircon, monazite and rutile was used.

1.3 Geological setting

The Caledonides of Greenland extend from c. 70˚ N to 82˚ N along the north-eastern coast (Figure 1). This gives the exposed part of the Caledonides of Greenland a length of about 1400 km in the north-south direction. The exposed width of the orogen is more than 300 km in the east-west direction (Haller 1985; Higgins 2001). The exposure of the Caledonian rocks terminates, to the south, under Tertiary plateau basalts, and to the north in the Arctic Ocean. The Caledonian rocks in the region from c. 70 °N to 79 °N are dominantly metamorphic and intrusive rocks of Precambrian and Palaeozoic age, with exceptions of local Carboniferous – Cretaceous and Palaeogene sedimentary basins, and Palaeogene intrusives and extrusives

(Haller, 1985; Higgins et al. 2004). The foreland fold- and thrust-belt in the thrust front in the west is covered by the Inland Ice along most of the orogen, except in the northernmost part (Kronprins Christian Land)(Figure 1)(Higgins et al. 2001). The main tectonic event in the area was the Ordovician to Upper Devonian Caledonian orogeny. The folding, thrusting and metamorphism related to this event overprints most of the older structures, but Archaean and Proterozoic terrains are recognized (e. g., Higgins et al., 2004).

This thesis focuses on the Caledonian orogeny, the result of the collision between Baltica and Laurentia which led to the formation of the continent Laurussia (Torsvik et al. 1996). The subduction of Baltica underneath Laurentia, and the eventual continent – continent collision, led to high grade metamorphism and thrusting of nappes onto both the Laurentia and the Baltica margins (e. g., Higgins et al., 2004; Tucker et al., 2004). A detailed outline of the geology of the East Greenland Caledonides will be given in Chapter 2.

2 Regional geological setting

2.1 Introduction

After the closure of the Iapetus Ocean during the Early Paleozoic, the collision of Laurentia, Baltica and Avalonia led to the formation of the Siluro - Devonian Caledonian orogen, a large scale mountain belt comparable to present-day Himalaya (Haller, 1971; Higgins et al., 2004; Torsvik et al., 1996). The remnants of this mountain range are now exposed in Eastern North America Western Scandinavia, on Svalbard, on the British Isles and North-East Greenland.

During the Silurian Baltica was underthrust below the Laurentian margin (e. g., Andersen et al., 1991; Tucker et al., 2004). Contemporaneous nappe stacking occurred, with allocthons being thrust in a south-eastern to eastern direction on to the Fennoscandian Shield with its thin Late Neoproterozoic to Early Paleozoic sedimentary cover (Bryhni and Andreasson, 1985; Roberts and Gee, 1985). The Scandinavian Caledonides are considered to consist of four main allochthonous units, named the Lower, Middle, Upper and Uppermost Allochthons, respectively (Roberts and Gee, 1985). The Lower and Middle Allochthons are interpreted to be of Baltic affinity, whereas the Uppermost Allochthon and parts of the Upper Allochthon are considered to be exotic to Baltica and derived from the Iapetus Ocean. Parts of the Uppermost Allochthon are interpreted to be derived from Laurentia's eastern margin (Roberts et al., 2002; Steltenpohl et al., 2003; Stephens and Gee, 1985; Yoshinobu et al., 2002).

Untill recently Haller (1971) described two principal lithogenetic units of the East Greenland Caledonides: the Precambrian basement complexes and a c. 16 km thick sequence of Neoproterozoic sedimentary rocks. The sedimentary sequence was divided into the Lower Eleonore Bay Group (EBG), the Upper Eleonore Bay Group and the Tillite Group.

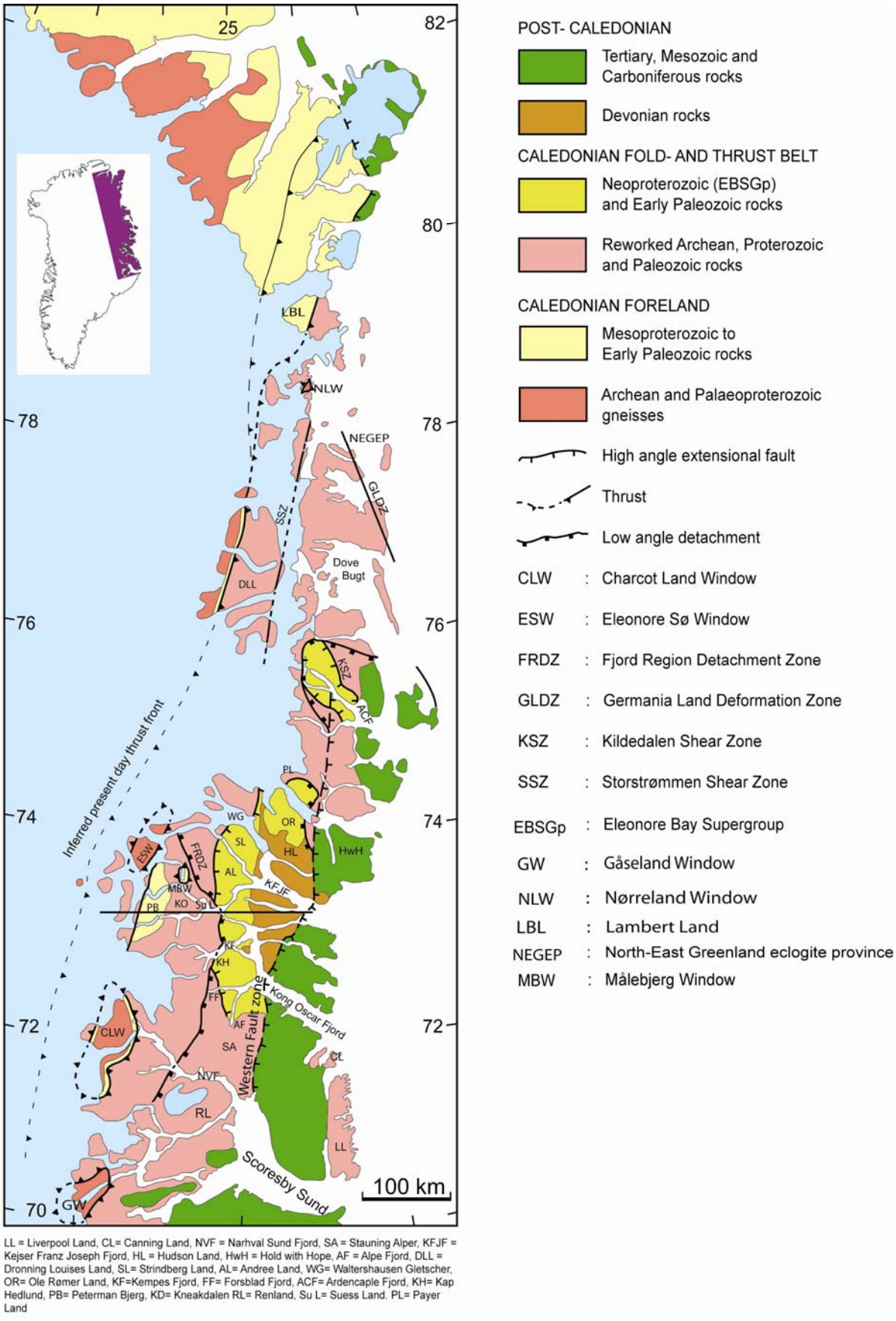

Figure 1: Map with legend of the main lithotectonic units of the East Greenland Caledonides. Modified after Andresen et al. (2007). Traverse of profile is shown by horizontal black line south of KFJF.

The lithological subdivision of Haller and previous authors (Haller, 1971, and references therein) for the Caledonian rocks in North-East Greenland has recently been revised. Now most authors agree that the East Greenland Caledonides comprise an autochthonous to parautochthonous basement complex of Paleo- to Mesoproterozoic age with Neoproterozoic to Lower Paleozoic cover (Figure 2), tectonically overlain by a regionally extensive thrust sheet. In the Fjord Region (70˚ N and 76˚ N), the allochthon has been divided in three main lithotectonic units (Higgins and Leslie, 2000). These are, in ascending order, (1) an Archean to Palaeoproterozoic basement complex, (2) a sequence of Mesoproterozoic supracrustals, commonly referred to as the Krummedal Sequence, (3) and a low grade metasedimentary sequence of Neoproterozoic and Early Palaeozoic age. The latter is sub-divided into the Eleonore Bay Supergroup (EBS), the Tillite Group, and the Lower Palaeozoic Kong Oscar Fjord Group (Higgins et al., 2004).

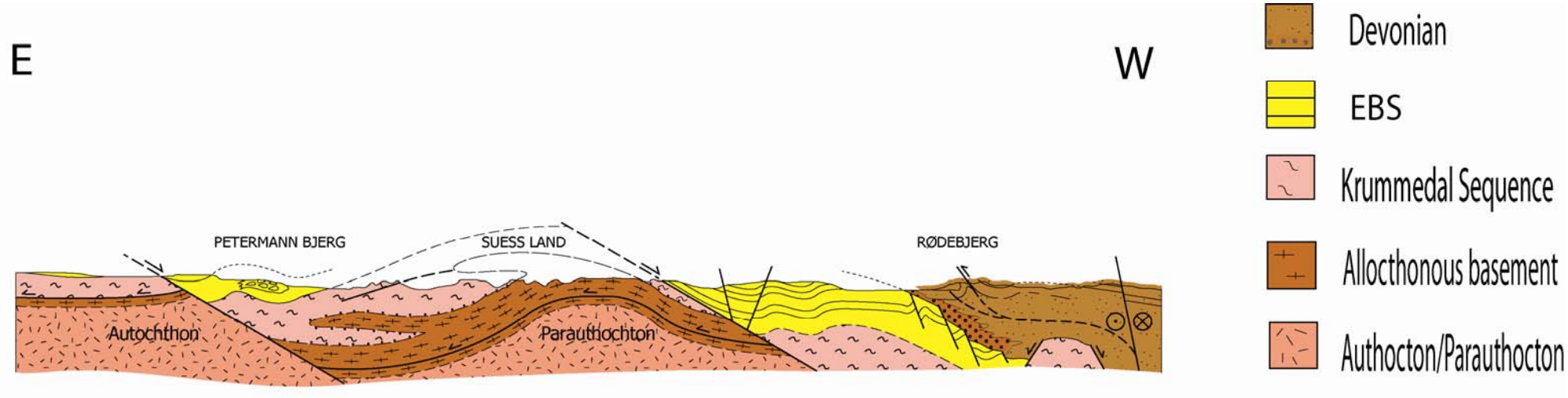

Figure 2: Schematic profile across the Caledonian orogen in the Fjord Region. Marked with a line just south of KFJF in Figure 1. After Andresen et al. (2007).

The Krummedal Sequence is variably migmatised, and this unit as well as the EBS are intruded by Caledonian granites. The Krummedal Sequence is also intruded by Grenvillian age granitoids (see below)(Hartz et al., 2001; Hartz et al., 2000; Kalsbeek et al., 2000; Leslie and Nutman, 2003; Watt et al., 2000; White et al., 2002; Andresen et al., 2007).

Different tectonic models exist regarding the internal structure/ tectonostratigraphy of the allochthon/thrust sheet in the Fjord Region (72-74 °N)(Figure 1)(Haller, 1971; Higgins et al., 2004; Higgins and Leslie, 2000; Andresen et al., 2007). Higgins and Leslie (2000) and Higgins et al.(2004) argue that the allochthon is composed of three tectonic units: (1) the lower Niggli Spids Thrust Sheet, consisting of Archean to Palaeoproterozoic crystalline basement and Mesoproterozoic metasediments of the Krummedal Sequence; (2) the middle Hagar Bjerg Thrust Sheet, consisting of the same two units, in addition to Grenvillian and Caledonian granitoid intrusives in the Krummedal Sequence; (3) and the upper Franz Joseph Allochthon consisting of EBS, locally with the overlying Vendian tillites and Lower Palaeozoic sediments. Also the Franz Joseph Allochthon is intruded by Caledonian granites. Whereas the two lower allochthons are thought to represent thrust sheets (Higgins et al., 2004; Higgins and Leslie, 2000), the contact between the Hagar Bjerg Thrust Sheet and the Franz Joseph Allochthon is considered to be a tectonically modified unconformity (Higgins et al., 2004).

Andresen et al. (2007) argue that the repetition of the units in the allochthon is due to recumbent folding (Figure 2) instead of repetition by thrusting. He considered the allochthonous rocks to belong to the same thrust sheet, and named it the Hagar-Niggli Thrust Sheet. The terminology and interpretation of Andresen et al. (2007) is followed here.

Both Higgins et al. (2004) and Andresen et al. (2007) agree that the entire nappe stack is dissected by two late orogenic extensional faults or detacments with down-to-the-east displacement, the Nunatak Fault (Andresen et al., 1998) or the Boyd Bastionen Fault (Higgins et al., 2004), and the Fjord Region Detachment (Andresen et al., 1998) (Figure 1)(Figure 2). The Fjord Region Detachment was active from late Silurian (Hartz et al., 2001) to at least Early Carboniferous (White and Hodges, 2002).

The autochthonous foreland of the East Greenland Caledonides is exposed in northern East Greenland/eastern North Greenland (Kronprins Christian Land)(Figure 1)(Higgins et al., 2001). The autochthonous/ parautochthonous basement with cover sequence is also exposed in several windows further south, the southernmost being the Gåseland Window (Figure 1).

2.2 The East Greenland Caledonides

2.2.1 The Caledonian basement-cover relationships

Kronprins Christian Land

The most complete section through the platform sequence along Laurentias eastern margin in East Greenland is exposed in the Kronprins Christian Land (Figure 1)(79°30´-81°30´N) (Higgins et al., 2001). The foreland-successions exposed in the tectonic windows further south all show evidence of Caledonian deformation, and are interpreted as parautochthonous (Higgins and Leslie, 2000). The Kronprins Christian Land foreland-succession comprises Palaeo- to Mesoproterozoic sequences overlain by Neoproterozoic to Lower Palaeozoic shelf sediments (Higgins et al., 2001). The older sequence consists of the Independence Fjord Group sandstones and interbedded red siltstones (Collinson, 1980), and is cut by c. 1382 ± 2 Ma doleritic dikes and sills related to the overlaying Zig Zag Dal Basalt Formation (Jepsen et al., 1980; Upton et al., 2005). Above the Neoproterozoic shelf sediments (Hagen Fjord Group) and below the Cambrian sediments (with Skolithos) of the Kap Holbæk Formation (Clemmensen and Jepsen, 1992), there is a hiatus. Another hiatus occurs between the Kap Holbæk Formation and the Ordovician to Silurian platform carbonates (Higgins et al., 2001). To the west the autochthonous foreland is bounded by the Vandredalen Thrust Sheet that displaces the Neoproterozoic sediments over Silurian flysch deposits, thus giving a maximum age of thrusting.

Lambert Land

In Lambert Land (79°20´N)(Figure 1) tectonic window, the Neoproterozoic shelf sediments (Hagen Fjord Group) are overlying crystalline basement gneiss complexes, and are locally overlain by Ordovician carbonates (Higgins et al., 2001).

Nørreland Window

Mesoproterozoic metasediments cut by dolerite dikes correlated with the Independence Fjord Group crop out in an anticlinal culmination exposing the Nørreland Window (78°40´N) (Figure 1)(Higgins et al., 2001). The Mesoproterozoic complex is overlain by deformed Ordovician metacarbonates with conodonts yielding CAI values of 5-6, indicating an overburden of 10-12.5 km (Rasmussen and Smith unpubl. data in (Higgins et al., 2001)). In the overlying thrust sheet, consisting of Palaeoproterozoic orthogneisses, Devonian eclogites

(c. 400 Ma) occur (Brueckner et al., 1998; Gilotti et al., 2004; Gilotti, 1993). Thus the thrust sheet in this part of the East Greenland Caledonides must have gone through substantial thinning before thrusting over the autochthon, not earlier than Mid-Devonian time (Gilotti et al., 2004)(see below).

Dronning Louise Land

In Dronning Louise Land (75°50´-77°25´N)(Figure 1) intense Caledonian deformation, manifested by N-S trending imbricate thrusts and folds, bounds the almost undeformed parautochthonous foreland (Strachan et al., 1994). Here a succession of metasediments (the Trekant 'series') cut by dolerite dikes is correlated with the Independence Fjord Group of Kronprins Christian Land (Clemmensen and Jepsen, 1992; Haller, 1971; Higgins et al., 2001). An overlying thin cover of sediments with Skolithos burrows (Zebra 'series'), are correlated with the Kap Holbæk Formation of Kronprins Christian Land (Clemmensen and Jepsen, 1992; Friderichsen et al., 1990; Strachan et al., 1994).

Eleonore Sø Window

The Eleonore Sø volcano-sedimentary complex (Figure 1) (73°35´-74°25´N) constitute a Palaeoproterozoic sequence of arkosic psammites, semipelites, a thick sequence of carbonate, a sequence of quartz psammites and black shale, with possibly rift related lavas on top. Quartz porphyry intruding the sequence is dated to c. 1900 Ma (Leslie and Higgins, 1998, in (Higgins et al., 2001)). Unconformably overlying is the Slottet Formation, a sedimentary sequence of up to 350 m, consisting of a basal conglomerate and several quartzite beds. In the Uppermost parts Skolithos burrows are abundant, and correlation can be made with the Kap Holbæk Formation of Kronprins Christian Land and the Zebra 'series of Dronning Louise Land (Higgins et al., 2001). Above the Slottet Formation, underlying a major Caledonian thrust, there is a thin carbonate cover containing abundant microfossils, interpreted to be of Cambro-Ordovician age (Higgins et al., 2001).

Målebjerg Window

Here, c. 35 km east of the Elonore Sø window (Figure 1), the Slottet Formation, overlie basement gneisses. Locally, in basement depressions, there is an up to 31 m clastic sequence containing diamictites interpreted as tillites (Smith et al., 2004). Again, carbonates of Cambro-Ordovician age (Målebjerg Formation) lie on top of the Slottet Formation, and the

occurrence of these formations allows correlation of the Målebjerg and Eleonore Sø Windows basement-cover sequence.

Charcot Land Window (71°30´-72°10´N)
Below an arched major thrust there is an infracrustal gneiss complex unconformably overlain by a volcano-sedimentary sequence (Charcot Land supracrustal sequence), with Paleoproterozoic quartz dioritic and granitic intrusions (Figure 1)(Higgins et al., 2001), thus suggesting correlation with the oldest supracrustals in the Eleonore Sø Window (Higgins et al., 2001). A small outcrop of diamictite, interpreted as tillite, correlated with the tillites in the Fjord Region (Henriksen, 1981; Moncreiff, 1989), is also present.

Gåseland Window
Cropping out in western Gåseland and the inner Scoresby Sund region (Figure 1)(70°10´-70°40´N), the southernmost of the Caledonian windows, is a crystalline basement complex unconformably overlain by a diamictite, interpreted to be a tillite (Phillips et al., 1973). Above the tillites, beneath the Caledonian thrust, is a marble cover, suggested to be Cambro-Ordovician (Phillips and Friderichsen, 1981). Phillips and Friderichsen (1981) also noted the similarities between the tillites here and the ones in the Fjord Region.

2.2.2 Basement-cover relationships along the orogen

As outlined above, there are several similarities between the autochthonous foreland in the north- easternmost part of Greenland and the parautochthonous units exposed in windows along the orogen (Higgins et al., 2001). The Early Paleozoic carbonates are found in all the described windows except in the Charcot Land window, indicating that the Iapetus margin was stretching at least 1300 km N-S (today's geography)(Higgins et al., 2001). The thrusts overlying the carbonates are sub-parallel to the bedding of the underlying strata, the youngest sediments deposited in the foreland areas prior to the Caledonian orogeny, and the carbonates probably acted as a decollement horizon where the major thrust sheet could propagate west-north-westwards during thrusting (Higgins et al., 2001). Skolithos bearing sediments are present in both the autochthonous foreland of Kronprins Christian Land and in the windows at Dronning Louise Land, and in the Eleonore Sø and Målebjerget areas. These and the diamictites occurring in the Charcot Land, Målebjerg and Gåseland Windows give further evidence of a coherent N-S striking continental Iapetus margin (Higgins et al., 2001).

Although there is a significant difference between the thin, hiati-disrupted sequences of the foreland and the thick, almost continuous Neoproterozoic to Ordovician sediment succession in the thrust sheet, a correlation is proposed (see below)(Higgins et al., 2001).

2.3 Tectonostratigraphy of the Hagar-Niggli Thrust Sheet

2.3.1 Allochthonous crystalline basement with eclogite-occurrences

The crystalline basement complexes occurring in the Hagar-Niggli Thrust Sheet can be divided into two units, Archean (c. 2.7-2.8Ga) gneisses south of c. 72°50´ N and Palaeoproterozoic (c. 1.9-2.0 Ga) gneisses north of this latitude (Thrane, 2002). A transition zone where Palaeoproterozoic granitoids have intruded Archean rocks was also reported (Thrane, 2002). The Palaeoproterozoic rocks extend further north and probably comprise all of the allochthonous crystalline basement rocks north of 72°40´ N. Samples from c. 77° N are dated to c. 1.74-1.97 Ga (Kalsbeek et al., 1993).

Eclogites and retrograded eclogites are widely documented in the generally felsic basement gneisses from c. 76° N to c. 80° N (North-East Greenland Eclogite Province, NEGEP)(Brueckner et al., 1998; Elvevold and Gilotti, 2000; Friderichsen et al., 1991; Gilotti, 1993; Gilotti and Krogh Ravna, 2002). Both Caledonian high pressure (HP)(Brueckner et al., 1998; Gilotti et al., 2004) and ultra-high pressure (UHP)(Gilotti and Krogh Ravna, 2002; Gilotti et al., 2004; McClelland et al., 2006) have been documented from this region. Gilotti et al.(2004) reported ages for HP-metamorphism at c. 410 - 400 Ma and for UHP-metamorphism at c. 360 Ma (Gilotti and Krogh Ravna, 2002). In situ SHRIMP-dating of zircons containing coesite from both kyanite-eclogites and the host gneiss (interlayered mafic to felsic quartzofelspathic gneisses), have yielded mean U-Pb-ages for the UHP-metamorphism from c. 360 to c. 347 Ma and zircon growth with HP mineral assemblages from c. 357 Ma down to c. 342 Ma (McClelland et al., 2006). The age spread from c. 400 Ma to c. 340 Ma for the HP- metamorphism and from c. 360 Ma to c. 347 Ma was by the latter authors interpreted to record prolonged residence time at eclogite facies to UHP conditions. McClelland et al. (2007) noted that UHP-metamorphism apparently coincided with a period of E-W rifting and formation of (Carboniferous) sedimentary basins. It should be noted that

where duplicate age determinations (U/Pb-zircon and Sm/Nd-garnet analysis) (Gilotti et al., 2004) are carried out, relatively large scatter between ages of the two methods occur.

The NEGEP is divided in three structural blocks by two major strike-slip shear zones, the Storstrømmen shear zone (sinistral) and the Germania Land deformation zone (dextral)(Figure 1)(Sartini Rideout et al., 2006). Eclogites in the westearn and central block give the older HP eclogite-ages referred above and samples from the eastern block give the younger UHP and HP eclogite-ages (Sartini Rideout et al., 2006). Sartini Rideout et al.(2006) attribute the initial exhumation of the HP-rocks to transpression and vertical extrusion along these shear zones. Late-stage exhumation was suggested to occur by continued movements at shallower crustal levels on the major shear zones and other brittle faults in the area (Sartini Rideout et al., 2006). This scenario resembles to some degree the suggested processes responsible for exhumation of the eclogites in Liverpool Land (see Chapter 5).

HP-granulites from Payer Land (74°28´-74°47´N)(Figure 1) have been described and dated to c. 405 Ma (Elvevold et al., 2003; McClelland and Gilotti, 2003). They are located below the Payer Land Detachment, occurring in paragneisses correlated with the Krummedal metasediments, although they differ somewhat in that they have been metamorphosed at c. 50 km depth and are not intruded by the S-type granites extensively occurring further south (Elvevold et al., 2003; McClelland and Gilotti, 2003). McClelland and Gilotti (2003) argue that the Payer Land Detachment, with the exhumation of the HP-granulites, may be a late stage, post-orogenic detachment, and indicate that much of the displacement of the East Greenland structure was synchronous with evolution on this detachment after HP-metamorphism (see below).

UHP-metamorphism has also been reported from Liverpool Land (Figure 1)(Figure 3)(Hartz et al., 2005), occurring at c. 399 Ma (see Chapter 3 and 4).

In northern Liverpool Land a sequence of metasedimentary rocks, possibly correlatable with the Krummedal Sequence has been described (Higgins, 1988). This might indicate that Liverpool Land belong to the same structural level as the Hagar-Niggli Thrust Sheet, and most workers include Liverpool Land in the allochthon (e. g., Higgins et al., 2004; Andresen et al., 2007).

2.3.2 Krummedal Sequence

The Krummedal Sequence is a thick, dominantly metasedimentary succession of Mesoproterozoic age originally described from the Scoresby Sund area (Figure 1)(Figure 2)(70° N) (Henriksen and Higgins, 1969). The age of deposition is constrained to between c. 1000-1100 and c. 930 Ma (Kalsbeek et al., 2000). The sequence rests unconformably on crystalline basement complexes, as observed several places (Andresen et al., 1998; Higgins et al., 1981), although the contact is generally highly tectonised (Higgins, 1988; Higgins et al., 1981). The lower part of the Krummedal Sequence is dominated by calcareous schists and marbles, locally with a basal quartzite. The major part of the sequence, however, is composed of alternating quartzites, semipelites and pelites, often brownish weathering (Higgins, 1988; Higgins et al., 1981). Based on the general development of the sedimentary facies, the great thickness and wide distribution of the sediments, Higgins (1988) suggested that the Krummedal Sequence could represent deep-water turbidite deposits.

The metamorphic grade varies from amphibolite facies with staurolite and kyanite as index minerals (Higgins, 1974; Higgins, 1988), via upper amphibolite facies, locally with abundant cordierite (Watt et al., 2000), to granulite facies, with migmatisation characterised by garnetiferous neosomes (Leslie and Higgins, 1999; Leslie and Nutman, 2003). In many areas retrograde mineral assemblages (chlorite, muscovite and phrenite) are partly overprinting the peak metamorphic paragenesis (Higgins, 1974).

The Krummedal Sequence is correlated with other Mesoproterozoic units (e. g. Smallefjord Sequence), and is considered to occur at least up to 76° N (Friedrichsen et al., 1994; Kalsbeek et al., 2000).

In Renland (Figure 1), tight isoclinal folds of the Krummedal Sequence metasediments, cut by and interfolded with augen-granites dated to between 900- 950 Ma, were described by Leslie and Higgins (1999; 2003). Ages in the same range were also reported by Kalsbeek et al. (2000) from the Kong Oscar Fjord region, both for metamorphic overgrowth on detrital zircons in the Krummedal Sequence and on cross-cutting granites. Leslie and Nutman (2003) take this as evidence for an Early Neoproterozoic event. However, converging metamorphic grade between the upper Krummedal Sequence and the overlying Eleonore Bay Supergroup

(see below) in the Petermann Bjerg and the Fjord Region (Figure 1)(Andresen et al., 1998; Higgins et al., 2004), argue against an extensive early Neoproterozoic orogenic event (Grenvillian) (Andresen et al., 2007). Where the contact between the Krummedal Sequence and the Eleonore Bay Supergroup is not an extensional fault, it is either a gradational contact (Andresen et al., 1998) or a bedding-parallel detachment, interpreted to be a modified unconformity (Higgins et al., 2004). This does also speak against a large scale "Grenvillian" orogenic event affecting the north-eastern margin of Greenland.

Caledonian metamorphism and magmatism is, however, regionally extensive within the Krummedal Sequence (Hartz et al., 2001; Higgins et al., 2004; Kalsbeek et al., 2001b; Leslie and Nutman, 2003; Watt et al., 2000; White et al., 2002; Andresen et al., 2007). The Caledonian metamorphism overprints c. 930 Ma granites (Kalsbeek et al., 2001a) and metamorphic monazite growth and zircon overgrowth from the Krummedal Sequence typically dates to c. 430 - 420 Ma (Andresen and Hartz, 1998; Leslie and Nutman, 2003; Watt et al., 2000; White and Hodges, 2003; White et al., 2002; Andresen et al., 2007).
Granitic rocks vary from cm wide veins to dikes and sheets several hundred meters wide. Felsic plutons more than 10 km across also appear, both undeformed and strongly foliated, and sometimes also folded (Kalsbeek et al., 2001a; Kalsbeek et al., 2001b). Most Caledonian granitoids are two-mica leucogranites, and the field relations mentioned above, as well as age distributions on inherited zircons (similar to those in the Krummedal Sequence metasediments), geochemical signatures and the absence of Caledonian (and Neoproterozoic) intrusives in the underlying basement rocks, suggest an anatectic Krummedal Sequence-origin (Hartz et al., 2001; Hartz et al., 2000; Kalsbeek et al., 2001a; Kalsbeek et al., 2001b; Leslie and Nutman, 2003; Watt et al., 2000; White et al., 2002).
The emplacement age of the Caledonian granites in the Krummedal Sequence generally range from c. 435 to 420 Ma (Hartz et al., 2001; Hartz et al., 2000; Kalsbeek et al., 2001b; Leslie and Nutman, 2003; Watt et al., 2000; White et al., 2002; Andresen et al., 2007), although recent work has revealed Late Ordovician to early Silurian magmatism (see below).

The high temperature metamorphism and partial melting of the Krummedal metasediments has been attributed to contraction and thickening in the Scandian phase of the Caledonian orogenesis (Andresen et al., 1998; Hartz et al., 2001; McKerrow et al., 2000; White et al., 2002; Andresen et al., 2007). Extension occurred in the upper crust synchronously with

contraction in the migmatised, ductile middle crust. The ductile lower middle crust experienced deformation by "flow", overturning folds into large scale recumbent folds (Figure 2)(Andresen et al., 2007). A clockwise P-T path was reported by White and Hodges (2003). Orogen-parallel, as well as East-West extension has been documented (Hartz et al., 2001; White et al., 2002). Generation of the late undeformed leucogranites has been related to (near) isothermal decompression, mainly caused by tectonic denudation on major detachments (Vold, 1997; Watt et al., 2000; White and Hodges, 2003). A similar P-T history has also been reported from the Smallefjord Sequence further north (Jones and Strachan, 2000).

Early calc-alkaline intrusions

Mafic and intermediate calc-alkaline intrusions are relatively abundant in the southernmost part of the East Greenland Caledonides (Rehnstrøm, written comm; Kalsbeek, written comm.). Rehnstrøm (written comm.) and F. Kalsbeek (written comm.) have obtained Ordovician ages on a granodiorite, a quartz-diorite and a leucogranite. Other calc-alkaline plutons from this area, with distinctly different chemistry than the anatecticly derived leucogranites in the Krummedal Sequence, have yielded ages from c. 430-420 Ma (Rehnstrøm, written comm.; F. Kalsbeek, written comm.). The geochemical signatures of the calc-alkaline intrusives in Renland indicate derivation from an enriched mantle or a mixed mantle/crustal source, and the older plutons have distinct negative Nb and Ti rock/chondrite spikes, typical for arc related rocks (F. Kalsbeek, written comm.). Hf- isotope data of the granitoids indicate derivation from a protolith with a crustal residence age of c. 1.7-2.0 Ga, mixed with juvenile mantle melts, the younger having the most juvenile component (Rehnstrøm, written comm.). High Ba- and Sr-concentrations, high K/Na, slightly lower ε_{Nd} and higher ε_{Sr} than proposed for lithospheric mantle values, support this interpretation (Kalsbeek, written comm.). Rehnstrøm (written comm.) suggests that the older intrusives are derived in a subduction zone setting, and that the younger intrusives might be the result of decompressional melting of an upwelling asthenospheric mantle in response to orogenic collapse.

2.3.3 The Eleonore Bay Supergroup

A thick Neoproterozoic succession of sedimentary rocks comprise the Eleonore Bay Supergroup (EBS), exposed in the Fjord Region (c. 72° to 74° N), in Payer Land, around Ardencaple Fjord and on Canning Land (Figure 1)(Higgins et al., 2004). The lower boundary of the EBS is either extensional faults (Figure 2), a bedding-parallel detachment or a gradational contact (see above)(Andresen et al., 1998; Higgins et al., 2004). In the base of the EBS, Caledonian metamorphism, resulting in new growth on detrital zircons, has recently been documented (Dhuime et al., 2007). The sedimentary sequence is up to over 13 km thick (in the Fjord Region) and is dominated by shallow marine siliciclastic sediments capped by platform carbonates (Tirsgaard and Sønderholm, 1997). The siliciclastic sediments were deposited on an extensive shelf, ranging from coastal plain to outer shelf environment, with a suggested N-S oriented coastline and basin-deepening to the east (Tirsgaard and Sønderholm, 1997). Fredriksen (2000; Ph. D thesis, in (Higgins et al., 2004)) suggested that carbonates of the Hagen Fjord Group in Kronprins Christian Land can be correlated with Upper Proterozoic carbonates in the Fjord Region, thus implying that the Eleonore Bay Supergroup basin stretched for more than 1000 km along the Laurentian margin. The deposition of the EBS is constrained to between c. 990 and c. 680 Ma (Dhuime et al., 2007).

2.3.4 Vendian Tillite Group

Conformably to unconformably overlying the EBS, is the Vendian Tillite Group, an 800-1000 m thick sequence with two diamictite units, correlated with the diamictites in the parautochtonous foreland (Hambrey et al., 1989; Higgins et al., 2004; Moncreiff, 1989).

2.3.5 Kong Oscar Fjord Group

The Cambro-Ordovician Kong Oscar Fjord Group is up to 4,5 km thick in the Fjord Region (Smith et al., 2004) The dominant lithologies are arenites fining upwards to shales in the lower part, succeeded by limestones and dolostones, the uppermost units being limestones of Ordovician age. The succession is continuous and the top is cut by the Caledonian erosion surface (Smith et al., 2004). The Kong Oscar Fjord sediments contrasts markedly with equivalently aged sediments in the autochthonous and parautochthonous foreland, the latter being thin and with a possible hiatus between the Lower Cambrian quartzites and the

overlying carbonates, thus indicating eastward deepening along the Laurentian Iapetus margin (todays geography)(Higgins et al., 2001).

Higgins et al. (2001) compared the foreland successions and the allochthonous Neoproterozoic-Lower Palaeozoic succession of the East Greenland Caledonides with corresponding similar aged sequences in Scotland, and concluded that the autochthonous and parautochthonous foreland of the East Greenland Caledonides laid further inland on the passive margin, and that the allochthonous sediments in the Fjord region laid outboard of the comparable successions in the Northwest Scotland (Torridon Group). The similarities of the EBS with the Murchinsonfjorden Supergroup of Spitzbergen and the Grampian Group of Scotland was pointed out by (Higgins et al., 2004). The Vendian tillites of East Greenland are according to Hambrey et al.(1989) correlatable almost on a "bed-by-bed" basis to the ones on NE Svalbard, and the Tillite Group are thought to have been deposited in a basin contiguous with the ones in Svalbard (Hambrey et al., 1989, and references therein).

2.4 Timing of thrusting and emplacement of the Hagar-Niggli Thrust Sheet

An important feature regarding the temporal and spatial evolution of the East Greenland Caledonides is the appearance of low grade rocks of the windows in tectonic contact with high grade allochthonous rocks (Gilotti et al., 2004; Andresen et al., 2007). Eclogites dated to c. 405 Ma (see above) occur above the Nørreland Window, which contains carbonates with conodonts showing colour alteration index of 5-6 (c. 12.5 km overburden)(Rasmussen and Smith, 2001). This indicates that thrusting of a thinned and partly exhumed thrust sheet happened after 405 Ma (Gilotti et al., 2004). The c. 360 Ma UHP rocks occurring further to the west might indicate that thrusting was even later than this (Gilotti et al., 2004). Dallmeyer and Strachan (1994) recorded muscovite $^{40}Ar/^{39}Ar$- ages of 392-385 Ma from a mylonitic quartzite in the marginal thrust zone of Dronning Louise Land. They interpreted these ages to closely date thrust related mylonite-formation, and thereby concluded that thrusting in the foreland occurred at this time. Hornblende $^{40}Ar/^{39}Ar$- cooling ages of c. 390-380 Ma from basement gneisses of Dove Bugt (Figure 1)(the central block, between Storstrømmen shear zone and Germania Land deformation zone), show that the HP-rocks here cooled below the

hornblende Ar-retention temperature at this time (Dallmeyer and Strachan, 1994). Since the samples from Dronning Louise Land were taken only 300-400 km from the thrust front in Andreé Land, the ages obtained for thrusting in Dronning Louise Land may likely also be valid for thrusting of the Hagar-Niggli Thrust Sheet (Andresen et al., 2007). A minimum age on thrusting in the south, is provided by a $^{40}Ar/^{39}Ar$- age of c. 357 Ma on biotite from a pseudotachylyte in the Fjord Region Detachment, which cuts across the Hagar-Niggli Thrust Sheet (White and Hodges, 2002; Andresen et al., 2007). From the easternmost tectonic window and the westernmost outcrop of the Hagar- Niggli thrust sheet, a minimum displacement distance of 100 km can be inferred (Andresen et al., 2007). These observations indicate that the main transport of allochthonous rocks occurred significantly later than the contractional and extensional events responsible for medium to high grade metamorphism and extensive granite generation in the Hagar-Niggli Thrust Sheet.

Schlindwein and Jokat (2000) described a west-dipping deep crustal reflector, proposed to be a large scale detachment, in the Fjord Region area. They also discussed the possibility that this sliver of high density lower crust was a relict of the westerly subducted Baltica crust. These authors noted that there were important differences in the crustal structure north and south of 76° N: (1) no Devonian basins have been recorded north of this latitude, neither has any major detachments; (2) a Devonian moho plateau observed in the Fjord Region, disappears towards the north (Schlindwein and Jokat, 2000, references therein). The difference in crustal stuctures north and south of 76° N, may explain the difference in timing of UHP-metamorphism in NEGEP and in Liverpool Land (see Chapter 5).

2.5 Devonian deposits

Middle Devonian N-S-striking extensional basins in the Fjord Region (72-74° N) preserve the oldest "post-Scandian" sediments in the East Greenland Caledonides, with upper Middle Devonian fossils as the oldest known (Figure 1)(Figure 2)(Jarvik, 1961; Larsen et al., 1989). The oldest sediments rest unconformably on Lower Paleozoic or Proterozoic rocks, and the up to c. 7 km thick succession also contains internal angular unconformities and are folded, witnessing the partly tectonically controlled sedimentation (Larsen and Bengaard, 1991; Larsen et al., 1989). The Devonian basin is bounded by a fault system with flower structures and extensional faults striking both NNW-SSE and E-W. Larsen and Bengaard (1991) related these faults to a N-S-striking sinistral wrench-fault zone.

Devonian sediments are also described from Canning Land just north of Liverpool Land, sometimes resting unconformably on Eleonore Bay Supergroup sediments, but affected by displacements on extensional faults (Caby, 1972).

As pointed out by Andresen et al. (2007) the indications that the Hagar Niggli Thrust Sheet was emplaced at Middle Devonian time (continued convergence between Baltica and Laurentia), may further imply that the Devonian sediments were deposited in a "piggy-back" setting, and that previously deposited sediments (in extensional basins generated by upper crustal extension from early Late Silurian) were continuously eroded away.

3 Geology of the study area

3.1 Introduction and previous work

The field area for this study is located on Liverpool Land, a high grade Caledonian terrain with several large intrusions of inferred Caledonian age (Figur 1)(Coe, 1975; Coe and Cheeney, 1972; Hansen and Steiger, 1971; Kranck, 1935). The Caledonian rocks are overlain unconformably by Late Permian and Mesozoic rocks. The unconformity dips to the west, and is suggested to be an old erosion surface (Coe, 1975).

Previous work in the area is limited, but important contributions was made especially by Kranck in the 1930's and Coe and Cheeney in the 1970's (Coe, 1975; Coe and Cheeney, 1972; Kranck, 1935). More recently some preliminary data has been presented by (Hartz et al., 2005). Kranck (1935) described migmatitic gneisses with both amphibolitic and eclogitic inclusions, cut by younger aplites and pegmatites. In his descriptions the migmatite gneiss terminated just south of Gubbedal (Figure 3)(see below). Coe and Cheeney (1972) redescribed the gneiss as a veined garnet-hornblende-biotite gneiss with a prominent N-S trending lineation. They also questioned the classification of some of the mafic inclusions as eclogites, as proposed by Kranck (1935) and Sahlstein (1935). More recently Smith and Cheeney (1981) reported serpentinised chromite-garnet ultrabasites from the same migmatite gneiss. North of the migmatite gneiss, Kranck (1935) reported a more than 400 km^2 large, pink, uniform granite, named the Hurry Inlet Granite (Figure 3). To the north of the Hurry Inlet Granite he described migmatitic biotite-garnet gneisses, and north of this gneiss, he described a granodiorite, later redescribed and named the Hodal-Storefjord Monzodiorite by Coe and Cheeney (1972)(Figure 3). Coe (1975) and Coe and Cheeney (1972) also described several other granitoids from Liverpool Land, ranging from monzonites to granodiorites and hornblende-bearing granites. In addition they redescribed the Hurry Inlet Granite and recognised five different phases, as well as xenoliths from the surrounding basement gneiss in the eastern part of the batholith. Coe (1975) did major and trace element geochemistry on 25 samples from the batholith (see Chapter 5). The Hurry Inlet Granite was dated by Rb/Sr on biotite to 434 ± 10 Ma (Hansen and Steiger, 1971). Later fission track dating on titanite, zircon and apatite from the Hurry Inlet Granite was conducted by Gleadow and Brooks (1979). They obtained an age of 413 ± 10 Ma for titanite, which is thought to have a retention

temperature of 250 ± 50 °C. Carboniferous and Mesozoic ages were obtained for zircon and apatite, respectively.

No major shear zones have been reported from Liverpool Land, but intense deformation of granodioritic gneisses, enveloped by a strongly lineated, fine grained hornblende schist of "mylonitic aspect" was reported from south of Lillefjord by Coe and Cheeney (1972) (thus the speculative extrapolation of the shear zone in the map) (Figure 3). Coe (1975) also described the contacts both on the southern and eastern side of the Hurry Inlet Granite as disrupted in most places, with occurrences of feldspar "porphyroblasts" and faulting. In the south he described "homogenisation" of the gneiss close to the granite. He attributed the "disruption" and "homogenisation" of the gneiss surrounding the Hurry Inlet Granite to the intrusion of the latter into the former.

Recently Hartz et al. (2005) confirmed the presence of true eclogites, and reported preliminary data indicating UHP-metamorphism at more than 25 Kbar, occurring at c. 397-393 Ma.

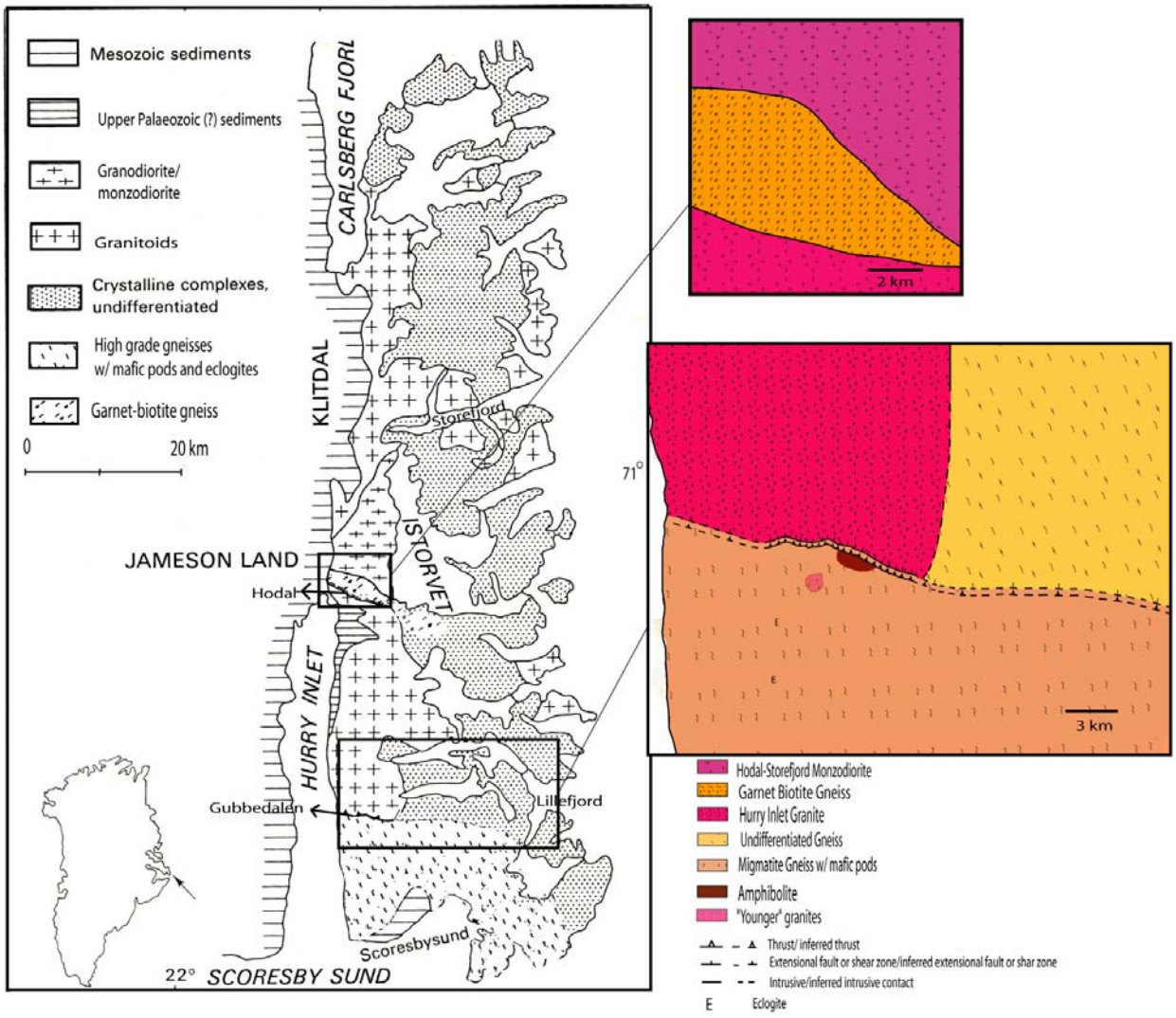

Figure 3: Map of Liverpool Land, modified after Coe (1975). Modifications partly based on Coe and Cheeney (1972) and this study. To the right detailed maps of the study area, based on mapping conducted during the summer of 2006. The extrapolation of the shear zone to the east coast is based on observations of a high strain zone "of mylonitic aspect" reported by Coe and Cheeney (1972).

Our mapping has shown that the Caledonian rocks on southern Liverpool Land are composed of two structural blocks/terranes; separated by a N-dipping shear zone, named the Gubbedalen Shear Zone (GSZ)(Augland et al., 2007)(Figure 3)(Figure 4) and a brittle extensional fault, the Gubbedalen Extensional Detachment Fault (GEDF). The footwall to the GSZ is composed of migmatitic gneisses with eclogite- and amphibolite-lenses and –layers, all intruded by granitic dikes and minor intrusives, whereas the hanging wall is dominated by undeformed Caledonian intrusives, where the Hurry Inlet Granite is the largest.

As stated in Chapter 1, the purpose of this study was to:

5) Document the presence of a shear zone (Gubbedalen Shear Zone) between the Hurry Inlet Granite and the high grade gneisses containing eclogites to the south of it.
6) Understand the kinematic evolution of the Gubbedalen Shear Zone.
7) Constrain the age of the high grade metamorphism in the footwall block using the ID-TIMS method.
8) Date the inferred Caledonian intrusions in the hanging wall north of the shear zone.

As only rocks from the footwall block appear in the shear zone, my description of the geology of the study area starts with this unit. Then a description of the tectonites and structures from the GSZ will follow. The descriptive part ends with a brief description of the main lithologies encountered in the granitoid dominated hanging wall.

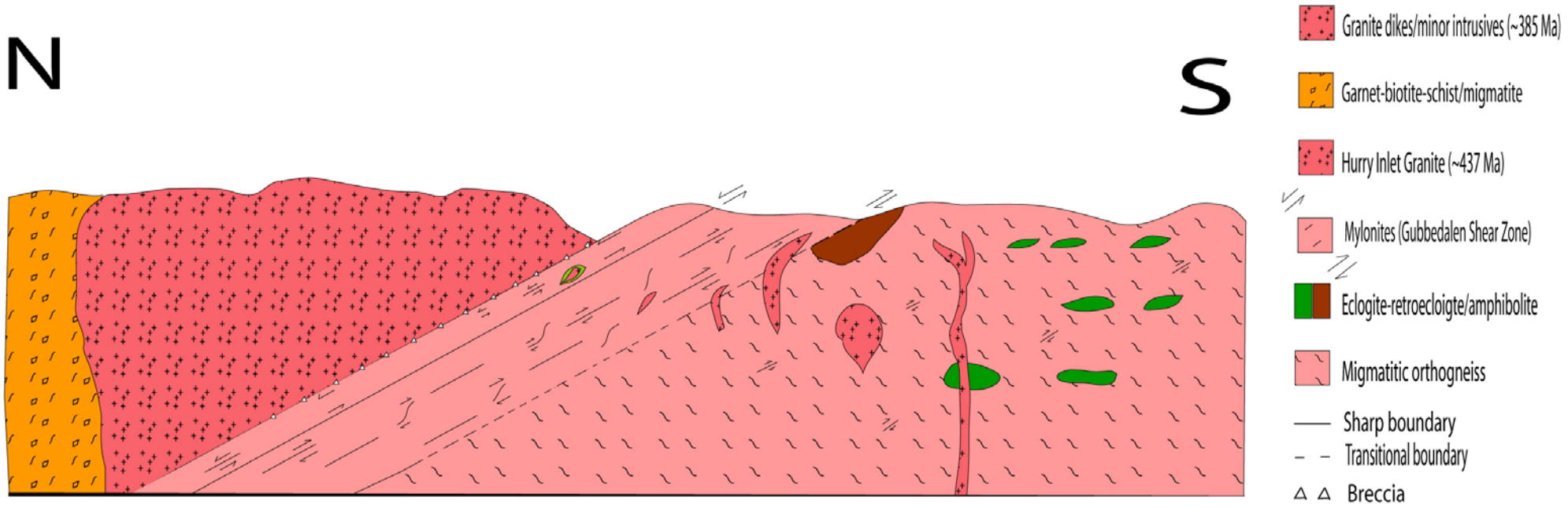

Figure 4: Schematic profile across the Gubbedalen Shear Zone, central/southern Liverpool Land. Not to scale.

3.2 Geology of the footwall (high grade) terrane

3.2.1 Introduction

The rock cropping out in the investigated area in Southern Liverpool Land is dominated by relatively homogenous, pink migmatitic gneiss, with different sized lenses and layers of mafic rocks. Both the migmatite and the mafic rocks are intruded by medium grained, pink granite dikes and smaller bodies.

3.2.2 Migmatite gneiss

The general foliation in the migmatite gneiss is shallowly dipping with a variable strike (Figure 5), due to wrapping around mafic lenses (see below) of variable size, from cm to several hundred meters scale. The dominant strike directions are NW-SE and NE-SW.

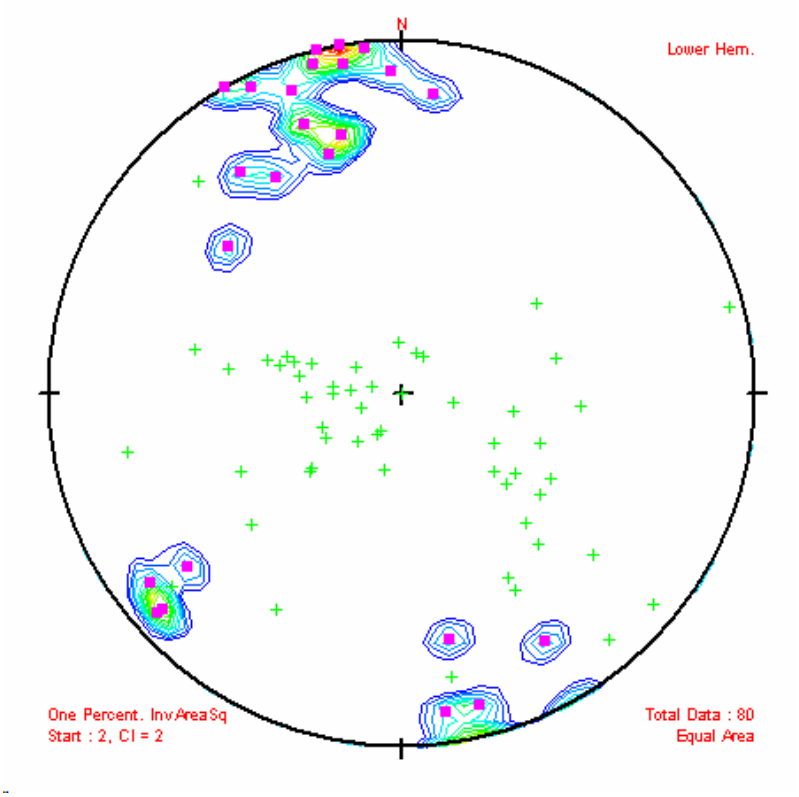

Figure 5: Stereographic presentation of poles to the dominant foliation in the migmatitic gneiss (green crosses). Measured elongation lineation has a NNW-SSE plunge (contour lines).

The gneiss in the study area is dominantly a felsic migmatite (Figure 6). The leucosomes of the migmatite are dominated by K- feldspar (almost 50 %), quartz (c. 40 %) and plagioclase (c. 10 %), with some biotite (c. 1 %), partly replaced by chlorite. The feldspars are altered, and in some of the K- feldspars, larger muscovite grains occur (Figure 7). The restite consists of biotite and amphibole with varying relative proportions, together with plagioclase, quartz and K- feldspar. Modal plagioclase is generally higher in the restite than in the neosome (Figure 7)(Figure 8). Locally, apparently more so close to the mafic boudins, garnet can be abundant in the restites. Pyroxene was observed in one sample (Figure 8). This rock is the equivalent of the garnet-hornblende-biotite gneiss of Coe and Cheeney (1972).

Figure 6: Migmatite gneis with flattend leucosomes, 10 cm scale bar laying on a nearly angular corner.

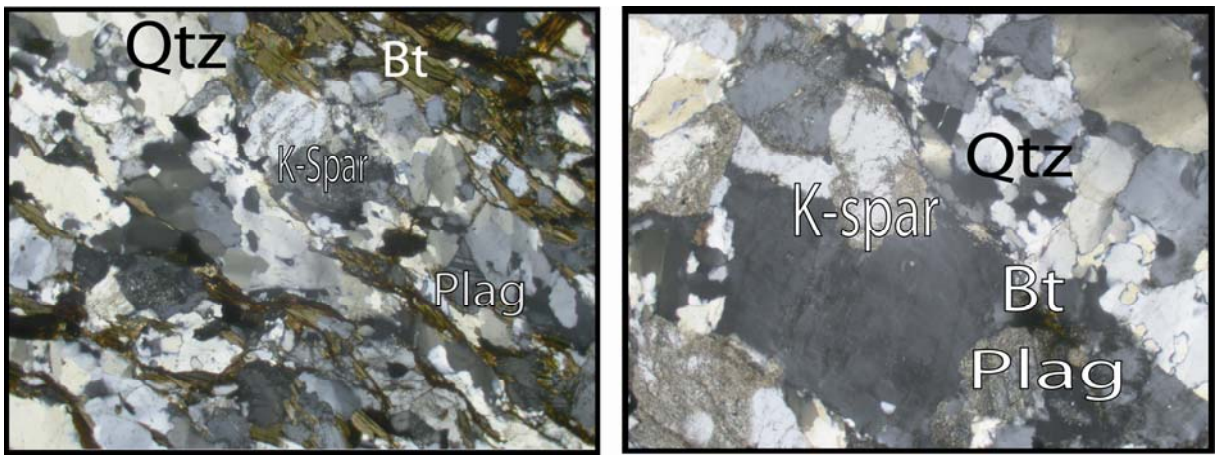

Figure 7: Photomicrographs taken with crossed nichols. The photomicrographs show the restite (left) and the neosome (right) of the migmatite gneiss (LEA 06-07). The sample is collected at 70 °36.04' N, 22° 14.238' W. Width of view in both pictures is 2.8 mm.

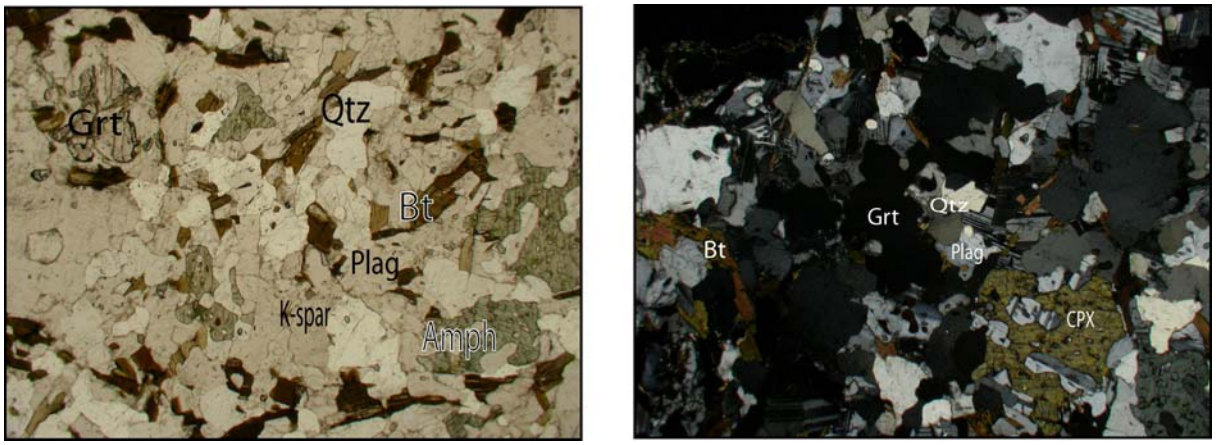

Figure 8: Photomicrograph of migmatite restite (LEA 06-11). Picture to the right is taken with crossed nichols (from a different spot). The sample is collected at 70° 35.211' N, 22 ° 14.177 W. Widt of view in both pictures is 5.5 mm.

Quartz in both restite and neosomes has experienced recrystallisation after migmatisation, showing development of small subgrains along grain margins and within larger grains, and beginning development of core and mantle structure, indicating recrystallisation by bulging recrystallisation and 'high temperature' bulging to slight subgrain rotation recrystallisation (Figure 7), the latter indicative of medium temperature metamorphism (Stipp, 2002; Stipp et al., 1999). The migmatite occur over a large area and is relatively homogeneous in both appearance and mineral composition. It is thus interpreted as an orthogneiss.

The deformation of the migmatite contemporaneous with and/or after crystallisation of the neosomes, has resulted in constrictional finite strain in the neosomes, with stretching (x) generally directed N-S (Figure 9)(Figure 10). There has, however, been a phase of initial flattening (Figure 6). Folded leucosomes, with general fold axes trending approximately N-S, are abundant. When unfolded, the leucosomes are flattened objects with $x \sim y >> z$ in the strain ellipsoid. At some sites the constrictional strain is not observed, and the flattening is most pronounced (Figure 6).

Figure 9: Leucosomes in the migmatite gneiss showing constrictional strain. Perpendicular view from Figure 10, and to the stretching direction.

Figure 10: Constrictional strain in the migmatite, leucosomes are stretched out. View is perpendicular to Figure 9 and in the foliation plane.

In the migmatite there is a pronounced aggregate lineation (mainly quartz aggregate lineation) trending approximately NNW-SSE (Figure 5), but with some local variations, due to wrapping around the mafic enclaves (see below).

3.2.3 Mafic lenses and layers

Mafic lenses and layers occur stratiformly (Figure 11), with varying distances between them and variable size on the individual lenses and layers (Figure 12). Most of the mafic lenses have typical boudin shapes, with stretched margins, and thick centres (Figure 12), and with the foliation of the migmatite gneiss wrapping around. Some of the lenses appear to have been rotated during boudinage (Figure 12). The boudins consist of eclogite, retrogressed eclogites

and amphibolites. Two of the freshest eclogites are shown in the map (Figure 3). The light green and red eclogite generally consist of 60 to 70 % garnet, c. 20 to 25 % clinopyroxene, c. 5 % rutile, c. 1 to 2 % ilmenite and accessory zircon (Figure 13), in addition to secondary amphibole and biotite (Figure 13)(Figure 14). The rock has an equigranular texture, with subhedral garnets and anhedral pyroxenes. The retrogressed eclogites consist of garnet, amphibole+plagioclase symplectites, amphibole, biotite, chlorite, rutile, some quartz and accessory zircon. Pyroxenes are also typically rimmed by amphibole. The jadeite component in the freshest sample was determined to c. 44 % (Table 1), showing that the clinopyroxene is a true omphacite. There are several stages of retrogression in the mafic boudins. The retrogression is dependent on fluid activity, as transitions from the typical retro-eclogite to amphibolite with no traces of the primary eclogite texture and mineralogy, are commonly observed around veins in the eclogite/ retro-eclogite (Figure 14). These amphibolites occur both within boudins with eclogite and retro-eclogite, and as separate boudins. They are fine grained, consist of amphibole, plagioclase, chlorite, quartz and some calcite. Amphibolite also occurs as a larger body bordering GSZ (Figure 3)(Figure 4). This competent body might have acted as a strain boundary, initiating the formation of the GSZ to the north of it.

	cpx-1	cpx-2	cpx-3	cpx-4
SiO_2	54.82	54.43	54.35	52.97
TiO_2	0.163	0.172	0.19	0.239
Cr_2O_3		0.004	0.016	0
Al_2O_3	12.055	12.211	12.242	12.55
FeO_{tot}	3.92	4.15	4.31	4.50
MgO	8.212	8.156	8.257	8.191
MnO	0.04	0.03	0.01	0.00
CaO	14.172	14.02	14.479	14.743
Na_2O	6.74	6.63	6.20	6.19
K_2O		0.017	0.002	0
SUM	100.12	99.79	100.04	99.38
X_{jd}^{Cpx}:	0.4445	0.4473	0.4277	0.4282

Table 1: Electron micro probe (EMP) analyses of four clinopyroxenes from a fresh eclogite (LEA 06-61). The analyses were performed on a Cameca 19939 EMP. The average jadeite component in the clinopyroxene is c. 44 %.

Figure 11: Large mafic boudins occuring stratiformly. Vidth of view is on the scale of 100 - 200 meters. Picture is taken at 70 °34.633' N, 22 °15,193' W.

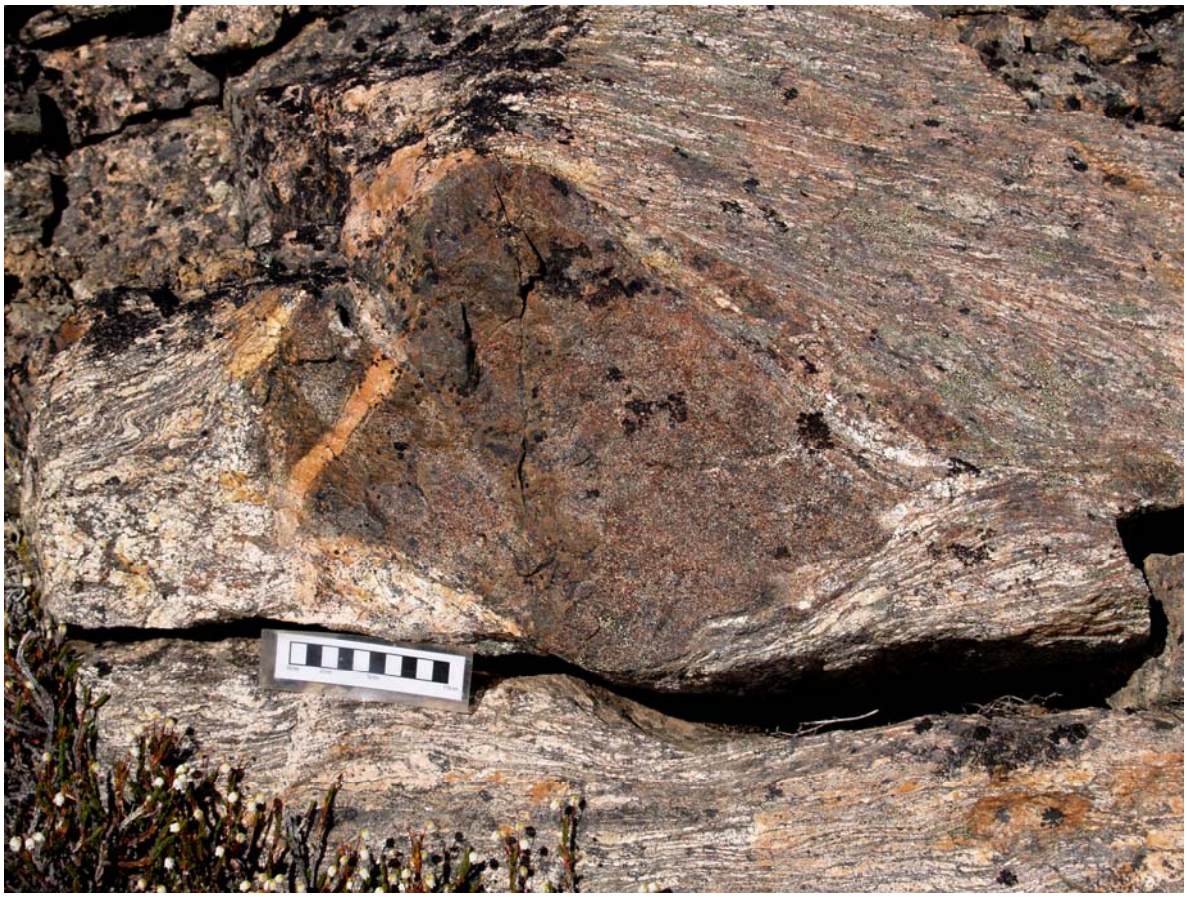

Figure 12: Mafic boudin in migmatite. A leucocratic pegmatite located in the neck of the boudin, and is also cutting it. Scale bar is 10 cm.

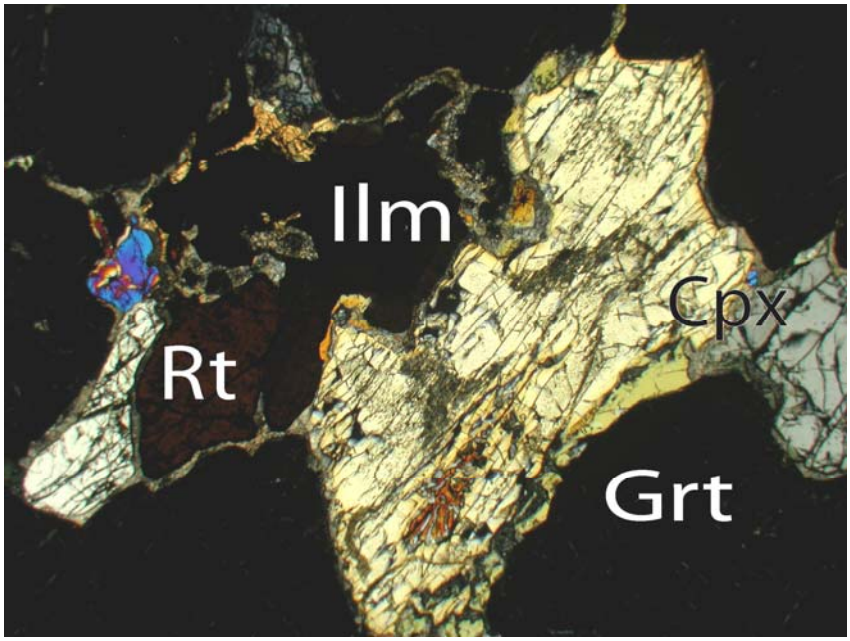

Figure 13: Photomicrograph taken with crossed nichols of eclogite (sample LEA 06-61). The rock consists of omphacite, garnet, rutile and ilmenite. Symplectites of plagioclase and amphibole are visible inside and along grain boudaries of cpx. Width of view is 5.5 mm. Sample collected at 70° 34. 633' N, 22° 15.223' W.

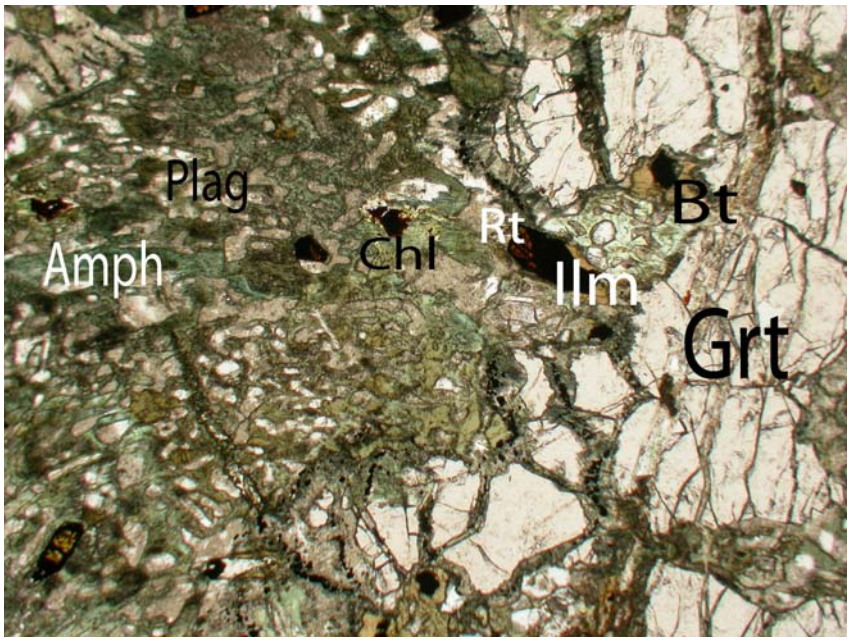

Figure 14: Photomicrograph of altered eclogite (sample LEA 06-23). Here the alteration of the eclogite can be observed in thin section, the slightly altered eclogite to the right, and progressive alteration towards the left. Altered rock occurs around a vein. Width of view 5.5 mm. Sample collected at 70° 34. 929' N, 22° 13.797' W.

3.2.4 Pegmatites

Leucocratic pegmatites are abundant in boudin necks, and can also be observed to cut through the boudins (Figure 12) (Figure 15). None of the pegmatites cut the surrounding gneiss (Figure 12)(Figure 15), indicating that the pegmatites crystallised earlier than, or at the same time as the generation of the visible foliation in the surrounding migmatite gneiss, and that the more competent mafic rocks protected the pegmatitic dikes, as opposed to the migmatite gneiss, in which the pegmatites were smeared out due to shearing under high temperatures. The pegmatite dikes have thicknesses of up to c. 2 meters. They consist mainly of plagioclase and amphibole, or plagioclase, K- feldspar, quartz and some biotite. The occurrence of amphibole indicates that the pegmatites crystallised under amphibolite facies conditions. These pegmatites crystallised at c. 388 Ma, probably due to decompressional anatexis of the high grade rocks (see Chapter 4).

Figure 15: Disrupted mafic layer in the migmatite gneiss. Note gradational transition from pegmatite to migmatite. Lens cap is 5 cm.

Figure 16: Banded eclogite (garnet- pyroxenite) lens with cross-cutting pegmatites consisting of large amfibole and plagioclase crystals. Hammer is c. 40 cm long. Eclogite located at 70 °34.633' N, 22 °15,193' W.

3.2.5 Mylonites

Around many of the mafic boudins, the migmatite gneiss, and in many cases the pegmatites, are mylonitised, with feldspars acting brittle and quartz ductile, with sub-grain rotation recrystallisation. Amphibole porphyroblasts were also observed in the mylonite at one locality, indicating long-lived deformation along the margins of the boudins, i.e. ductile shearing under amphibolite facies condition, down to below 3-400 ºC (brittle deformation). There is a distinct lineation associated with the mylonite zones, defined by both quartz aggregate lineation and alignment of porphyroclasts. Where kinematical indicators (i.e. S-C bands, small scale asymmetric folding and stacking of clasts) are present in the mylonites, top-to-the-south displacement is evident (Figure 17).

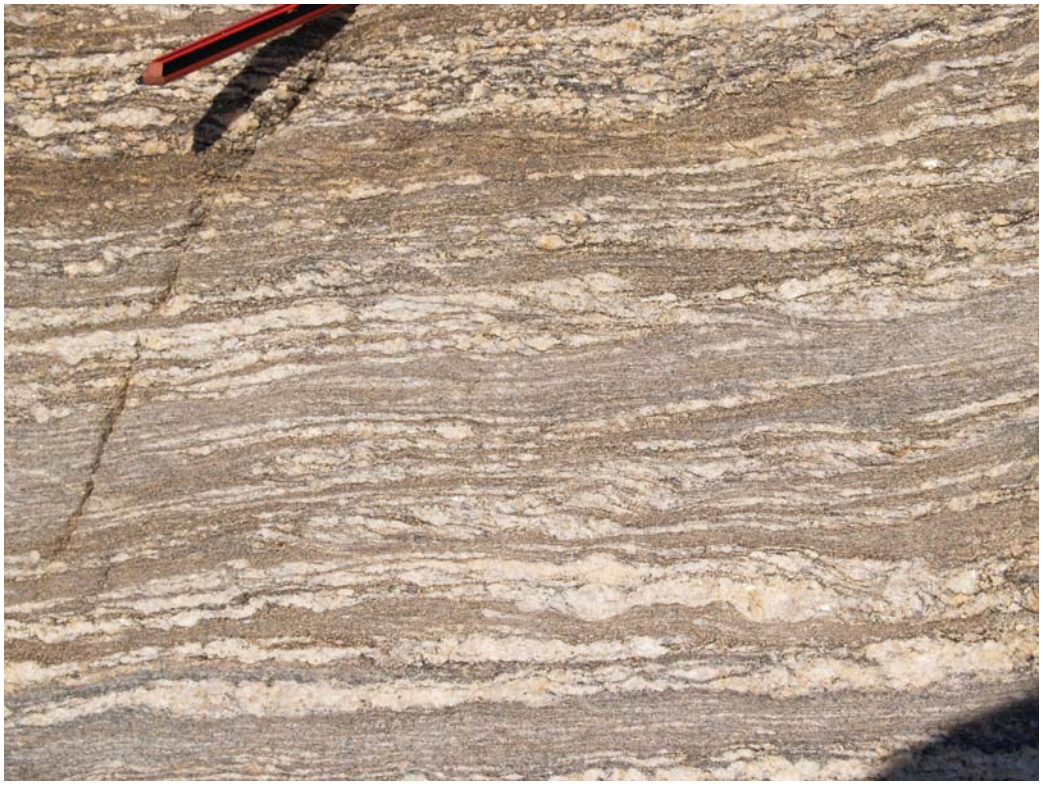

Figure 17: S-C- bands, small scale asymmetric folds and stacking of porphyroclasts in the mylonite around a mafic boudin. Shear sense is top-to-the-south (left in the picture). Pencil for scale.

3.2.6 Young Granites

The migmatite gneiss, the mafic boudins with their pegmatites, and sometimes the mylonites, are cut by medium grained granitic dikes of a few cm to c. 10 m width, and by smaller bodies (up to ca 100-200 m diameter bodies were observed)(Figure 18)(Figure 19), probably resembling the aplites described by Kranck (1935). At one locality a granite dike appears as an intrusive breccia with xenoliths of both the migmatite and the mafic rocks (Figure 20). The granite dikes are in most cases unfoliated, but in high strain zones, especially in the north close to the GSZ, these are foliated (Figure 21). The rock consists of c. 40 % K-feldspar, c. 35 % quartz, c. 10 % plagioclase, c. 5 % biotite partly altered to chlorite, some muscovite and accessory zircon, rutile and opaques (Figure 22). The feldspars are partly altered to clay minerals. The apparently undeformed granite dikes, has experienced a slight degree of bulging recrystallisation in the quartz grains (Figure 22). Quartz and K-feldspars also show undulose extinction, indicating that some deformation also has affected these dikes later. There is evidence of late fluid activity associated with the granite dikes, with coarse grained quartz and K-feldspar pegmatite veins occurring on both margins of the granitic dikes (Figure

23). These pegmatites are contemporary, or younger than the granite dike intrusion, and not related to the anatectic pegmatites associated with the mafic boudins. The granite dikes have been dated to c. 386 Ma (see Chapter 4).

Figure 18: Granite dike cutting anatectic amphibolite, showing that the granite dikes are younger than the anatectic pegmatites and aplites. Geologist is Mark Steltenpohl.

Figure 19: Young granite dike cutting mylonites surrounding a mafic boudin within the migmatite gneiss. Scale is 10 cm.

Figure 20: Granite dike with xenoliths of mafic rocks. Note book is 21 cm high.

Figure 21: Foliated granite dike around mafic boudin. Relict foliation in the boudin is rotated towards the foliation of the granite.

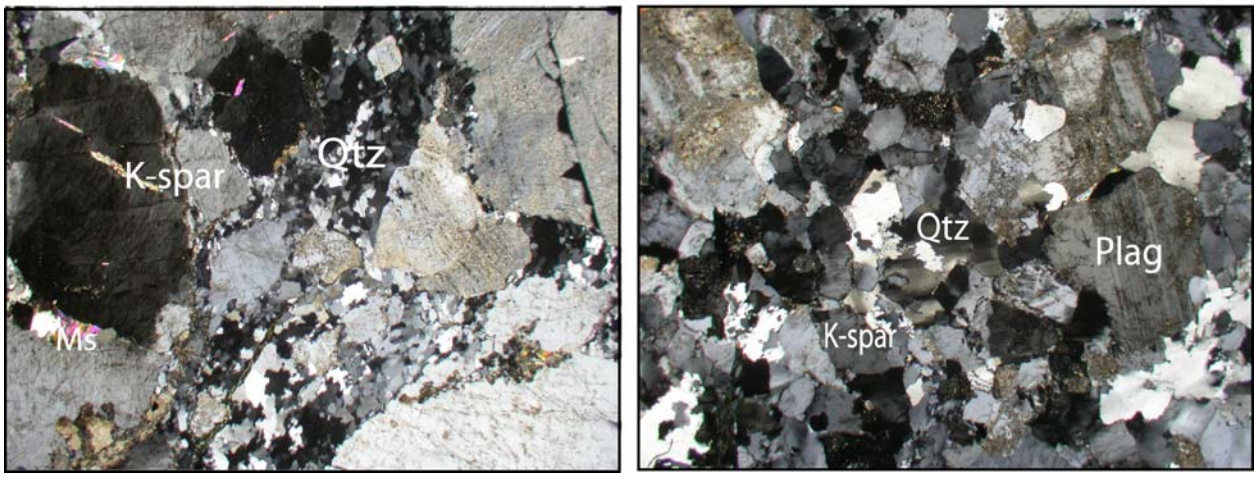

Figure 22: Photomicrograph taken with crossed nichols of unfoliated granite dike (sample LEA 06 - 35 equivalent to sample LEA 06-62) to the right. Foliated granite dike (sample LEA 06 - 66) to the left. Note that quartz is recrystallised, in LEA 06 - 35 by bulging recrystallisation and in LEA 06 - 66 by subgrain rotation recrystallisation. K- feldspar is highly strained in LEA 06 - 66, which is sampled from within the shear zone, and both K- feldspar and plagioclase are partly altered to clay minerals. Width of view is 5.5 mm in each photo. LEA 06-35 was collected at 70 °34. 481' N, 22 °13.181' W and LEA 06-66 at 70 °35.922' N, 22 °13.479' W.

Figure 23: Undeformed granite dike (left) with pegmatite margin (right). Pegmatites occur on both margins of the granite dike. Length of scale bar is 10 cm.

3.3 The Gubbedalen Shear Zone

3.3.1 Introduction

In the northern part of the footwall block, and bounding the upper plate Hurry Inlet Granite, there is a high strain zone, named the Gubbedalen Shear Zone (GSZ)(Augland et al., 2007). The GSZ is about 500 m thick, and consists mainly of pink mylonites with variable grain size, with local mafic lenses. There is a transition zone between the high grade terrane and the GSZ. The fabric in the GSZ ranges from ductile to semi-ductile, indicative of shearing at decreasing temperatures. The lower c. 400 m has only top-to-the-south contractional kinematic indicators. The upper c. 100 m show top-to-the-north extensional kinematic indicators. The uppermost c. 20 m is brecciated, and the contact to the upper plate is sharp, marked by a fault, here named the Gubbedalen Extensional Detachment Fault.

3.3.2 Transition zone

As described above, amphibolite grade top-to-the-south shear zones occur sporadically in the footwall block to the GSZ. But the frequency of these shear zones increases as one approaches the GSZ, and just south of the GSZ a c. 100 m thick zone with abundant top-to-the-south kinematic indicators occurs (Figure 4)(Figure 25)(Figure 26).

Foliation in this zone of the footwall block is mainly east-west striking, with a consistent north trending lineation (Figure 24), but with the relict migmatite foliation visible (Figure 25)(Figure 26).

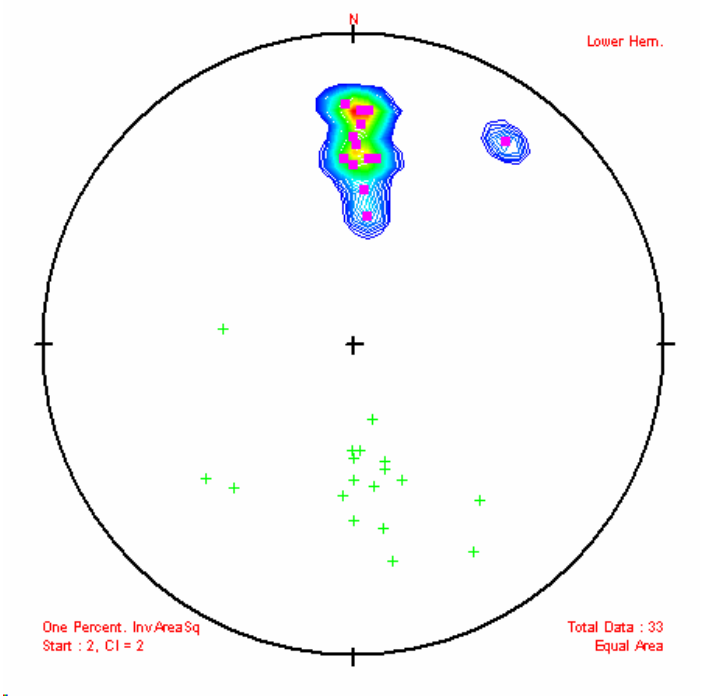

Figure 24: Foliation (green crosses) and lineation (contour lines) from the transition zone to the GSZ, and in the GSZ itself. Foliation strikes mainly east - west, and lineation trends northwards.

After this transition zone, where relict migmatite-foliation is observed discordant to the top-to-the-south shear-related foliation (Figure 25) (Figure 26)(Figure 28), the latter foliation overprints everything (Figure 29).

Typically foliated (grain shape fabric) and mylonitised granitic dikes occur in the shear planes in the transition zone, and the relict foliation of the surrounding migmatite is rotated towards the shear planes. The mineralogy of the granitic dikes here is the same as in the apparently undeformed granitic dikes in the high grade terrane (see above). The differences are a non-equigranular texture, with quartz having subgrains along the grain boundaries, indicative of bulging recrystallisation, and development of subgrains indicative of sub-grain rotation recrystallisation (Figure 22). Quartz recrystallised by subgrain rotation, indicates temperatures of at least 400˚ C, depending on strain rates, during deformation (Stipp, 2002; Stipp et al., 1999). In addition the ductile fabrics are in some cases overprinted by protomylonitc textures, indicating that shearing continued at lower temperatures. The granitic dikes do at some localities also have limonitic rims indicative of late stage movements with hydrothermal fluids present (Figure 26). At one locality in the transition zone to the GSZ a "megaporphyroclast" of granite is observed within highly sheared migmatite (Figure 27). The consistent observations of sheared granite dikes that have experienced medium grade

recrystallisation to lower temperature deformation, occurring in the shear plane, parallel to the foliation associated with top-to-the-south shear, indicates that the granite dikes intruded into high strain zones during shearing, i.e. the granite dikes are syn- tectonic. The deformed granite dikes give the same U-Pb age as the undeformed dikes in the high grade terrane, and further strengthen our observation that the deformed and the undeformed dikes are co-magmatic (see Chapter 4). This means that top-to-the-south shear was active under amphibolite facies conditions at c. 386 Ma or later (see below).

Figure 25: Sheared, mylonitic granite dike parallel with shear plane. The margin of the dike contains large porphyroclasts. The relict surrounding migmatite foliation is rotated into the shear plane. Shear sense is top-to-the-south. Pencil is c. 20 cm.

Figure 26: Sheared granite dike parallel to the shear plane. Granite is mylonitised, and has a red limonitic rim. Sample LEA 06-66, used for age dating, is from this rock. Lens cap is 5 cm across.

Figure 27: Megaporphyroclast of the "young" granite, showing top-to-the-south displacement. Hammer is c. 40 cm long.

Figure 28: Sheared migmatite just south of the GSZ. Shear sense is top-to-the-south. Lens cap is c. 5 cm long.

Figure 29: Northerly dipping foliation in the GSZ. North is to the left in the picture.

3.3.3 Top-to-the-south shear

In the map (Figure 3) the GSZ is marked as the zone between the thrust and the extensional fault, and in the cross-section (Figure 4) it is marked as a zone with top-to-the-south and top-to-the-north shear sense indicators, respectively. In the field the GSZ is a mylonite zone with a relatively uniform north-dipping foliation and a north trending lineation (Figure 24).

The mylonites in the GSZ probably consist of both granite dike and migmatite "protoliths". They are non-equigranular with foliation constituted by oriented micas and grain shape fabric of quartz, and alternation of mica and amphibole rich layers and quartzo-feldspathic layers. In the deformed and recrystallised granite dikes in the shear zone, quartz is recrystallized by subgrain rotation, and biotite is in many cases buckled as a response to deformation. K-feldspar porphyroclasts are highly strained, fractured and fragmented in some samples. In other samples K-feldspars have relatively poorly pronounced boundaries between the porphyroclasts and small recrystallised grains mantling them, indicating that recrystallisation occurred (Figure 30)(Figure 31). Quartz myrmekite-growth in K-feldspars is also observed (Figure 32). K-feldspar recrystallisation and myrmekite growth indicate deformation under amphibolite facies conditions (Simpson and Wintsch, 1989; Vidal et al., 1980). The feldspars are partly altered to clay minerals. Mica fish and quartz aggregate fish, S – C – C′- structures (Figure 30) (where S – structures are constituted by quartz grain shape fabric and cleavage in mica fish, C – bands by the general foliation and C′ - bands by fine grained mica occurring in the C′- planes), and winged porphyroclasts show top-to-the-south displacement. In some of the deformed granite dikes in the GSZ, growth of garnet and white mica is observed. In thin section the garnets appear subhedral, but fragmented. White mica appears as fish, and is frequently buckled. Metamorphism under amphibolite facies conditions is indicated from the growth of garnet. Lower temperature deformation led to the fracturing of the garnet porphyroblasts.

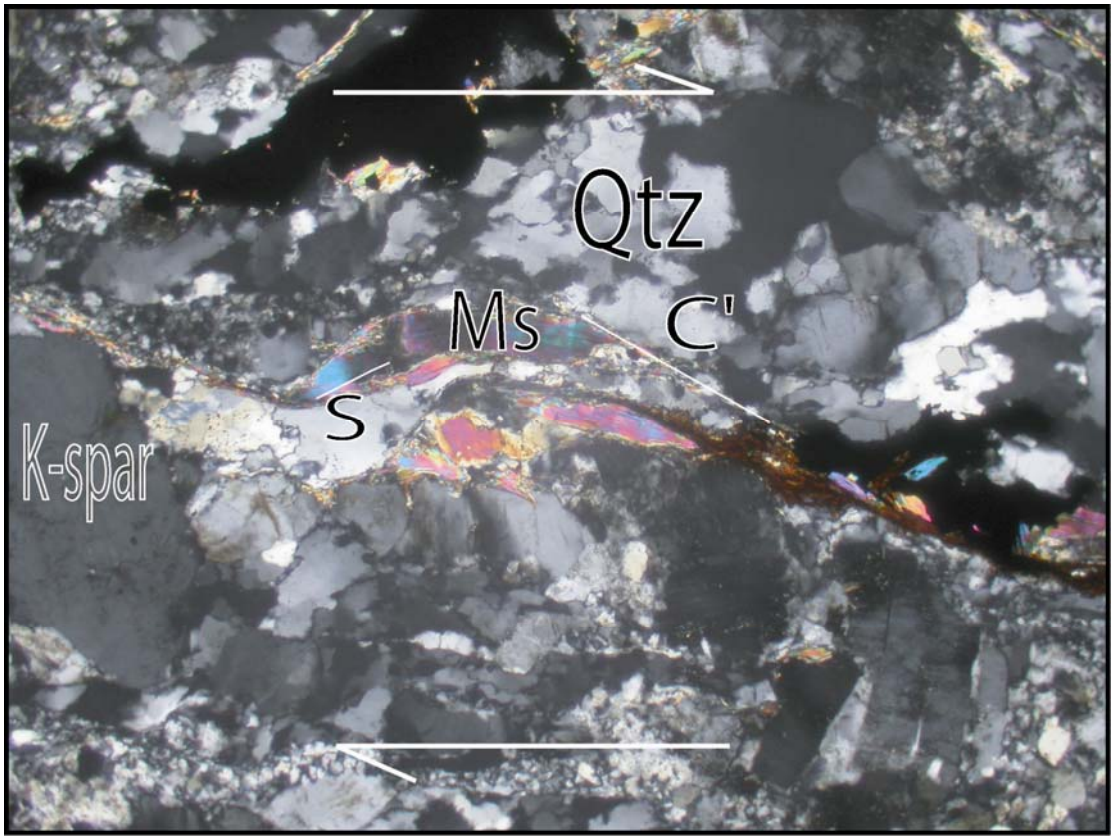

Figure 30: Photomicrograph taken with crossed nichols of deformed and recrystallised granite dike (sample LEA 06 - 67). C'- and S-bands is mostly defined by mica grains. Top-to-the-south shear sense. Width of view 2.8 mm. Sample collected at 70 °36.046'N, 22 °12.995' W.

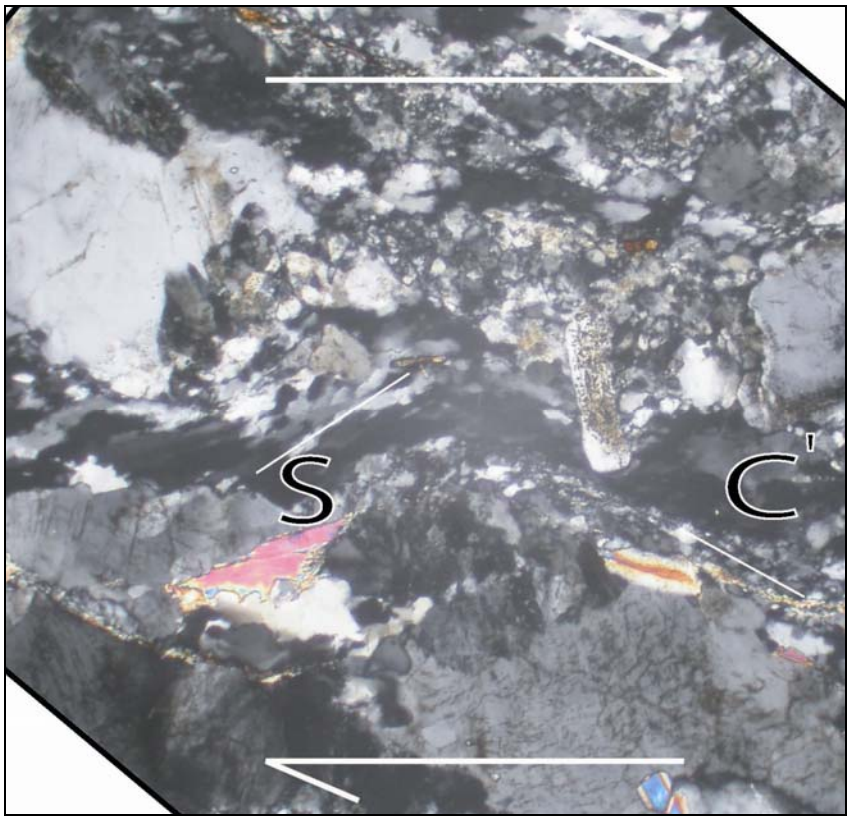

Figure 31: Photomicrograph taken with crossed nichols of deformed and recrystallised granite dike from the high strain zone (sample LEA 06-67). S-bands defined by quartz grain shape fabric and C'-bands defined by small mica grains. Shear sense is top-to-the-south. Note recrystallised quartz and K-feldspar. Width of wiev is 1.8 mm.

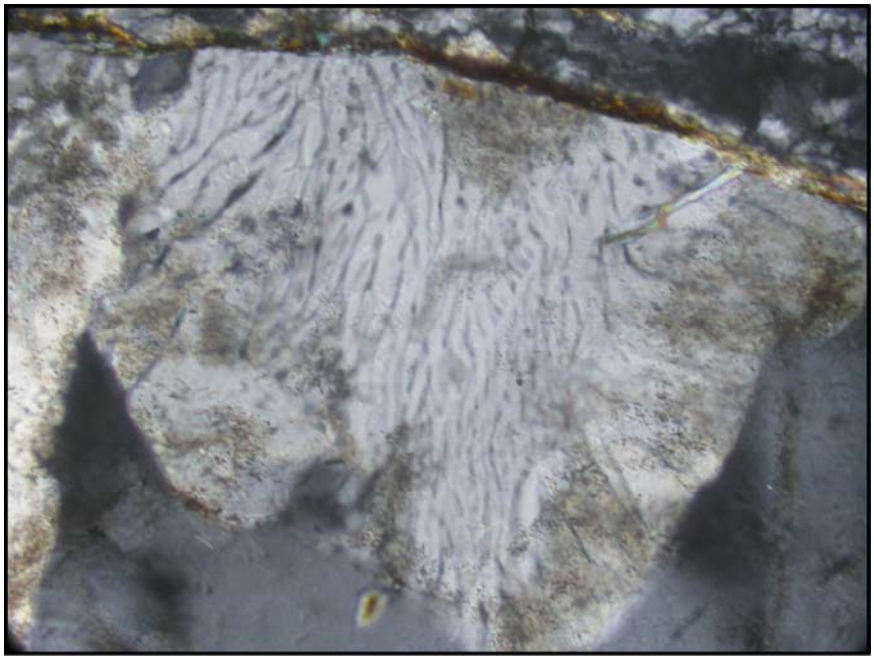

Figure 32: Photomicrograph taken with crossed nichols of deformed and recrystallised granite dike from the high strain zone (sample LEA 06-67), showing myrmekite growth in K-feldspar. Width of view is 0.5 mm.

There are also some mafic lenses of variable size and composition, from amphibolitic bodies of 10's of m to c. 1-2 m ultramafic serpentinite lenses, occurring in the high strain zone. The larger amphibolites have behaved more rigidly and taken up less strain than the surrounding felsic rocks. In one of the mafic lenses, the intrusive relationship between the mafic rock and the younger granite is preserved (Figure 33). The granite dikes are cutting the amphibolite relict ductile fabric, and contain inclusions of the mafic rock. The granite dikes have a grain shape fabric foliation that is parallel to the main GSZ-foliation (Figure 33).

Figure 33: Part of a mafic lens with relict foliation in the northern part of the top-to-the-south high strain zone. Granitic dikes are cutting, and containing xenoliths of, the mafic rock. Hammer is c. 40 cm long.

There is a pronounced north trending lineation through most of the GSZ (Figure 24) (Figure 34). The lineation is defined by amphibole mineral lineation/quartz aggregate lineation, and alignment of porphyroclasts on foliation surfaces (Figure 34).

The observation that top-to-the-south kinematic indicators range from amphibolite facies textures, down to more brittle mylonite structures indicates that the displacements on the shear zone took place at decreasing temperatures.

Figure 34: Lineation on a foliation surface in the GSZ. Quartz aggregate lineation and alignment of porphyroclasts make out the lineation. Metal top on pencil is ca 1 cm long.

3.3.4 Top-to-the-north shear

The upper (northernmost) part of the GSZ is a c. 100 m thick zone with shear sense indicators showing top-to-the-north displacement (Figure 3)(Figure 4). These structures are both semi-ductile and brittle (Figure 35)(Figure 36) (Figure 37)(Figure 38)(Figure 39)(Figure 40)(Figure 41)(Figure 42). Typical, semi-ductile structures occur in the lowermost part of this zone of extension and constitute small scale steep (c. 60º dip) or listric extensional shear zones with drag folding and flat-ramp structures (Figure 35)(Figure 36)(Figure 37). Further up in this zone of extension, i.e. the uppermost c.70 m, the rocks are typically more altered and fine grained, and consists of mostly alternating leucocratic, feldspar and quartz rich layers and melanocratic, mica rich layers (Figure 38)(Figure 40)(Figure 41)(Figure 42). Some layers are phyllonitic and in these, S-C bands, with S-C intersection lineation, are pronounced, showing

top-to-the-north displacement (Figure 38). Within some of the mica rich layers, micro folds of quartz also show top-to-the-north shear sense (Figure 39).

Figure 35: Top-to-the-north, ductile extensional structure in the upper part of the shear zone. Pencil ca 20 cm long.

Figure 36: Ductile extensional structures showing top-to-the-north sense of shear. Lens cap is 5 cm across.

Figure 37: Extensional structure in the GSZ. Listric small scale shear zone with drag folding and flat-ramp structures. Sense of shear is top-to-the-north. Pencil is c. 20 cm long.

Figure 38: Phylonite in the upper part of the GSZ, showing top-to-the-north displacement. Metal top of pencil is c. 1 cm.

Figure 39: Small scale assymetric folds of quartz veins in micaceous unit, showing top-to-the-north displacement. Metal top of pencil is c. 1 cm long.

Figure 40: Brittle contractional structures in the uppermost part of the GSZ showing top-to-the-north displacement. The overall structures in this part of the GSZ are extensional, but locally show contraction due to spacing problems. c. 50 cm long sledgehammer for scale.

Figure 41: Alternating leucocratic, feldspar and quartz rich, and melanocratic, micasceous layers in the uppermost part of the GSZ. Folds in the leucocratic layers show top-to-the-north displacement.

Figure 42: Brittle to semi- brittle extensional structures in the uppermost part of the GSZ. Drag folding into the fault planes is common. Sense of shear is top-to-the-north. Width of view c. 20 m.

In this uppermost part of the GSZ larger scale extensional, semi-brittle and brittle faults, some with drag folding are widespread, all showing top to the north displacement (Figure 42). Brittle contractional faults with top-to-the-north displacements also occur (Figure 40). The contractional structures are also related to the top-to-the-north extension, but are contractional due to spacing problems. All extensional structures overprint the contractional mylonite foliation observed in the lower part of the GSZ.

3.3.5 Breccia and the Gubbedalen Extensional Detachment Fault

A c. 20 m wide, highly brecciated, disrupted zone, with both chlorite and carbonate breccia (Figure 43) is located between the foliated GSZ and the upper plate Hurry Inlet Granite (see below). The GEDF separating the upper plate and the highly brecciated zone is sharp and is oriented east-west.

Figure 43: Breccia with carbonate in the fault zone between the lower and upper plate over the GBZ. 5 cm lens cap for scale.

3.4 Hanging wall block

3.4.1 Introduction

Three main lithologies were studied from the hanging wall block above the GDEF, the Hurry Inlet Granite, a batholith consisting of several compositionally and texturally different phases, the Hodal-Storefjord Monzodiorite, a large pluton, and a garnet-biotite gneiss, situated between the two intrusives. In addition lamprophyres and dolerites occurrs in the hanging wall block. There was no intention to study this area in detail, but the aim of the work here was to constrain the relationships between the major intrusives and the gneisses, and to sample the large granitoids for age dating.

3.4.2 Banded garnet-biotite gneiss

North of the Hurry Inlet Granite, a belt of partly migmatised garnet-biotite gneiss with relict metasedimentary inclusions, occurs (Figure 3)(Figure 4). The contacts to the granitoid rocks are intrusive (Figure 44). The Hurry Inlet Granite has satellite dikes intruding the gneiss, and in these, assimilated inclusions of the gneiss are widespread (Figure 44). However, as noted by Coe and Cheeney (1972), brittle faults are abundant along the contact between the Hurry Inlet Granite and the gneiss.

Figure 44: Hurry Inlet Granite with inclusions of the garnet-biotite gneiss to the north of it. The inclusions are baked and assimilated in to the granite.

The garnet-biotite gneiss is a medium to coarse grained rock with c. 50-60 % plagioclase, c. 20 % quartz, from c. 15 to c. 20 % biotite and up to c. 15 % garnet. Muscovite and accessory zircon, apatite and opaques are observed. Foliation is only weakly defined by sub-parallell biotite in thin section. Some biotites are slightly buckled and quartz show undulose extinction. Plagioclase is partly altered to clay minerals. In some samples garnet appear to be consumed. The metamorphic "protolith" of the garnet-biotite gneiss can be observed in large xenoliths within the gneiss (Figure 45)(Figure 46). The protolith occurs as a layered rock with metapsammite, micaschist and calc-silicates interlayered. Within the same gneiss complex the garnet, biotite bearing rock also occurs as an igneous rock, where the garnets either are xenocrysts or grown from a melt, as shown from migmatites in south-western Renland (Leslie and Nutman, 2003). The (almost) complete melting of the rock could be due to the heat flow from the surrounding granitoid intrusives. The igneous variant of the garnet-biotite gneiss is a garnet bearing diorite.

Figure 45: Garnet, biotite gneiss with relict metapsammite.

Figure 46: Garnet, biotite gneiss with relict metapsammite.

Muscovite bearing, granitic pegmatites are cutting both the diorite and the gneiss.

The sedimentary origin of this high grade gneiss complex, with its metasedimentary inclusions and high alumina content, points to a possible correlation with the Mesoproterozoic

Krummedal sequence that is suggested to occur further to the north on Liverpool Land (Higgins, 1988).

The contact to the Hodal-Storefjord Monzodiorite to the north of the garnet-biotite gneiss is also an intrusive contact, evident from the assimilated inclusions of the garnet-biotite gneiss in the monzodiorite. Also, the garnet-biotite diorite was observed only in contact with, or close to, the monzodiorite. Along the contact, the intrusion is more quartz and biotite rich, and contains several cm large feldspar crystals (Figure 47). Around the contact there are also abundant feldspar and quartz rich pegmatites (Figure 48).

Figure 47: Large euhedral feldspar crystals in the monzodiorite near the contact to the the garnet, biotite gneiss.

Figure 48: K-feldspar, and quartz pegmatite cutting monzodiorite.

Both the garnet-biotite gneiss, the Hurry Inlet Granite and the Hodal-Storefjord Monzodiorite to the north of the gneiss (see below), are cut by lamprophyre dikes, probably related to the c. 420 Ma lamprophyres observed further to the north (Andresen et al., 1995) (Figure 49). The lamprophyre dikes contain up to 5 cm large phenocrysts of phlogopite and zoned amphibole in a fine grained matrix. The gneiss is also cut by dolerite dikes (see below).

Figure 49: Lamprophyre with large phenocrystals of phlogopite and amphibole cutting monzodiorite. 5 cm lens cover for scale.

3.4.3 Hurry Inlet Granite (batholith)

In the lowermost part of the Hurry Inlet Granite the rocks are cataclastic and altered. But already less than 100 m from the contact, the rocks appear to be unaffected by the displacements along the GEDF. The rock is, however, cut by late brittle faults and fractures. The most prominent of the granitoid phases in the southern part of the batholith, is a pinkish red, medium grained, equigranular rock. It contains c. 45 % K- feldspar, c. 30 % quartz, c. 15 % plagioclase, around 10 % mafic phases, i. e. a true granite (Figure 50)(Figure 51). The mafic mineral in the freshest samples, is mostly amphibole, with minor amounts of clinopyroxene. Close to the GEDF, the granodiorite is hydrothermally altered to a certain extent, and the amphibole is largely chloritised, with only tiny relic amphibole grains preserved in some of the chlorite grains. In the most altered rock, plagioclase is completely altered to clay minerals, but with relic albite twins preserved. The presumably minor phases of Hurry Inlet Granite found in the south, generally has the same mineralogy, but with varying relative amounts of the major phases, still with K-feldspar as the dominating mineral. There are also grain size variations between the different phases, one of them appearing as fine grained granite, with maximum grain size of c. 1 mm, and another coarse grained (Figure 50) (Figure 51). From the northern part of Hurry Inlet Granite, one sample was studied in thin section (Figure 51). It is medium grained, and contains c.45 % K-feldspar, both with and without microcline cross hatch twins, c. 35 % plagioclase with albite twins and c. 20 % amphibole. Minor amounts of clinopyroxene, quartz, chlorite, titanite, opaqes, calcite and zircon were also observed. This rock is thus a monzonite, rather than granite.

The texture is cut by mineralised veins, clearly fragmenting grains in the rock. Feldspars are partly altered to clay minerals, and amphibole sometimes appears grumpsy, with rims clearly altered to chlorite. The alteration and fragmenting seen in thin section, is in agreement with the large number of brittle faults cutting the Hurry Inlet Granite observed in the field. The granite is seen to intrude the high grade metasediments described above.

Two phases of this batholith were dated, giving ages of c. 445 Ma and c. 438 Ma, respectively (see Chapter 4).

Figure 50: The Hurry Inlet Granite batholith. As shown in the picture several different varieties occur within less than a m^3. The pinkish red, medium grained, most common variety to the left, two more fine grained, grey varieties in the right centre, and a bright coarse grained phase to the right. Scale 5 cm diameter.

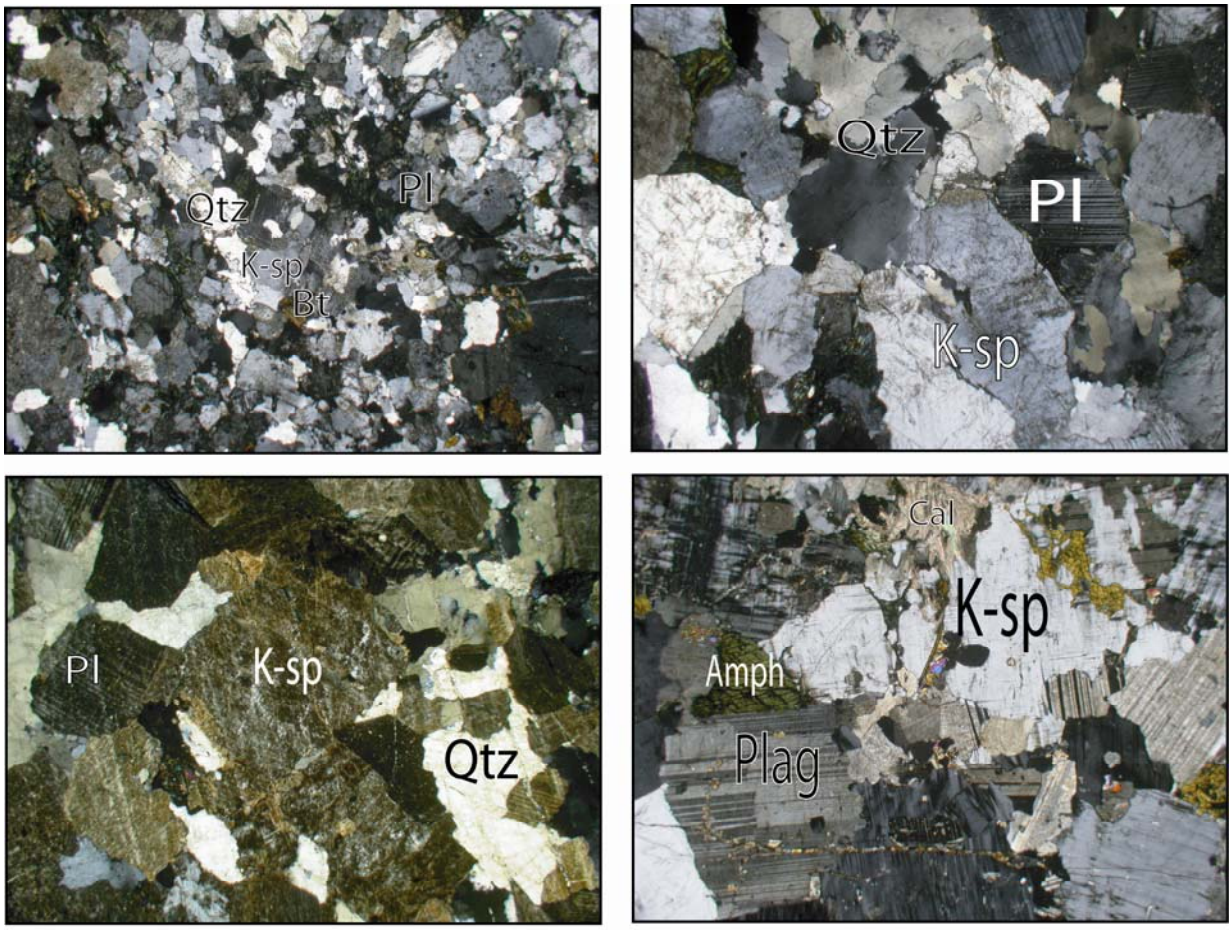

Figure 51: Photomicrograph of four different samples of the Hurry Inlet Granite batholith, all taken with crossed nichols. Upper left: fine grained granite (sample LEA 06-71C), upper right: medium grained granite (sample LEA 06-71A), lower left: medium grained granite (sample LEA 06-71D), all from the southernmost part of the batholith, collected within c 200 m of each other at c. 70 °36.307' N, 22 °16.502' W. Medium grained monzonite (sample LEA 06-89) in the lower right, from the northernmost part of the batholith (70 °51.558' N, 22 °21.551' W). Width of view in all photos are 5.5 mm.

3.4.4 Hodal-Storefjord Monzodiorite

To the north of the garnet-biotite gneiss, there is a large pluton dated to c. 424 Ma (see Chapter 4), covering more than 50 km^2 (Figure 3). The sample examined in thin section in this study, is a monzonite to a monzodiorite consisting of more than 50 % plagioclase, c. 15 % chlorite, c. 10 % K-feldspar, c. 10 % orthopyroxene, c. 5 % quartz, c. 5 % amphibole, c. 3 % clinopyroxene and c. 2 % opaqes (Figure 52). This rock was named the Hodal-Storefjord quartz monzodiorite by Coe and Cheeney (1972), on the base of two different samples, with quartz content of 5 and 15 %. The contact to the garnet biotite gneiss is intrusive and the rock is cut by both lamprophyres and dolerites.

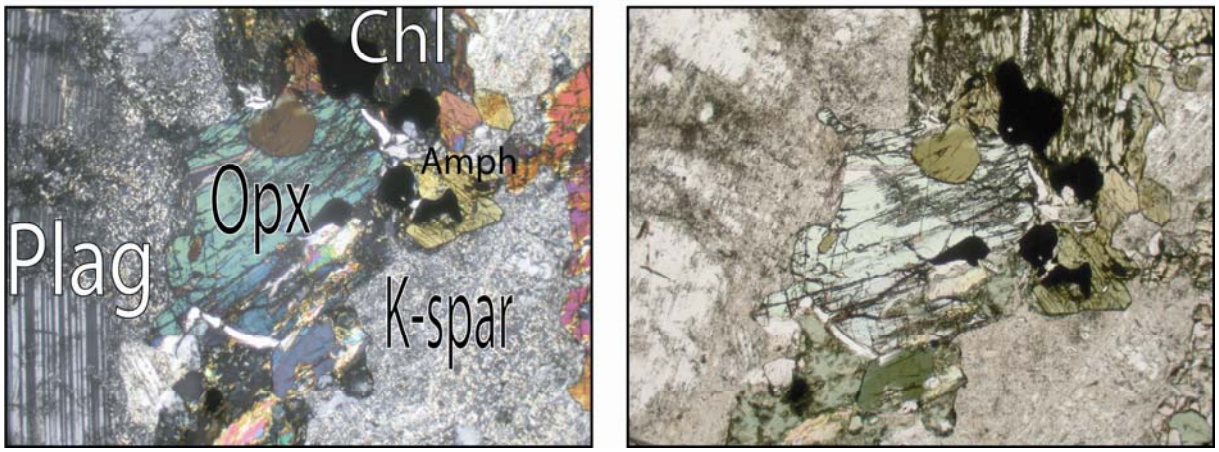

Figure 52: Photomicrograph of the Hodal-Storefjord Monzodiorite (sample LEA 06-79) with (left) and without (right) crossed nichols. Width of view is 2.8 mm. Sample collected at 70° 52.483' N, 22° 19.451' W.

The lamprophyres are porphyritic, with phenocrysts of dark mica (phlogopite) and amphibole (Figure 49). Their contacts to the monzodiorite are sharp, with no evidence of deformation along the contacts. Xenoliths of the host rock are abundant in the lamprophyres. Similar occurrences of lamprophyres intruding granitoids was also reported from Canning Land, just to the north of Liverpool Land (Caby, 1972).

The dolerites intruding the monzodiorite (and the other rocks in the area), are fine grained, with small plagioclase phenocrysts. The monzodiorite is brecciated and rusty brown along the dike's margin, clearly showing that the pluton was behaving brittle when the dolerites intruded. These dikes are presumably Tertiary, related to the plateau lavas now exposed south of Scoresby Sund.

4 U/Pb-chronology; results and interpretation of data

4.1 Introduction

Eight samples collected during the summers of 2005 and 2006 were dated by the Isotope Dilution-Thermal Ionization Mass Spectrometry (ID-TIMS) method. Positions of the different samples are given in Table 2. Sample preparation and analytical work was carried out in the laboratory facilities of the Institute of Geosciences at the University of Oslo from October 2006 to March 2007. Methodology and results are presented in the following.

4.2 Analytical Procedure

All samples, weighing c. 0.5-1 kg, were ultrasonically cleaned, crushed with a jaw-crusher and milled down to < 0.3-0.5 mm particles in a Retsch crusher. Minerals were then separated out using a Wilfley table, Franz magnetic separators and heavy liquid ($CH_2 I_2$, DJM; d= 3.2 g/cm^3) flotation.

Mineral grains selected for analysis were picked in alcohol under a binocular microscope, discriminated on the basis of morphology, transparency, colour and internal textures (i. e. presence of cores, inclusions and degrees of metamictization and alteration)(Corfu et al., 2003). Air-abrasion was then carried out using the method described by Krogh (1982), to remove the marginal areas of the mineral grains most likely to have experienced lead loss. Further discrimination of grains and division into fractions for analysis was sometimes done after abrasion. Most samples were photographed using a digital camera mounted to a binocular microscope. The phases used for age dating in this study include zircon, monazite and rutile. Mineral samples were washed in dilute HNO_3, H_2O and acetone using an ultrasonic bath, to remove any contamination. Each sample was then weighed on a microscale, spiked with a mixed ^{202}Pb - ^{205}Pb – ^{235}U tracer. The double Pb-tracer is used to determine source fractionation during measurements, which when incorporated in the error calculation, gives better precision estimates. The zircon and rutile were dissolved in HF and a drop of HNO_3 in Teflon bombs at c. 190° C for 5 days. Monazite was dissolved in 6N HCl and a drop of HNO_3 in Teflon Savillexes on a hotplate at c. 125° C for 5 days. Zircon samples weighing more than 0.005 mg, two of the monazite samples and the rutile samples were chemically separated using micro-columns and anion-exchange resin (AG1-X8), following the method originally

outlined by (Krogh, 1973). The solutions of zircon, monazites and rutile were transferred to the columns, and treated with HCl (zircon and monazite) and a mixture of HCl and HBr (rutile) to retain U and Pb in the resin, and to wash out other cations. U and Pb were then extracted using HCl and H_2O. After adding a drop of H_3PO_4, the U/Pb-solutions were dried down and loaded on degassed single Re filaments with silica gel.

The samples were measured on a Finnigan MAT 262 mass spectrometer, using either Faraday cups in static mode or, for low-intensity samples, a Secondary Electron Multiplier (SEM) in peak jumping mode. $^{207}Pb/^{204}Pb$ ratios were measured on SEM for all samples. SEM data were corrected for non-linearity based on measurements of the standard NBS 982-Pb + U500. Measurements of the standard are also used to monitor the reproducibility of the mass spectrometer. The standard was always measured at the start of the day, before measuring the samples.

Measurements were corrected for a 2 pg Pb and 0.1 pg U blank, with blank compositions: $^{206}Pb/^{204}Pb = 18.3$, $^{207}Pb/^{206}Pb = 0.85$ and $^{207}Pb/^{204}Pb = 15.555$. Common Pb corrections were employed using the Pb-evolution model of Stacey and Kramers (1975), using the $^{207}Pb/^{206}Pb$ age as the assumed crystallization age. U source fractionation was estimated to be 0.12 % / a.m.u. Pb source fractionation was corrected for using the measured $^{205}Pb/^{202}Pb$ tracer ratio, normalized to the certified value of 0.44050. A standard fractionation error of 0.06 % /a.m.u. is incorporated in the calculations if the $^{205}Pb/^{202}Pb$ ratio is determined very precisely and the fractionation corrections become unrealistically precise. If $^{205}Pb/^{202}Pb$ is not determined, or the measured $^{205}Pb/^{202}Pb$ are far of from 0.44050, Pb fractionation is set at 0.1 %/a.m.u. Pb fractionation values between 0.02-0.16 % /a.m.u. are generated by this procedure.

The analytical errors and corrections were then incorporated and propagated using the ROMAGE 6.3 program, originally developed by T. E. Krogh. Graphic presentations and age-calculations were performed using the ISOPLOT program of Ludwig (2003).

4.3 Results

4.3.1 Hurry Inlet Granite (batholith)

Sample descriptions

As described in the previous chapter the Hurry Inlet Granite batholith consists of several phases, and in this study three samples were dated, PIM 05-Li02, collected in the summer of 2005 by Per Inge Myhre and Arild Andresen, LEA 06-71A and LEA 06-89, both collected by the author in the summer of 2006. Hand specimens and photomicrographs of the two latter samples are shown in (Figure 51)(Figure 53). LEA 06-89 was collected from the northernmost part of the batholith, and the two other samples from the southern part. Positions of the different samples are given in table (Table 2). LEA 06-71A and PIM 05-Li02 are from two granitic phases, and LEA 06-89 is from a monzonitic phase of the batholith. See Chapter 3 for sample descriptions and field relations.

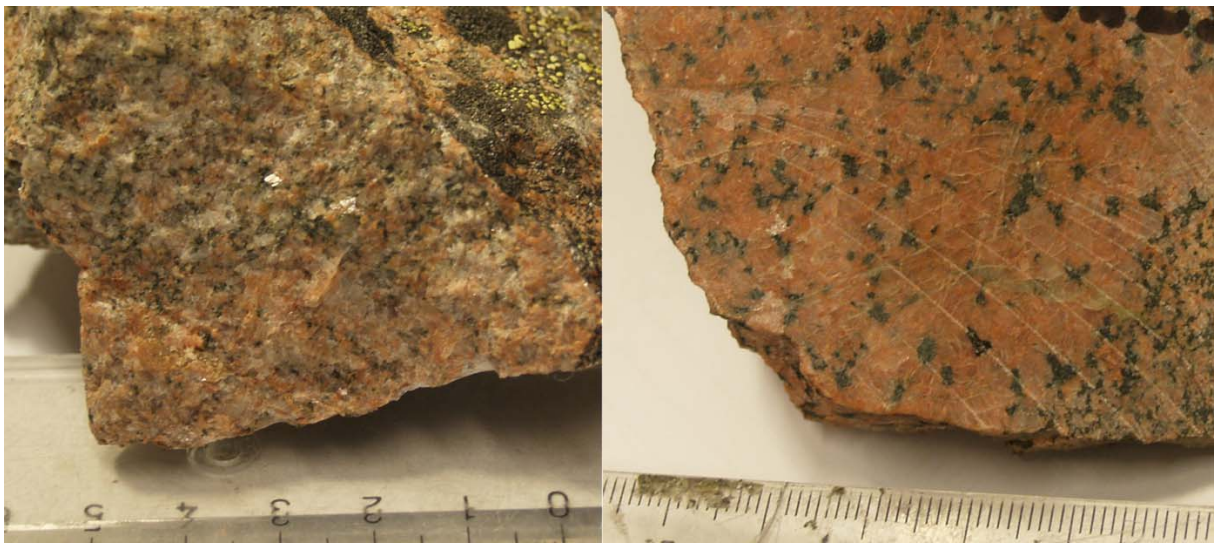

Figure 53: Hand specimen of sample two phases of the Hurry Inlet Granite batholith. Granite (sample LEA 06-71A) to the left and monzonite (sample LEA 06-89) to the right. Centimeter ruler for scale.

Sample	Description	Locality	Lattitude	Longitude	Use
LEA 06-59	Retrograded eclogite	9.5	70°34.939' N	22°13.777' W	Age dating
LEA 06-62	"Young" Granite dike	11.5	70°35.700' N	22°17.952' W	Age dating
LEA 06-66	"Young" Granite dike from GSZ	12.2	70°35.779' N	22°13.479' W	Age dating
LEA 06-18	Pegmatite in boudin neck	3.1	70°35.030' N	22°13.838' W	Age dating
PIM 05-Li02	Hurry Inlet Granite		70°36.460' N	22°16.177' W	Age dating
LEA 06-71A	Hurry Inlet Granite	13.1	70°36.307' N	22°16.502' W	Age dating
LEA 06-89	Hurry Inlet Granite	20.5	70°51.809' N	22°20.176' W	Age dating
LEA 06-101	Hodal-Storfjord Monzodiorite	23.1	70°52.949' N	22°20.117' W	Age dating
LEA 06-61	Eclogite	10.4	70°34.633' N	22°15.223' W	EMP*
	*EMP: Electron Micro Probe				

Table 2: GPS-positions for the samples used for age-dating and the eclogite used for electron microprobe analyses.

Analytical results

A total of four zircon fractions of 1-6 grains were analysed from PIM 05-Li2; eight zircon fractions of 2-9 grains were analysed from LEA 06-71A; two fractions of 5 and 6 grains from LEA 06-89. Results are given in (Figure 54)(Figure 55) and (Table 3).

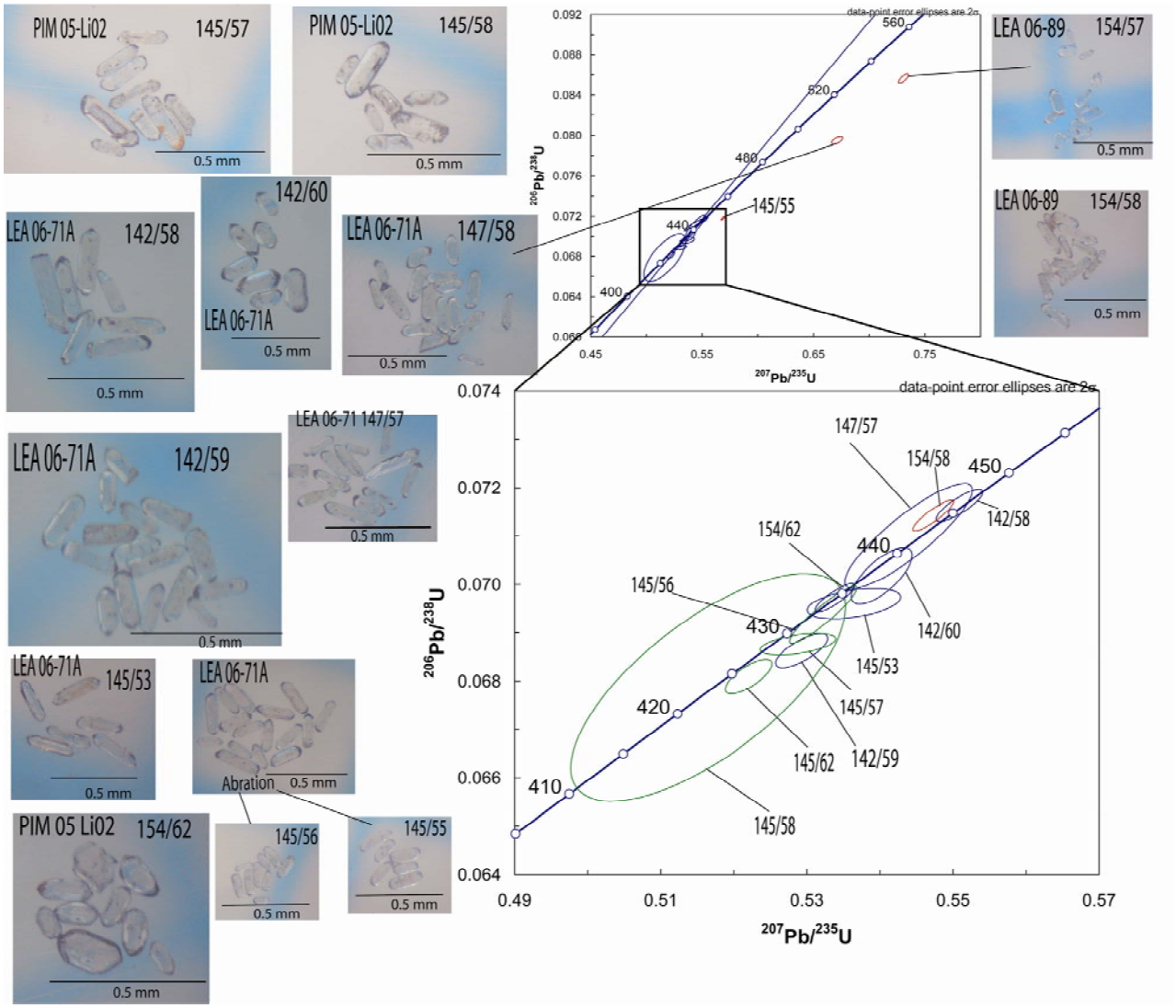

Figure 54: Concordia plot for the samples from Hurry Inlet Granite, with binocular microscope photographs of the different zircon fractions. All photos and data point error ellipses are numbered according to Table 3. Blue data point error ellipses represent LEA 06-71A, green ellipses represent PIM 05-Li02 and red ellipses represent LEA 06-89. The red ellipses in the upper plot are both from LEA 06-89 and LEA 06-71A and are not included in any calculations. Decay constants errors are ignored.

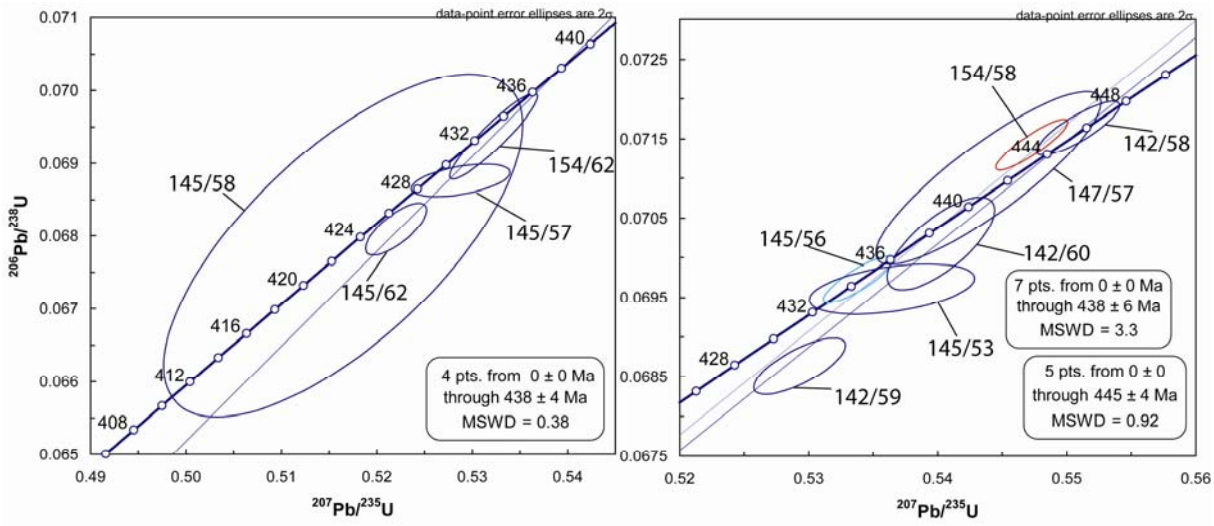

Figure 55: The concordia plot of Figure 49 split in two, showing that there are two distinct age groups of zircons. An older phase of the batholith crystallised at c. 445 Ma, and a younger phase crystallised at c. 438 Ma. The left-hand plot shows the four fractions of PIM 05-Li02 and the right-hand plot shows LEA 06-71A. The light blue ellipse is not included in calculation of the older age. The red data point error ellipse represents analysis 154/58 of sample LEA 06-89. This analysis is not included in the calculation of the older age. Decay constant errors are ignored.

Zircons

The zircon population of LEA 06-71A (Figure 54) is relatively homogenous, mostly colourless, with some weakly red and yellow metamict grains. Prismatic grains dominated by (100) and (101) forms are most common, with elongation ratios ranging from 2 to 6. The dominance of (101) pyramidal and 100 prismatic morphologies of the zircons, point to a classification of this granite as a monzogranite-alkaline granite in the calc-alkaline series following Pupin (1980). The grains are generally rich in inclusions and seldom contain visible cores. All fractions, except for the most discordant (147/58), have low common lead (c. 0.0-1 ppm), and U content varying from c. 130 to c. 1700 ppm (Table 3). The fractions used for age calculation are either concordant or up to 2 % discordant (Table 3). The zircons in PIM 05-Li02, are, on the other hand, heterogeneous, with colourless to reddish to brown grains, some are metamict and some contain cores. Elongation ratio is ranging from 2-6. The analysed grains had prismatic morphologies dominated by (100) and (101), were clear, colourless to weakly red and containing few inclusions, and no visible cores (Figure 54). They have low common Pb (c.0.0-2 ppm), and relatively high U-content (c. 380-1000 ppm) and are 0.8 % to 3.4 % discordant (Table 3). Sample LEA 06-89 contains a heterogeneous zircon population, differing in colour and morphologies. Many grains are metamict and rounded, cores are relatively common. Two fractions were analysed, one with stubby prisms and large fragments, with length to width ratio of 2 to 4, and one with long thin grains with elongation ratios of up

to 6 (Figure 54). Most of the analysed grains contained inclusions. Both fractions had low common lead, and U-contents of c. 2800 ppm (154/58) and 415 ppm (145/57). The fraction with the stubby prisms (154/57) yielded a highly discordant age. The other fraction (154/58) yielded a reverse discordance of 2.2 %. All fractions from the Hurry Inlet Granite batholith have moderate Th/U-ratios (0.29-0.53).

Interpretation

Of the fourteen fractions analysed, 4 points are concordant and 10 are discordant, 7 of these are less than 3.4 % discordant. The data point error ellipses of LEA 06-71A are coloured blue, LEA 06-89 are coloured red and PIM 05 Li02 are coloured green (Figure 55). From (Figure 54) it is clear that there is an age spread in the zircons of the Hurry Inlet Granite. Thus the analyses have been plotted separate for different samples (Figure 55). The two discordia ages calculated are thought to represent the crystallisation age of two phases of the batholith. A discordia age for LEA 06-71A based on all analyses plotted in (Figure 55) has a poor fit (MSWD=3.3), so analysis 145/56 and 154/58 (LEA 06-89) are excluded. A discordia age calculated on the base of the rest of the analyses (five points) thus gives the age of the older phase, 445 ± 4 Ma (2σ, MSWD=0.92). A younger phase of the batholith, represented by all the analyses of PIM 05-Li02 (four points discordia age), crystallised at 438 ± 4 Ma (2σ, MSWD=0.38). The fraction yielding the young concordant analysis (145/56) of LEA 06-71A, might have experienced differential U- and Pb-loss, possibly as a response to the intrusion of the younger phase. Alternatively, some of the grains in the fraction might have been reset during intrusion of the later phase, or the younger age might be due to some analytical error. Since only two zircon fractions of LEA 06-89 were analysed, and one of these is highly discordant and the other slightly reversely discordant (154/58), it is not completely clear which group, if any, this belongs to. If the reversely discordant analysis is the result of open system behaviour with U-loss (or Pb-gain), this could mean that the data point has moved along a U-loss line from 438 Ma. However, the $^{206}Pb/^{238}U$-age and the $^{207}Pb/^{235}U$-age (444.7 ± 1.6 and 443.2 ± 1.5 Ma, respectively) are both close to the calculated older age, so it is most likely that also this sample belongs to an older phase of the batholith. As the U-content of this sample is high (c.2800 ppm), metamict zones could have been prone to U-loss, possibly during washing in HNO_3. The reverse discordance could also be due to some undetected analytical error.

The large error of analysis 145/58, is due to low intensity during measurement (little material) and, hence, poor precision (Figure 55)(Table 3). The discordant analyses lying in the upper

right of the concordia diagram are all thought to contain inherited isotope signatures (Figure 54).

Fraction Analysed	No of grains	Weight	Pbt]	U	Th/U	Pbc	Pbcom	206/204	207/235	2 sigma	206/238	2 sigma	Rho	207/206	2 sigma	206/238	2 sigma	207/235	2 sigma	207/206	2 sigma	Disc.
HURRY INLET GRANITE		[ug]	[ppm]	[ppm]		[ppm]	[pg]			[abs]		[abs]			[abs]		[abs]		[abs]		[abs]	[%]
LEA 06-71A 142/58	ZR 3	5	56	721	0.53	1.08	7.4	2200	0.55088	0.00262	0.07163	0.00028	0.84	0.05578	0.00014	446.0	1.7	445.6	1.7	443.5	5.7	-0.6
LEA 06-71A 142/59	ZR 2	5	16	239	0.29	0.30	3.5	1472	0.52929	0.00291	0.06863	0.00029	0.74	0.05593	0.00021	427.9	1.7	431.3	1.9	449.7	8.1	5.0
LEA 06 71A 142/60	ZR 4	7	21	292	0.44	0.34	4.4	2070	0.54024	0.00340	0.07018	0.00048	0.73	0.05583	0.00027	437.2	2.9	438.6	2.2	445.7	10.8	2.0
LEA 06 71A 145/53	ZR 1	1	12	191	NO VALUE	0.00	1.1	764	0.53645	0.00523	0.06960	0.00026	0.43	0.05590	0.00049	433.8	1.6	436.1	3.5	448.3	19.5	3.3
LEA 06 71A 145/55	ZR 6	12	27	377	0.42	0.06	2.7	7452	0.56888	0.00145	0.07182	0.00016	0.90	0.05745	0.00006	447.1	1.0	457.3	0.9	508.7	2.5	12.5
LEA 06 71A 145/56	ZR 9	6	40	549	0.46	0.16	3.0	4848	0.53384	0.00221	0.06973	0.00024	0.85	0.05553	0.00012	434.5	1.4	434.4	1.5	433.6	4.8	-0.2
LEA 06 71A 147/57	ZR 4	3	9	134	NO VALUE	0.00	1.2	1530	0.54392	0.00713	0.07100	0.00089	0.87	0.05556	0.00036	442.2	5.3	441.0	4.7	434.8	14.4	-1.8
LEA 06 71 147/58	ZR 6	1	149	1701	0.52	10.58	12.6	691	0.67125	0.00408	0.07951	0.00029	0.62	0.06123	0.00029	493.2	1.7	521.5	2.5	647.3	10.2	24.7
LEA 06 89 154/57	ZR 4	3	34	415	NO VALUE	0.06	2.2	3076	0.73082	0.00359	0.08564	0.00037	0.76	0.06189	0.00020	529.7	2.2	557.0	2.1	670.4	7.0	21.9
LEA 06-89 154/58	ZR 4	1	205	2824	0.39	0.00	1.9	6689	0.54729	0.00228	0.07142	0.00026	0.89	0.05558	0.00010	444.7	1.6	443.2	1.5	435.4	4.1	-2.2
PIM 05-LI02 145/57	ZR 1	1	30	432	0.37	0.25	2.3	842	0.52878	0.00423	0.06876	0.00018	0.49	0.05577	0.00039	428.7	1.1	431.0	2.8	443.3	15.6	3.4
PIM 05 LI02 145/58	ZR 1	1	67	1025	NO VALUE	2.03	4.0	1096	0.51648	0.01538	0.06787	0.00192	0.70	0.05519	0.00124	423.3	11.6	422.8	10.2	420.0	49.3	-0.8
PIM 05 LI02 145/62	ZR 1	1	73	1034	0.50	0.00	1.1	4124	0.52203	0.00261	0.06809	0.00029	0.74	0.05560	0.00019	424.7	1.8	426.5	1.7	436.4	7.6	2.8
PIM 05-LI02 154/62	ZR 5	11	27	379	0.37	0.37	6.1	2978	0.53224	0.00376	0.06937	0.00048	0.93	0.05564	0.00015	432.4	2.9	433.3	2.5	438.1	5.9	1.4
HODAL STORFJORD MNZ																						
LEA 06 101 142/52	ZR 8	9	14	176	0.82	0.32	4.9	1384	0.51634	0.00262	0.06747	0.00025	0.73	0.05550	0.00019	420.9	1.5	422.7	1.8	432.5	7.7	2.8
LEA 06-101 142/56	ZR 3	1	125	1651	0.75	0.60	2.6	2703	0.51791	0.00375	0.06780	0.00058	0.71	0.05540	0.00034	422.9	3.5	423.8	2.5	428.6	13.6	1.4
LEA 06-101 142/57	ZR 1	1	5	61	0.87	0.38	2.4	127	0.51357	0.02641	0.06773	0.00041	0.49	0.05499	0.00268	422.5	2.5	420.8	17.6	411.9	100.0	-2.7
LEA 06 101 145/59	ZR 1	10	22	225	0.82	4.67	48.7	215	0.51688	0.00877	0.06822	0.00021	0.24	0.05495	0.00091	425.4	1.3	423.1	5.9	410.3	36.4	-3.8
LEA 06 101 145/60	ZR 1	3	6	68	0.89	0.45	3.4	277	0.51188	0.00912	0.06777	0.00027	0.42	0.05478	0.00091	422.7	1.7	419.7	6.1	403.2	36.6	-5.0
LEA 06 101 145/61	ZR 1	2	6	89	NO VALUE	0.00	1.0	784	0.53892	0.02908	0.07162	0.00314	0.54	0.05457	0.00261	445.9	18.9	437.7	19.0	394.8	100.0	-13.4
LEA 06 101 147/59	ZR 2	5	8	22	NO VALUE	9.89	51.4	27	0.47133	0.17095	0.06634	0.00265	0.07	0.05153	0.01865	414.1	16.3	392.1	111.9	264.4	100.0	-58.5
LEA 06 101 147/60	ZR 9	6	14	179	0.74	0.20	3.2	1429	0.51703	0.00260	0.06782	0.00019	0.67	0.05529	0.00021	423.0	1.1	423.2	1.7	424.0	8.4	0.2
ECLOGITE																						
LEA 06-59 147/55	ZR 13	2	62	696	0.53	0.00	0.9	8343	0.80750	0.00529	0.08408	0.00072	0.70	0.06965	0.00043	520.5	4.3	601.1	3.0	918.1	12.7	45.1
LEA 06-59 147/56	ZR 8	29	22	274	0.83	0.15	6.2	5827	0.62308	0.00190	0.07279	0.00018	0.89	0.06208	0.00009	453.0	1.1	491.8	1.2	676.8	3.0	34.2

LEA 06 59 154/59	ZR 15	13	5	70	0.35	0.09	3.2	1164	0.50486	0.00469	0.06477	0.00032	0.59	0.05653	0.00042	404.6	1.9	415.0	3.2	473.2	16.5	14.9
LEA 06 59 154/60	ZR 14	18	24	283	0.38	0.04	2.8	9370	0.77194	0.00399	0.08224	0.00039	0.94	0.06808	0.00012	509.5	2.3	580.9	2.3	870.9	3.7	43.1
LEA 06 59 159/54	ZR 8	25	21	298	0.33	0.00	2.1	15551	0.58947	0.00146	0.07070	0.00016	0.92	0.06047	0.00006	440.4	1.0	470.5	0.9	620.5	2.1	30.0
LEA 06 59 154/61	RT	410	1	23	0.02	0.08	34.0	1088	0.45903	0.02264	0.06083	0.00296	0.89	0.05473	0.00128	380.7	18.0	383.6	15.6	401.0	51.4	5.2
LEA 06 59 159/53	RT	12	1	16	0.01	0.02	2.3	333	0.43713	0.00947	0.05869	0.00062	0.53	0.05402	0.00099	367.7	3.8	368.2	6.7	371.9	40.8	1.2
PEGMATITE																						
LEA 06-18 147/61	ZR 1	1	734	12743	0.12	0.24	2.3	21737	0.46012	0.00246	0.06136	0.00031	0.96	0.05439	0.00008	383.9	1.9	384.3	1.7	387.1	3.4	0.9
LEA 06-18 147/62	ZR 1	1	953	16633	0.14	11.69	13.7	4588	0.45013	0.00171	0.06000	0.00019	0.91	0.05441	0.00009	375.6	1.2	377.4	1.2	388.2	3.5	3.3
LEA 06 18 154/55	ZR 1	1	1274	21619	0.13	17.21	19.2	4374	0.46249	0.01318	0.06172	0.00174	1.00	0.05435	0.00014	386.1	10.6	386.0	9.1	385.4	5.6	-0.2
LEA 06-18 154/56	ZR 1	1	1208	21249	0.14	3.62	5.6	14214	0.45012	0.00214	0.05998	0.00027	0.95	0.05442	0.00008	375.5	1.6	377.4	1.5	388.6	3.2	3.5
GRANITE DIKE/MINOR INTR																						
LEA 06 62 142/54	ZR 2	1	197	3274	0.32	12.66	14.7	813	0.42596	0.00201	0.05680	0.00015	0.60	0.05439	0.00021	356.1	0.9	360.3	1.4	387.2	8.5	8.2
LEA 06-62 142/55	ZR 1	1	130	2226	0.15	2.03	4.0	2111	0.45278	0.00170	0.06066	0.00020	0.78	0.05414	0.00013	379.6	1.2	379.2	1.2	376.7	5.4	-0.8
LEA 06 62 145/51	ZR 2	7	82	1426	0.19	0.70	6.9	5439	0.44747	0.00146	0.05973	0.00018	0.90	0.05434	0.00008	374.0	1.1	375.5	1.0	385.1	3.1	3.0
LEA 06 62 145/52	ZR 3	1	558	9366	0.23	0.08	2.1	17227	0.46184	0.00221	0.06143	0.00027	0.95	0.05452	0.00008	384.3	1.6	385.5	1.5	392.8	3.4	2.2
LEA 06-62 147/51	MON 2	8	540	1617	16.21	0.47	5.8	8636	0.45791	0.00243	0.06128	0.00031	0.97	0.05419	0.00007	383.4	1.9	382.8	1.7	379.1	3.0	-1.2
LEA 06-62 147/53	ZR 2	1	200	3298	0.24	7.75	9.8	1291	0.44981	0.00210	0.06008	0.00019	0.73	0.05430	0.00017	376.1	1.2	377.1	1.5	383.4	7.1	1.9
LEA 06-62/154 54	MON 2	1	2563	6747	18.76	2.62	4.6	5645	0.46182	0.00286	0.06160	0.00038	0.92	0.05437	0.00013	385.3	2.3	385.5	2.0	386.6	5.5	0.3
LEA 06 66 154/51	ZR 1	1	78	1329	NO VALUE	0.00	0.9	5652	0.46638	0.00585	0.06217	0.00077	0.98	0.05441	0.00015	388.8	4.7	388.7	4.0	388.1	6.2	-0.2
LEA 06 66 154/52	ZR 1	1	21	314	NO VALUE	0.00	1.5	927	0.58903	0.01690	0.06918	0.00192	0.97	0.06175	0.00046	431.2	11.5	470.2	10.7	665.6	15.8	36.4
LEA 06 66 154/53	ZR 2	1	32	552	NO VALUE	0.69	2.7	804	0.45915	0.00422	0.06137	0.00023	0.53	0.05426	0.00043	384.0	1.4	383.7	2.9	381.9	17.6	-0.6

Table 3: Analytical results. Samples of the different rock units are listed to the left. Numbers on the form "142/58" refer to the fractions analysed. Errors in weight are always 0.001 mg. This error propagates to concentrations of U and Pb. These errors are not shown as they do not affect the U/Pb-ratios. Th/U-ratios are modelled from the $^{208}Pb/^{206}Pb$ measurements. Analyses where $^{208}Pb/^{206}Pb$ were not measured have "NO VALUE" in the Th/U column. Errors are given as absolute errors at the 2σ level. Rho is a correlation coefficient. Abbreviations: Pbt: total Pb; Pbc: common Pb; Disc: discordancy in percent: zr: zircon; mon: monazite; rt: rutile.

4.2.2 Hodal-Storefjord Monzodiorite

Sample description

One sample (LEA 06-101) of the Hodal-Storefjord Monzodiorite, situated in the north of the study area (Table 2)(Figure 3), collected in the summer of 2006, was dated (Figure 56). The rock is plagioclase-rich (c. 50 %) and also contains chlorite, pyroxene, amphibole, K-feldspar and quartz (Figure 52). Zircons and opaques are common accessory phases. The monzodiorite has an intrusive relation to high grade metasedimentary rocks in the south. See Chapter 3 for further sample and field descriptions.

Figure 56: Picture of the Hodal Storefjord Monzodiorite. Sample LEA 06-101 is collected from this rock. Compass for scale.

Analytical results

Eight zircon fractions of 1-9 grains were analysed. The results are given in (Table 3) and (Figure 57).

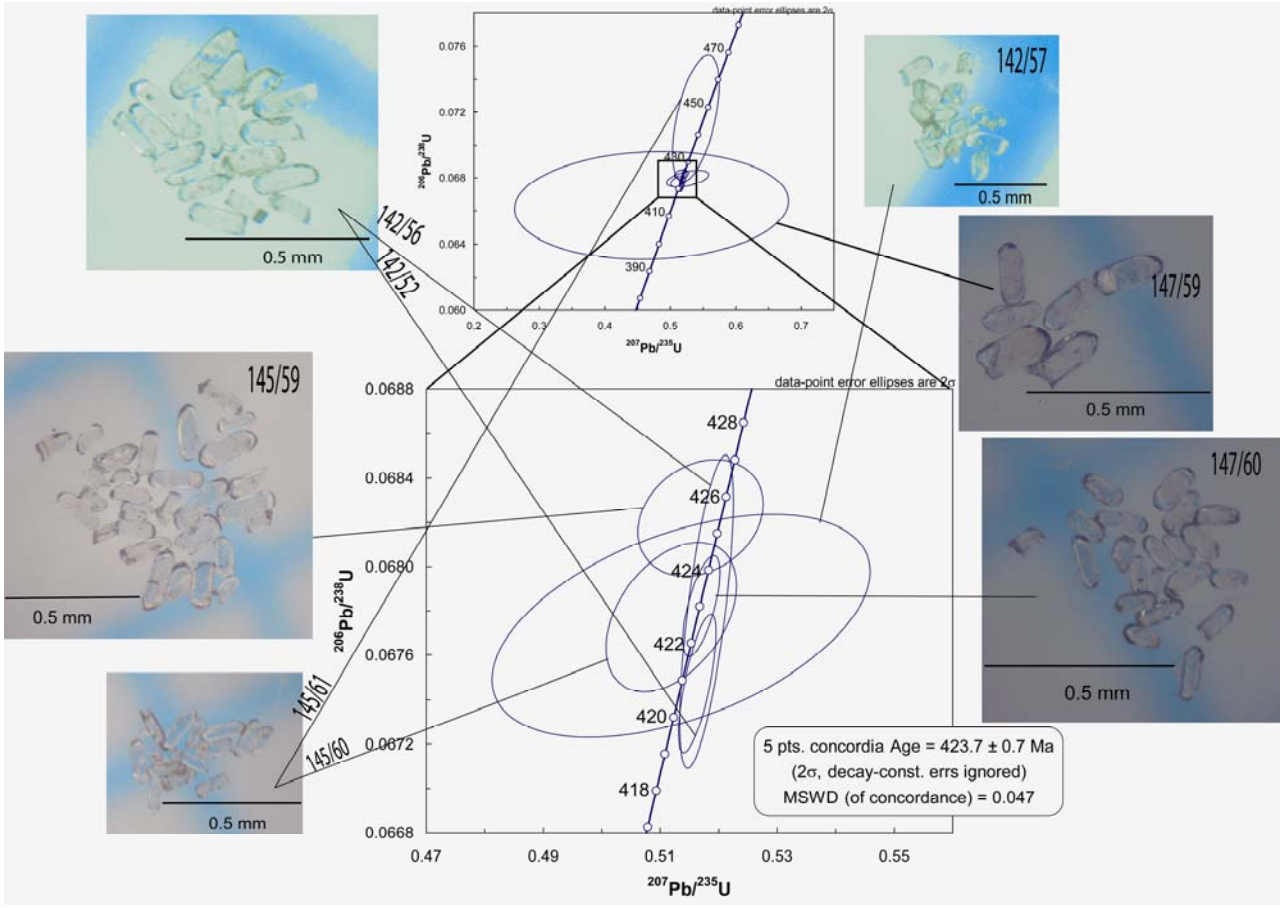

Figure 57: Concordia plot from the Hodal-Storefjord Monzodiorite. With binocular microscope photographs of the analysed zircon fractions. The photos are numberd according to Table 3 and linked to their respective data point error ellipses. A 5 point concordia age is interpreted as the crystallisation age of the pluton at 423.7 ± 0.7 Ma. Decay-constant errors are ignored.

Zircon

The zircon population of this sample is relatively homogeneous, with colourless, prismatic shapes dominated by (100) and (101) (Figure 57). The zircon morphology, where (101) dominate over (211) pyramidal forms, and the 100 prismatic form dominate overall, fall in the calc-alkaline group zircons following Pupin (1980). Most grains contain inclusions and about one third of the grains have smooth subrounded terminations. No cores were observed. The elongation ratio varies from 2 to 5, and the analysed fractions were generally in the upper range of these values. One fraction of tips was also analysed. Common Pb is below 0.6 ppm for all fractions except two, 145/59 with c. 4.7 ppm and 147/59 with c. 10 ppm (Table 3). U-content is low to moderate, varying from 21-225 ppm, except for one fraction 142/56, with a U-content of c. 1650 ppm. Th/U-ratios range between 0.74 and 0.81.

Interpretation

Seven of the eight data points are concordant, but two of them are not included in the age calculation due to very large errors. The one point not included in the age calculation (142/52) is 2.8 % discordant (Figure 57). A five point concordia age of 423.7 ± 0.7 Ma (2σ, MSWD=0.047) is considered the crystallisation age for the Hodal-Storefjord Monzodiorite (Figure 57). The relatively low U-content (and for 147/59 high common Pb) in many samples give data with relatively poor precision, but the best data points cluster tightly and give a precise age. The lower discordant point is probably due to recent lead loss. An option is that several fractions have experienced some lead loss, and thus have moved slightly down concordia (but not enough to appear discordant), giving a younger age than the real. This scenario is, however, not supported by the data that all cluster around the same point on the concordia, and the fact that the most precise analysis is concordant close to 424 Ma.

4.2.5 Eclogite metamorphism

Sample description

One sample of a retrogressed eglogite boudin, LEA 06-59 (Figure 58), sampled during the summer of 2006 (Table 2), was analysed. The rock consists of c. 50 % garnet almost 50 % symplectised clinopyroxene (plagioclase, and secondary clinopyroxene and amphibole), accessory rutile, opaques (probably ilmenite) and zircon (Figure 59). For further descriptions and field relations see Chapter 3.

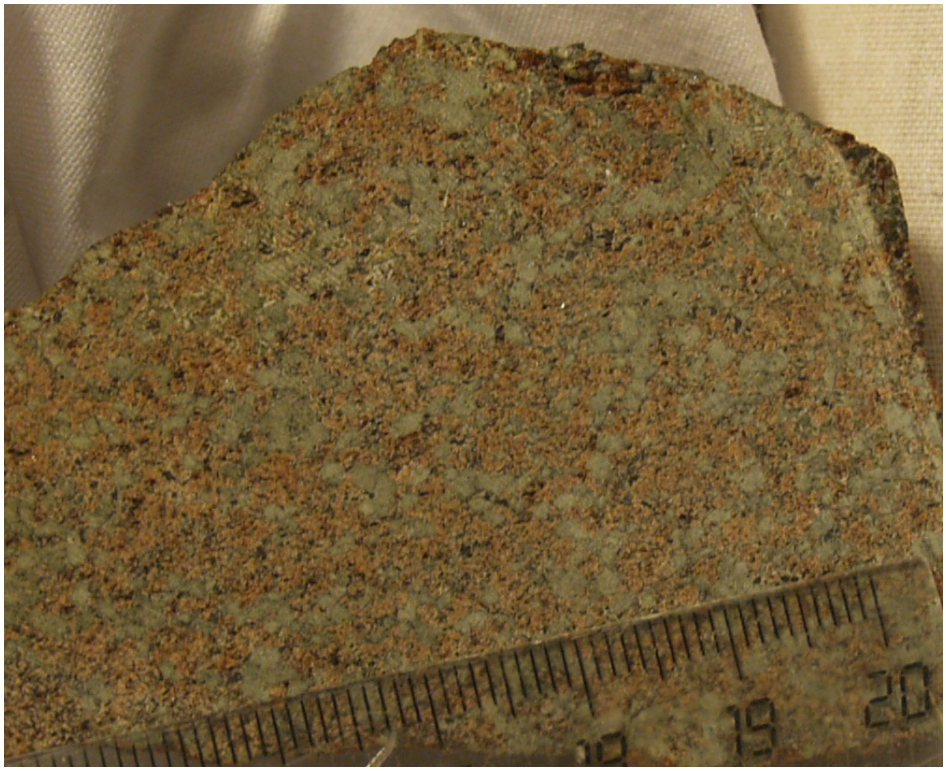

Figure 58: Hand specimen of retro-eclogite (sample LEA 06-59). Note ruler for scale.

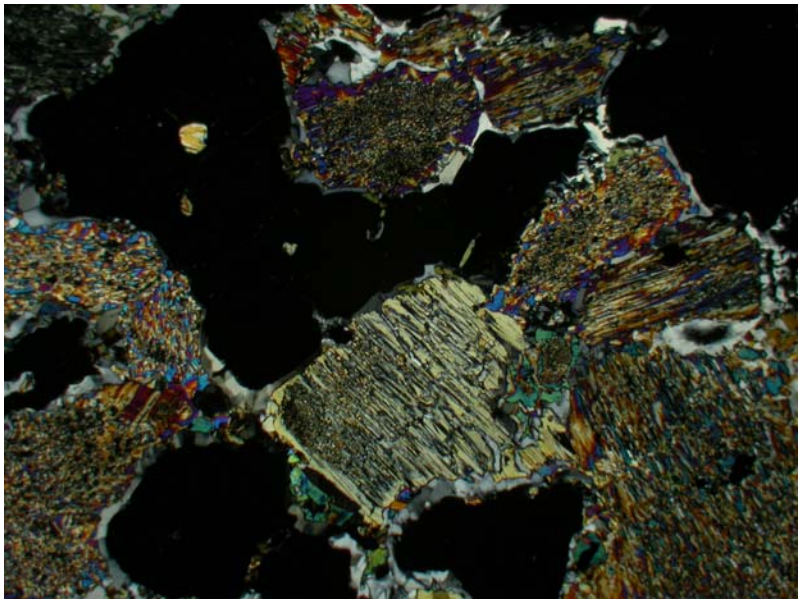

Figure 59: Photomicrograph taken with crossed nichols of sample LEA 06 - 59, showing a retro-eclogite with black garnets and coloured symplectitic relicts of pyroxene. Symplectites of plagioclase and diopside or amphibole. Width of view is 5,5 mm.

Analytical results

Five zircon fractions of 9-18 grains and two fractions of c. 20 and c. 50 rutile grains, respectively, were analysed. Results are given in (Table 3) and (Figure 60).

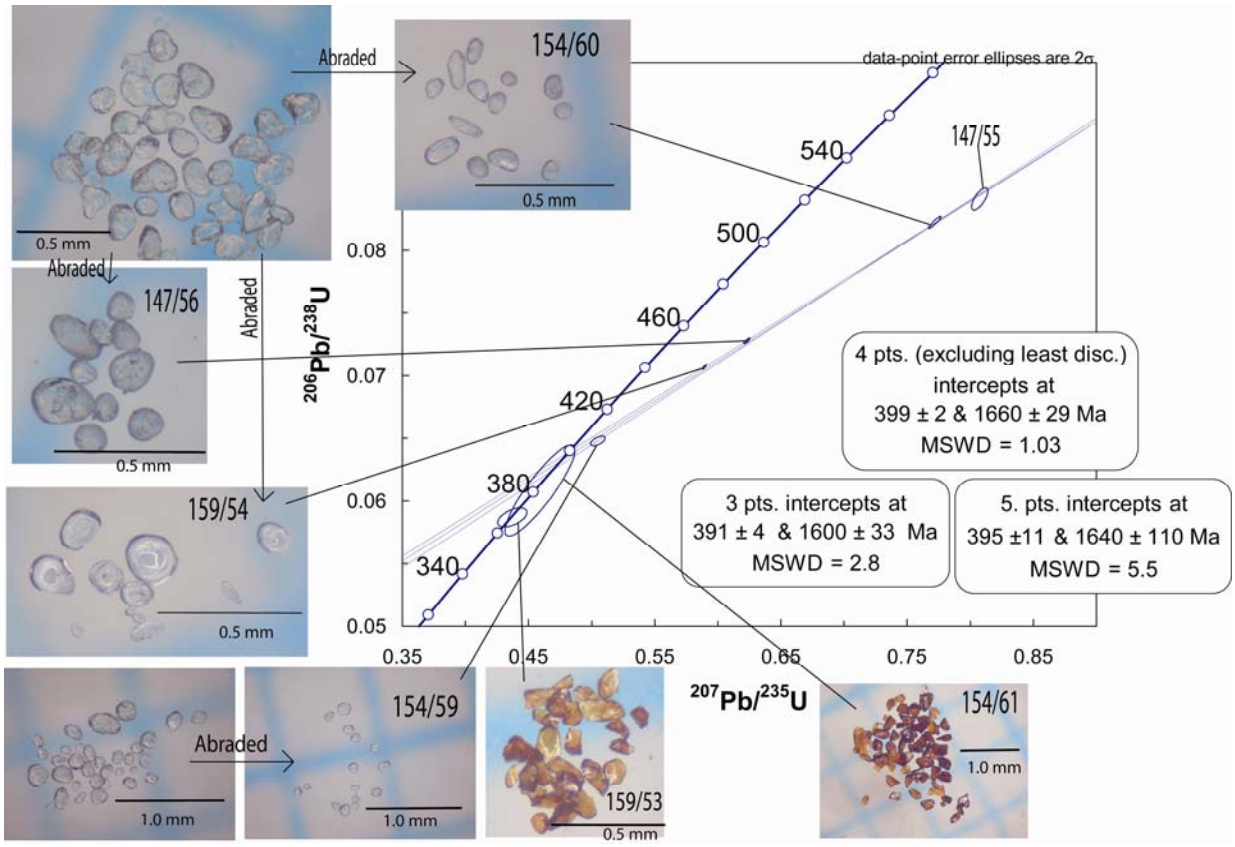

Figure 60: Concordia plot for retro-eclogite, LEA 06-59, with binocular microscope photographs of the fractions analysed. 5 zircon fractions and 2 rutile fractions were analysed. 147/55 is not pictured. Fractions are numbered according to Table 3. Decay constant errors are ignored. See text for discussion.

Zircon

The zircons of LEA 06-59 are rounded clear grains of varying size (Figure 60). The grains are generally inclusion free. The different fractions selected for analysis, were discriminated based on size and degree of rounding. Common Pb is low for all fractions, U-content is low to moderate (c. 70-700 ppm) and Th/U-ratios are ranging from 0.33 to 0.83 (Table 3).

Rutile

The rutiles selected for analysis were clear, brown, inclusion-free fragmented grains of varying size (Figure 60). Common Pb is 0.02 and 0.08 ppm for 159/53 and 154/61, respectively. U-content is low (16 and 23 ppm) (Table 3).

Interpretation

Of the five zircon fractions analysed none were concordant, but the four most discordant data points line up well. The most concordant data point is hanging a bit down from the line

defined by the other points (Figure 60). The two rutile analyses are concordant, but fraction 154/61 is highly imprecise. A lower intercept for all five zircon fractions analysed give an imprecise age of 395 ± 11 Ma (2σ, MSWD=5.5). A four points lower intercept age, excluding the least discordant analysis, give 399 ± 2 Ma (Figure 60)(2σ, MSWD=1.03). Whereas the lower three points give a line with an intercept age of 391 ± 4 Ma (2σ, MSWD=2.8). The most precise age of 399 ± 2 Ma is considered the age of eclogite metamorphism. This implies that the least discordant analysis has been prone to later lead loss, or new zircon growth, possibly related to retrogression (and fluid activity). The upper intercept age at 1660 ± 29 Ma probably reflects the protolith age, likely intrusion of mafic dikes. A Concordia age of the two rutile analyses gave 369 ± 4 Ma, controlled by the most precise analysis (159/53). Although the Th/U-ratios are moderate, and far from as low as expected for metamorphic zircons, a metamorphic age for the zircons is suggested by the morphology of the zircons, with rounded zircons generally accepted as metamorphic (except detrital)(Corfu et al., 2003; Hoskin and Schaltegger, 2003) and the geologic context (e. g. the eclogites on Liverpool Land are occurring in a region where Caledonian metamorphism and magmatism are widespread, and being exhumed partly by displacements on a late Caledonian shear zone; GSZ. See Chapter 5).

Comment on Rutile

The closing temperature of rutile (c. 600 °C (Cherniak, 2000) to 400-450 °C (Schmitz and Bowring, 2003)) is significantly lower than that for zircon (>950 °C (Cherniak and Watson, 2003)). This means that depending on the temperature conditions during metamorphism, rutile could reflect a cooling temperature (related to the exhumation), rather than the crystallisation temperature. Thus the rutile age reflects coling through 400-600 °C under retrograde conditions.

4.2.4 Pegmatite in mafic boudin neck

Sample description and field relations

One sample, LEA 06-18, from a pegmatite occurring in the neck of a retrogressed eclogite boudin, sampled during the summer of 2006 (Table 2), was analysed. The rock is coarse grained, K-feldspar- and quartz-rich containing some biotite (see Chapter 3 for general field descriptions of the mafic boudins and the pegmatites). Zircon is present as an accessory phase.

Analytical results

Four single grain fractions were analysed. The results are given in (Table 3) and (Figure 61).

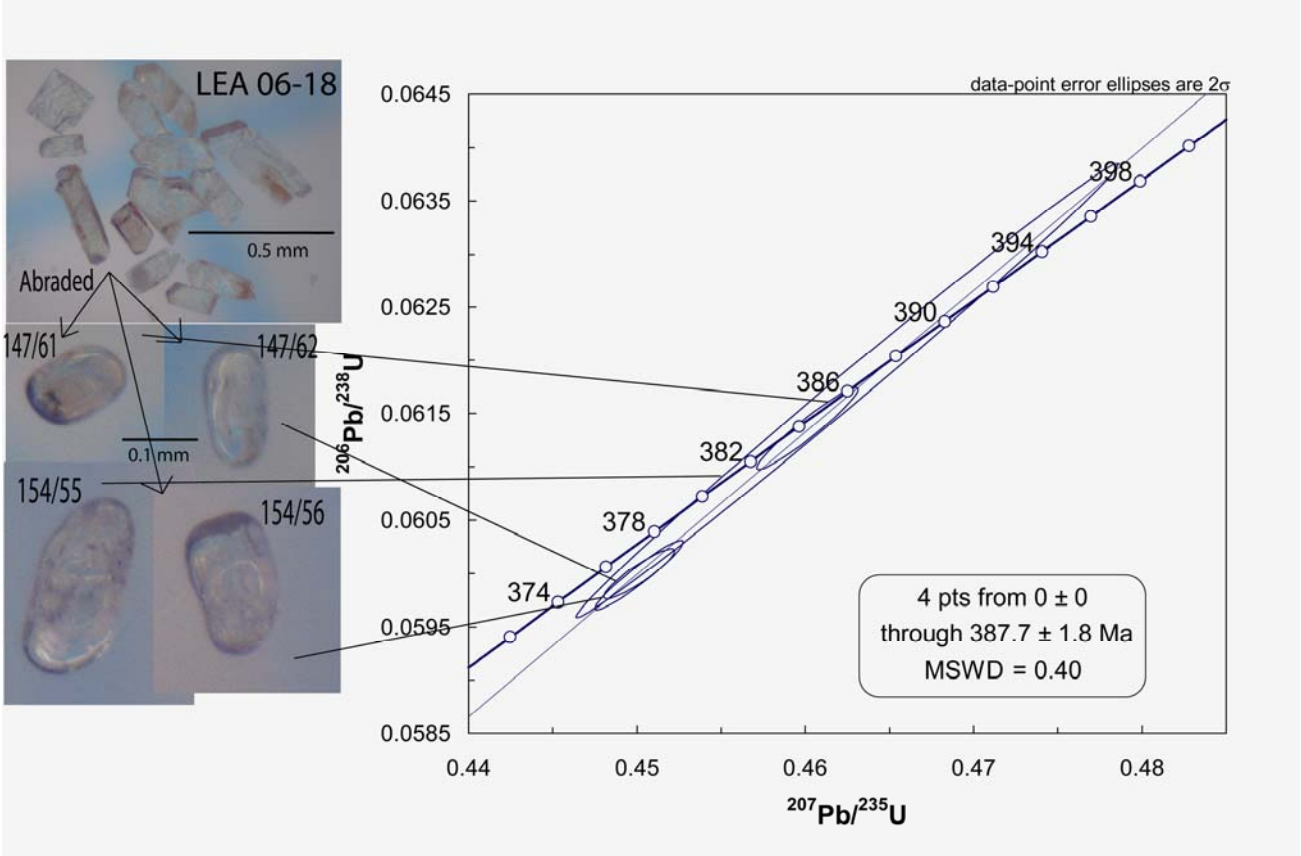

Figure 61: Concordia plot for the pegmatite (sample LEA 06-18), with binocular microscope photographs of zircon fractions. Photos of the fractions (single grain) analysed, are linked to their respective data point error ellipses and numbered according to Table 3. A 4 point discordia age of 387.7 ± 1.8 Ma is considered to represent the crystallisation age of the pegmatites. Decay-constant errors are ignored.

Zircon

Relatively few zircons are occur in this sample, but the grains present can be divided in two: partly metamict, brownish to reddish long prisms, mostly fragmented (Figure 61)(dominated by (110) morphology), and rounded, clear grains. The rounded grains are possibly xenocrysts from the eclogite/retroeclogite (see above). Common Pb is low for 147/61, moderate for 154/56, and high for 147/62 and 154/55 (Table 3). Uranium is very high in all fractions, ranging from c. 12700 ppm to c. 21700 ppm. Th/U-ratios are 0.12 for 147/61 and 147/62, and 0.13 for 154/55 and 154/56.

Interpretation

Three of the four analysed zircons are discordant (Figure 61). Only the less precise analysis, 154/55, is concordant. All data points line up closely. A four point discordia age of 387.7 ± 1.8 Ma (2σ, MSWD=0.40), anchored at 0 Ma, is considered the crystallisation age of the pegmatite. The low precision of 154/55 is due to high common Pb.

4.3.2 Granite dikes and minor intrusives in the footwall block

Sample description

One sample from a small, undeformed granite body intruding the migmatite (LEA 06-62; see Chapter 3)(Figure 62) and one sample of a granite dike intruding, and deformed by top-to-the-south shear (LEA 06-66; see Chapter 3) (Figure 26), sampled during the summer of 2006 (Table 2), were analysed. Both the undeformed and the deformed rock are rich in K-feldspar and quartz, with c. 10 % plagioclase and some biotite, partly altered to chlorite. Some muscovite, and accessory zircon, rutile and opaques occur. The dike in the shear zone is recrystallised. See Chapter 3 for further sample descriptions and field relations.

Figure 62: Minor intrusion and dikes of the "young" granite. Note the amphibolitic xenoliths. Sample LEA 06-62 is collected from this locality. Geologist is Arild Andresen.

Analytical results

Five fractions of 1-3 zircons, two fractions of 2 monazites from sample LEA 06-62, and three fractions of 1-2 zircons of sample LEA 06-66, were analysed. Results are given in (Table 3) and (Figure 63).

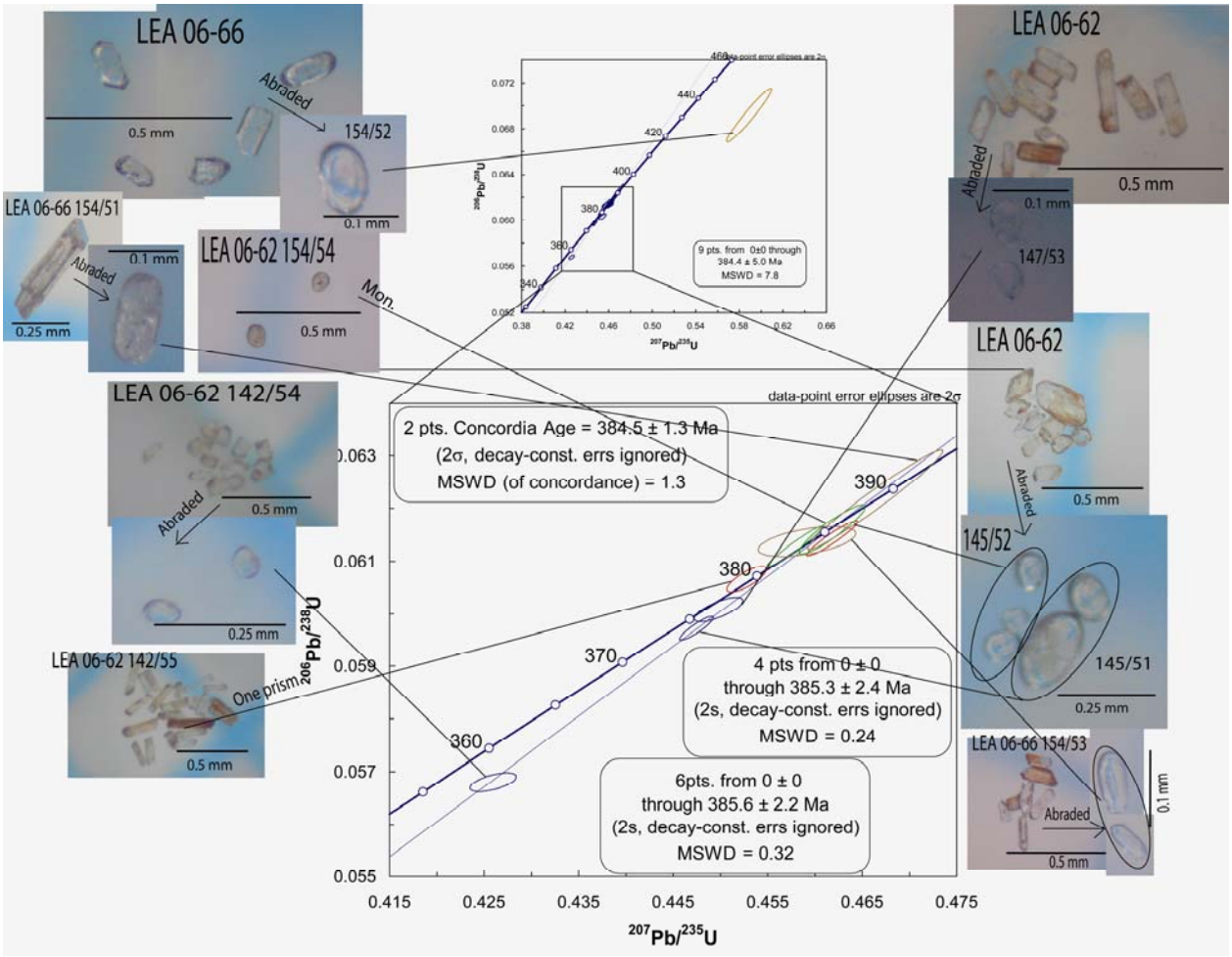

Figure 63: Concordia plot from the granite dikes in the high grade terrane and in the GSZ. Red, blue and green ellipses are analyses from LEA 06-62, where green are monazite analyses and red and blue zircon analyses. Brown ellipses represent analyses of LEA 06-66. A discordia age of 385.3 ± 2.4 Ma from 4 data points, including one concordant point from LEA 06-62 and a concordia age of 384.5 ± 1.3 from LEA 06-66 are joined, and the best estimate for the crystallisation age is thought to be the 6 point discordia age of 385.6 ± 2.2 Ma. Decay-constant errors are ignored. Binocular microscope photographs of zircon and monazite fractions analysed are linked to the respective data point error ellipses. The different fractions are numbered according to Table 3.

Zircons

LEA 06-62 is characterised by a heterogeneous zircon population, with many grains containing visible cores and being metamict. The analysed fractions were weakly yellow to reddish, some were slightly metamict and some had a rusty surface colour (partly altered surfaces). Elongation ratios of the analysed grains were generally high, ranging from 3.5 to 7, but most grains were fragmented, so the real maximum elongation ratio is uncertain. As most of the analysed grains were fragmented, equant prisms, (110) are most likely the dominating morphology (Figure 63). The typical (100) morphology with high elongation ratios occurring in LEA 06-62, is indicative of rapid crystallisation, probably from a water rich melt (Corfu et al., 2003). Common Pb is low to moderate for all fractions except 142/54, with c. 12.7 ppm, and 147/53, with c. 7.7 ppm (Table 3). The relatively high common Pb does, however not give as poor precision as expected, as the U-content, and hence the radiogenic Pb-content, is high. U-content of the fractions lye in the range c. 1425 ppm to 9366 ppm, and Th/U- ratios varies between c. 0.15-0.32.

The zircon population of LEA 06-66 is also heterogeneous, dominated by large fragments. Many grains are metamict and contain visible cores. Grains are colourless to reddish, some with a rusty, altered surface. Of the non-fragmented grains, the elongation ratio varies from 2 to 6. The analysed fractions comprise one large fragmented, slightly metamict prism, a stubby, clear prism, and one fraction of two small, colourless prisms (Figure 63). The zircon morphology seem to be much the same as in LEA 06-62, but the grains are generally more fragmented and it is hard to give good characteristics. Common Pb is very low, less than c. 0.7 ppm for all fractions. U-content is relatively high, ranging from c. 300 to 1300 ppm (Table 3). $^{208}Pb/^{206}Pb$-ratios were not measured, and thus no Th/U-ratio is modelled.

Monazite

The two fractions of clear yellow monazite fragments (only 154/54 post-abrasion is pictured in Figure 63) analysed have common Pb content of c. 0.47 ppm (147/51) and 2.64 ppm (154/54). U-contents of the two samples are 1616 ppm (147/51) and 6747 ppm (154/54). Th/U-ratios are c. 16.2 and 18.6 for 147/51 and 154/54, respectively. Monazite fraction 147/51 yields a slightly reversely discordant data point.

Interpretation

The red, blue and green ellipses represent analyses of LEA 06-62, where the blue are zircon analyses which are used for age calculation, the red are zircon analyses not included in the age calculation, and green are monazite analyses, where one is included in the age calculation (Figure 63). Brown data point error elipsses represent analyses of LEA 06-66 (Figure 63). Four zircon analyses and one monazite analysis of LEA 06-62 are discordant. One zircon analysis of LEA 06-66 is discordant. Six of these data points are used for age calculation. First the individual ages for the two different samples were calculated. A four point discordia age of 385.3 ± 2.4 Ma (2σ, MSWD=0.24) is considered the crystallisation age of the undeformed granite dike. A two point concordia age of 384.5 ± 1.3 Ma (2σ, MSWD=1.3) is considered the crystallisation age of the deformed dike from GSZ. Based on the field relation between the undeformed granite dikes south of GSZ and the deformed granite dikes in the shear zone, showing that these are of the same generation (see Chapter 3), the points are put in the same concordia diagram. A six point discordia age of the points mentioned above, anchored at zero Ma, giving 385.6 ± 2.2 Ma (2σ, MSWD=0.32)(Figure 63), is thus calculated. This age is interpreted as the crystallisation age of the dikes. The fraction responsible for the discordant red error ellipse (145/52) is thought to have experienced recent Pb-loss and to contain a component of inheritance. The upper right discordant point (154/52) has a larger component of inheritance. The three discordant points 142/54,145/51 and 147/53, have experienced recent lead loss. The concordant 142/55 (single zircon), that has a younger age than the preferred crystallisation age, might have experienced some early Pb loss, although no independent evidence proves that. Alternatively the slightly younger age could be due to some analytical error.

The amphibolite facies metamorphism (and deformation) in the GSZ was synchronous with emplacement of the dikes, as the dikes are heavily sheared, foliated, occurring parallel to the mylonite foliation and are traceable from outside the intensely deformed zone (see Chapter 3). One monazite analysis is reversely discordant, probably due to excess ^{230}Th, resulting in unsupported ^{206}Pb, common for high Th-affinity minerals (Harrison et al., 2002; Oberli et al., 2004). The ^{235}U/^{207}Pb-age is then considered the most reliable. The ^{235}U/^{207}Pb-age for 147/51 (not pictured) is a bit younger (382.8 ± 1.7 Ma; 2σ) than the discordia age calculated. The younger age could reflect "slow" cooling through the monazite closure temperature (650-750 °C)(Harrison et al., 2002).

5 Discussion

5.1 Introduction

In this chapter the structural observations and the isotopic ages presented in the preceeding chapters will be discussed and put into the regional context. The chapter ends with a model for the generation of the large volumes of granitic melts and the exhumation of the eclogites on Liverpool Land based on these data.

5.2 Magmatic history of the Upper Plate

5.2.1 The Hurry Inlet Granite and the Hodal-Storefjord Monzodiorite

Two of the major granitoid bodies of Liverpool Land have been studied in this work: the Hurry Inlet Granite (batholith) and the Hodal-Storefjord Monzodiorite (see Chapter 3 and 4), both described by Coe and Cheeney (1972). Coe (1975) reported xenoliths of the surrounding basement gneiss from the eastern part of the Hurry Inlet Granite batholith. He described the contact between the Hurry Inlet Granite and the surrounding gneisses as disrupted in most places, with occurrences of feldspar "porphyroblasts" and faults. The southern contact was described as being "homogenised" gneiss close to the granite. The latter locality probably represents the Gubbedalen Shear Zone documented in this study. The composition of the two abovementioned intrusives, is distinctly different from most granitoids commonly described from the Niggli-Hagar Thrust Sheet. The other granitoids of Liverpool Land, according to Coe (1975), range from monzonites to granodiorites and hornblende-bearing granites, and also apparently differ significantly from the common type. The Caledonian granites widely distributed further west are generally peraluminous S-type, two-mica granites derived by migmatisation of the Krummedal Sequence (Kalsbeek et al., 2001b). Both the different phases of the Hurry Inlet Granite batholith and the Hodal-Storefjord Monzodiorite, on the other hand, have abundant amphibole, and the latter is also orthopyroxene-bearing. The differences indicate that the genesis of the Hurry Inlet Granite batholith and the Hodal-Storefjord Monzodiorite is different from that of the well-studied leucogranites (e. g., Kalsbeek 2001a). This difference is further supported by the geochemical signature of the Hurry Inlet Granite compared to the S-type leucogranites found elsewhere in the Niggli-Hagar Thrust Sheet (Coe, 1975; Kalsbeek et al., 2001a). The Hurry Inlet Granite and the Hodal-Storefjord

Monzodiorite seem instead to be comparable to the calc-alkaline granitoids of Renland (Figure 1)(Rehnström, written comm.; Kalsbeek, written comm.)

The two different phases of the Hurry Inlet Granite batholith which have been dated in this study appear to differ in age by c. 7 m. y. The older phase has been dated to c. 445 Ma and the younger phase to c. 438 Ma. Although there is a slight overlap of the two calculated discordia ages, this age difference is most likely real, as individual concordant analysis show a clear age gap between the two phases (Figure 55). The older phase of the Hurry Inlet Granite batholith is almost identical to the age of the Danmark Ø quartz diorite of Renland (Figure 64) (Rhenström, written comm.).

The Hodal-Storefjord Monzodiorite on the other hand is dated to c. 424 Ma, which is contemporaneous with the bulk of Caledonian leucogranite magmatism in North-East Greenland and with the younger generation of magmatism in Renland (Figure 64)(Rehnstrøm, written comm.).

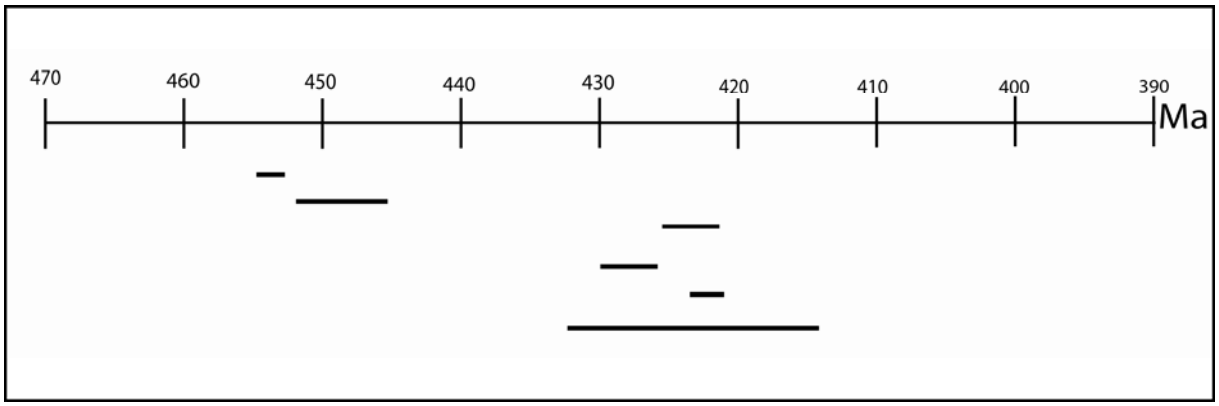

Figure 64: Calc-alkaline magmatism in Renland, East Greenland. U/Pb ages plotted with 2σ errors. Ages from Rehnström (written comm.).

Coe (1975) did major element and a limited number of trace element analyses of 25 samples from the Hurry Inlet Granite (Table 4). Based on these analyses certain features should be emphasised. The analyses show a calc-alkaline trend in the AFM-diagram (Figure 65). All samples except two, plot in the high-K field (Figure 66). The rock is peraluminous (Table 4), and plot in the volcanic arc granite field of the (Y+Nb) vs Rb discrimination diagram (Pearce et al., 1984) (Figure 67). The trace element data, when plotted in a chondrite normalised (chondritic normalisation values from Thompson, 1982) spider-diagram (Figure 68) show a

Major Elem.	1	2	3	4	5	6	7	8	9	10	11	12	13	14	15	16	17	18	19	20	21	22	23	24	25
SiO2	70.18	62.83	68.06	64.39	72.56	63.31	69.6	60.1	70.57	70.13	70.55	71.77	72.84	71.03	52.49	70.53	69.53	70.68	73.86	66.17	68.77	73.07	55.31	68.65	69.4
Al2O3	14.44	16.7	14.89	16.21	14.43	17.18	16.65	17.59	15.48	15.92	15.33	14.82	14.75	15.78	18.72	15.66	16.21	15	13.83	16.24	15.55	14.44	10.29	14.98	14.68
Fe2O3	1.73	2.51	1.77	2.04	0.76	2.35	0.66	2.37	1.22	1.39	1.53	1	0.8	0.93	3.03	0.97	1.25	0.94	0.46	1.79	1.81	0.86	1.55	1.26	1.25
FeO	1.02	2.02	1.43	2.36	1.53	2.34	1.33	3.09	1.25	1.21	1.07	1.03	0.75	1.29	3.16	1.17	1.34	1.46	0.48	1.68	1.34	1.35	2.81	1.25	1.68
MnO	0.09	0.1	0.08	0.09	0.07	0.09	0.07	0.1	0.08	0.08	0.08	0.08	0.07	0.09	0.11	0.08	0.08	0.08	0.06	0.09	0.09	0.07	0.12	0.09	0.09
MgO	0.76	2.05	1.2	1.35	0.79	1.4	0.68	2.04	0.6	0.5	0.56	0.34	0.4	0.34	2.89	0.64	1.09	0.27	0.2	0.89	0.54	1.04	6.01	1.27	0.87
CaO	1.06	3.1	1.86	3.63	0.6	3.52	2.54	4.41	1.93	1.87	1.53	1.57	1.29	2.05	5.72	2.07	2.67	1.91	0.58	2.55	1.95	1.52	11.26	1.6	1.22
Na2O	4.23	3.84	4.32	3.77	2.8	4.22	4.5	3.73	4.45	4.3	3.62	4.15	4.34	3.99	4.4	4.47	4.57	3.87	4.75	4.42	4.64	3.83	1.66	4.33	4.58
K2O	4.8	4.16	4.37	3.07	4.99	3.25	3.68	3.46	3.75	3.85	3.78	4.38	4.78	3.88	3.73	3.92	3.34	4.11	4.37	3.84	3.87	4.61	5.55	5.02	4.21
P2O5	0.21	0.41	0.23	0.3	0.18	0.34	0.13	0.45	0.13	0.15	0.15	0.17	0.11	0.13	0.69	0.13	0.16	0.11	0.12	0.24	0.15	0.17	1.52	0.25	0.23
Trace Elem.	1	2	3	4	5	6	7	8	9	10	11	12	13	14	15	16	17	18	19	20	21	22	23	24	
Ti	4700	8800	5400	7900	4600	8500	3800	10600	3700	4000	3800	3000	2300	3400	18000	3500	4300	4500	1200	6800	4400	3500	6500	5700	
Ni	40	44	41	42	43	42	34	47	38	37	35	36	38	35	73	33	37	36	37	32	34	38	192	56	
Rb	138	82	125	54	162	78	84	93	90	94	96	111	118	99	69	107	86	100	178	104	101	117	122	185	
Sr	979	1389	815	1269	373	1160	718	1613	640	619	591	491	424	588	1773	707	779	549	173	789	792	380	969	1000	
Ba	1679	3202	1877	2224	1641	2314	1678	3120	1844	2120	1778	1630	1064	1546	2800	1711	1886	1672	541	1878	1743	1749	1063	1313	
Y	20	29	18	20	18	9	17	25	18	16	18	17	14	16	15	14	11	17	15	18	25	23	41	19	
Zr	244	394	249	352	207	363	239	351	246	271	253	218	153	220	496	218	264	241	73	308	254	231	104	300	
Nb	10	18	12	8	11	6	4	3	5	8	5	7	10	12	16	4	5	4	17	8	8	8	5	16	
Ce	70	116	89	121	104	148	79	174	82	85	90	71	66	71	145	72	89	87	34	121	61	89	167	158	
Pb	36	35	46	37	47	36	47	31	42	45	39	40	62	37	30	42	31	37	41	40	31	41	20	59	
Ga	22	26	19	27	27	27	24	28	21	22	20	21	18	19	26	21	23	19	19	22	21	17	16	24	
Zn	69	111	87	109	42	106	50	116	69	73	67	60	42	62	130	57	70	65	23	91	76	72	89	96	

Table 4: Major element data of 25 samples and trace element data of 24 samples from the Hurry Inlet Granite batholith. From Coe (1975).

characteristic trend, with high Ba (up to more than 3000 ppm) and Sr (up to c. 1600 ppm) values, a distinct negative Nb-peak, and for most samples also a small negative Ti-peak. The Hurry Inlet Granite samples have an average K/Na-ratio of c. 0.7.

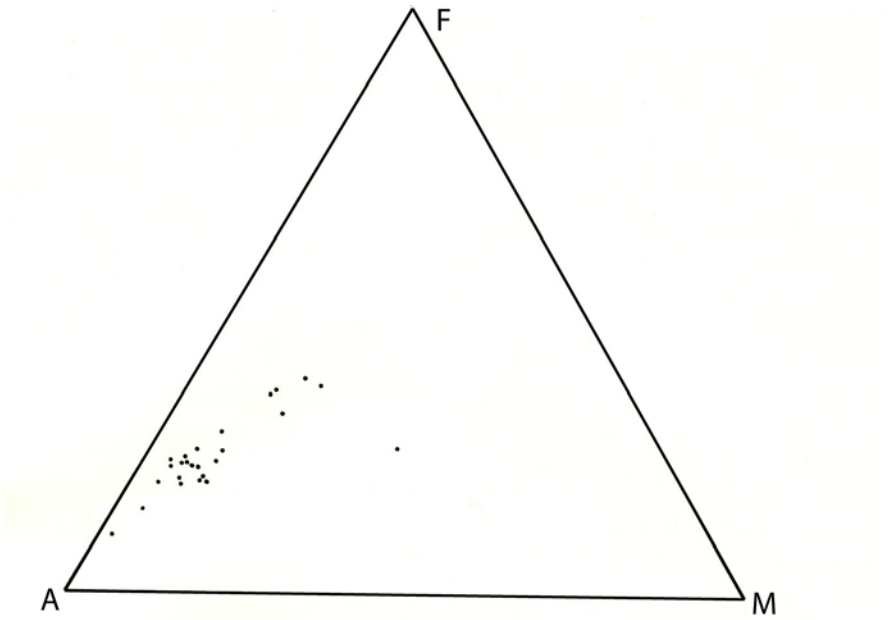

Figure 65: AFM diagram for 25 samples from the Hurry Inlet Granite. After Coe (1975).

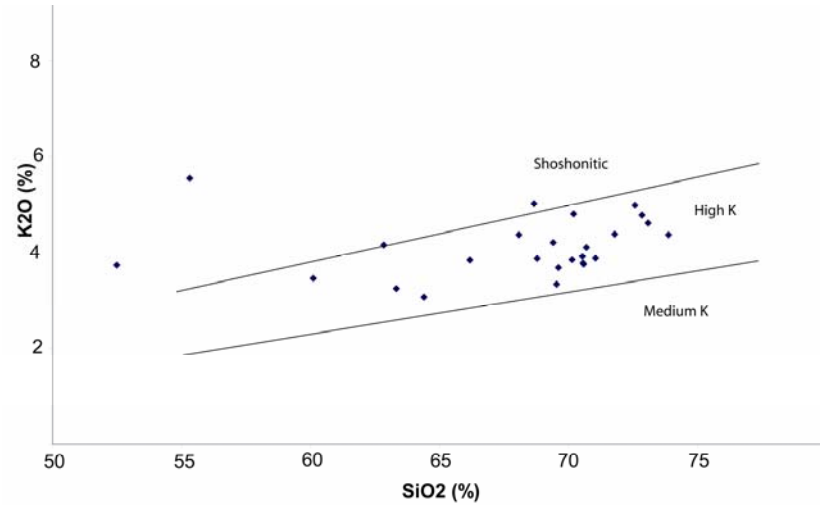

Figure 66: SiO_2-K_2O diagram for 25 samples of the Hurry Inlet Granite. Analysed by Coe (1975).

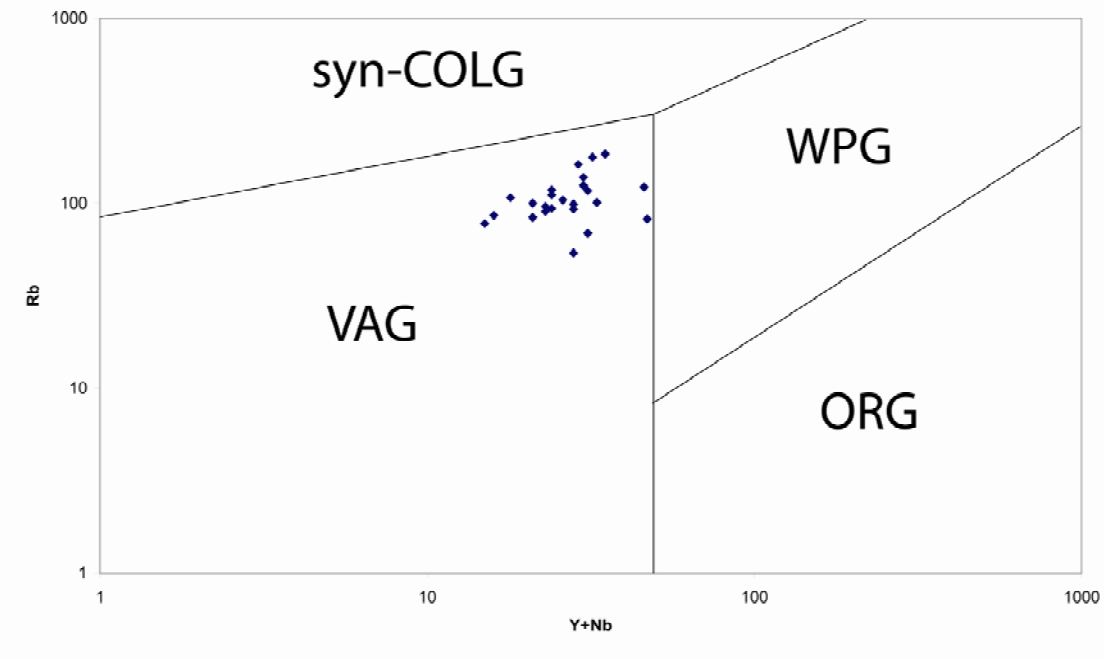

Figure 67: Nb+Y vs Rb discrimination diagram after Pearce et al. (1984). Analyses by Coe (1975). Abbreviations: syn-COLG: syn-collision granite; VAG: volcanic arc granite; WPG: within plate granite; ORG: ocean ridge granite.

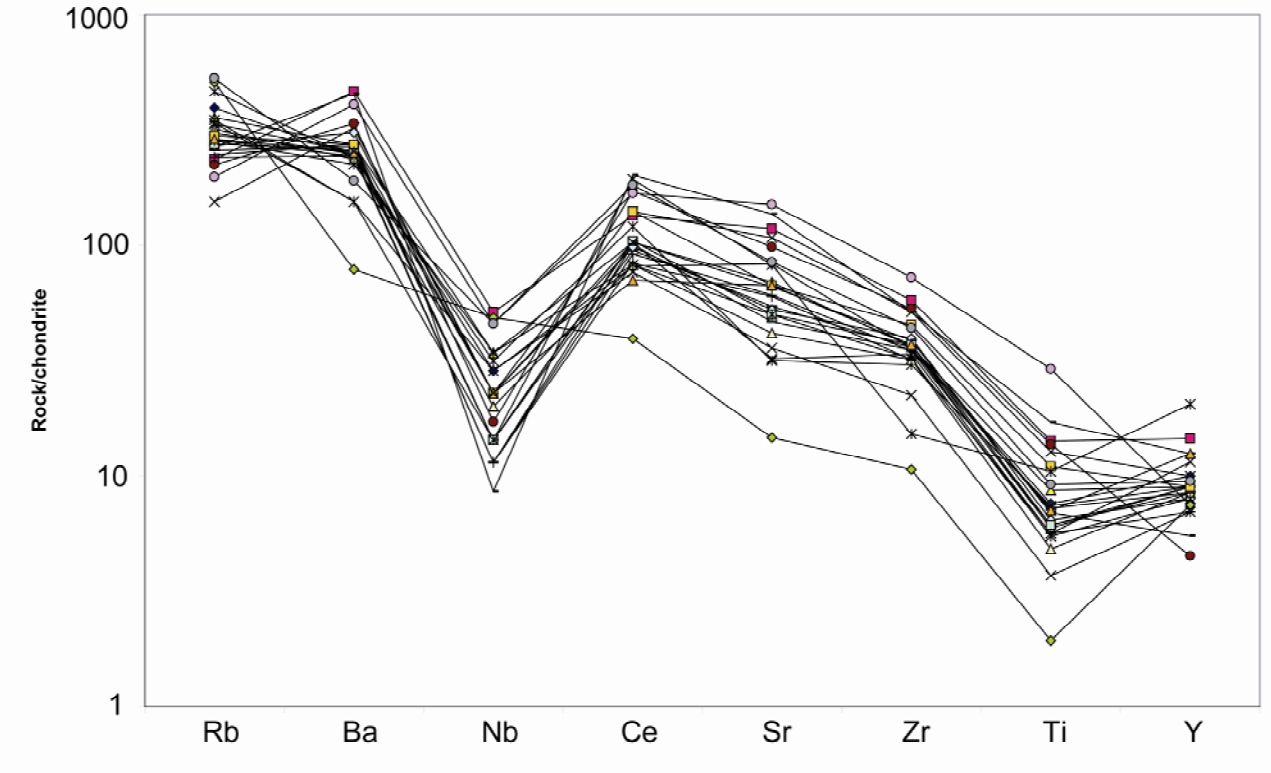

Figure 68: Limited element spider-diagram of trace elements analysed by Coe (1975). Chondritic normalisation values from Thompson (1982).

5.2.2 The Liverpool Land granitoids in a regional context

To explore the possibility that the Hurry Inlet Granite batholith forms part of an orogen-wide magmatic event, data from Liverpool Land have been compared with data from Renland. The calc-alkaline granitoids of Renland occur in two distinct age groups, one at c. 450 Ma and one at c. 430-420 Ma (Figure 64). Geochemical work has been done on two granitoids belonging to the older generation (Rehnström, written comm.; Kalsbeek, written comm.). Major and trace element analysis only include the Korridoren granodiorite. This rock plots in the high-K field and in the volcanic arc granite field of the Nb+Y vs Rb discrimination diagram, has an average K/Na-ratio of 0.5, and shows a trace element pattern similar to the Hurry Inlet Granite, with negative Nb- and Ti-peaks and relatively high Ba. Ti and Nb concentrations are about the same for the Hurry Inlet Granite and the Korridoren granodiorite, but Ba and Sr concentrations are higher in the former. Isotope signatures indicate a mixed mantle-crust source.

The younger granitoids have high K/Na, enriched incompatible trace elements and isotopic signatures also indicative of a mixed crust-mantle source (Kalsbeek, written comm.; Rehnström, written comm.). Most of these granitoids also show distinct negative Nb- and Ti-peaks in the spider diagrams. The Ba and Sr concentrations are similar to those for the Hurry Inlet Granite. However, many of these granitoids plot in different fields of the Nb+Y vs Rb discrimination diagram and the K_2O-SiO_2 diagram. Many also have distinct negative Sr peaks in the spider diagram.

It is argued that decompressional melting of an upwelling asthenosphere and mixing of juvenile magmas with crustal material, give the observed isotope signatures for the younger granitoids (Rehnström, written comm.). The older generation is interpreted to be linked to westward subduction of the Iapetus oceanic plate under Laurentia, and Andean-type magmatism (Rehnström, written comm.).

The Hurry Inlet Granite batholith has geochemical and petrographical similarities with both groups of granitoids in Renland, and an age of one of the phases identical, within error, to the older group. This indicates that the Hurry Inlet Granite batholith is related to arc-magmatism, probably also represented by the older granitoids in Renland. It also seems likely that Hurry Inlet Granite batholith is composed of several magmatic pulses emplaced over a time interval

of at least 7 m. y. The tectonic setting of the Hurry Inlet Granite batholith is illustrated in Figure 69.

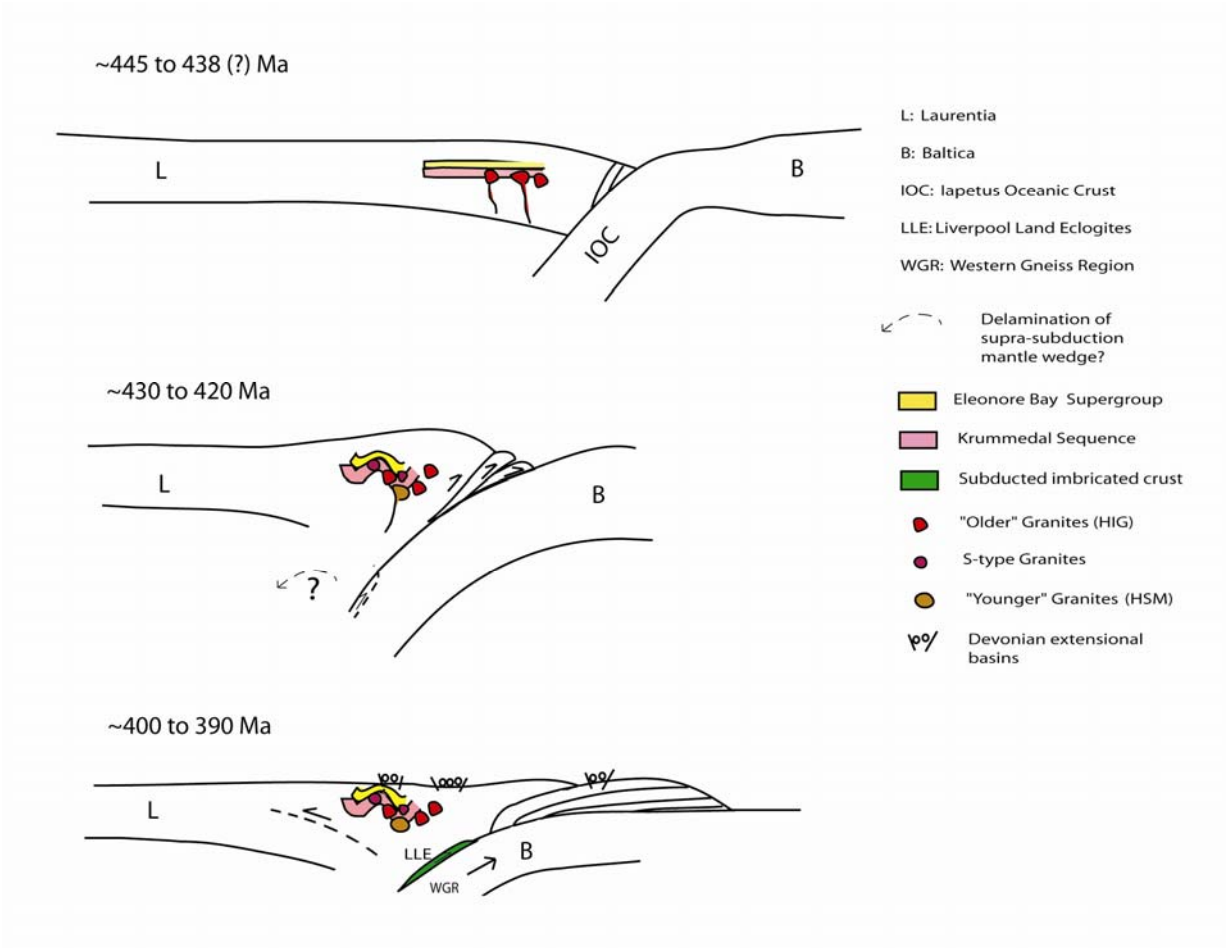

Figure 69: Cartoon showing the proposed tectonic setting at the time intervals relevant for main events in the field area prior to the last extrusion and exhumation of the eclogites (shown in Figure 70). Eclogite formation and imbrication of the subducted Baltic crust is here interpreted to be contemporaneous with emplacement of the Hagar-Niggli Thrust Sheet (see Chapter 2). The development on the Baltic continent is simplified from Tucker et al. (2004). HIG: Hurry Inlet Granite batholith; HSM: Hodal-Storefjord Monzodiorite.

The ages of the Hurry Inlet Granite also overlap with the ages obtained for calc-alcaline intrusives occurring in the Upper and Uppermost Allocthons of the Scandinavian Caledonides (448-430 Ma) (Nordgulen et al., 1993; Tucker et al., 2004; Yoshinobu et al., 2002). The Uppermost Allocthon is now considered to be of Laurentian origin (Roberts et al., 2002; Yoshinobu et al., 2002).

The Hodal-Storefjord Monzodiorite is similar to the monzonites of the younger generations in Renland, both in age (the age of the Hodal-Storefjord Monzodiorite is overlapping with three

of the dated plutons from Renland) and in petrography (i. e. abundant amphibole, low modal quartz and occurrence of orthopyroxene). This could indicate a relationship with the later generation in Renland.

Attention should also be made to the lamprophyres occurring in the study area, cutting the two granitoids dated here. Lamprophyres intruding the Eleonore Bay Supergroup in the Fjord Region have been dated to c. 420 Ma (Andresen et al., 1995). Lamprophyres are also cutting granitoids and a succession of Eleonore Bay Supergroup sediments in Canning Land just north of Liverpool Land, indicating that this area can be correlated with Liverpool Land (Caby, 1972).

Lamprophyres are generally accepted to represent water-rich melts with enriched mantle origin (Shand et al., 1994; von Seckendorff et al., 2004). Occurrences of lamprophyres associated with granitoids, is amongst other known from the Caledonian Scottish Highland and the Variscides of Mid-Germany (Rock et al., 1988; Shand et al., 1994; von Seckendorff et al., 2004). Geochemical data suggest that the lamprophyres associated with the "Newer Granites" in Scotland could represent parental magmas for these granitoids (Rock et al., 1988). Several authors (Shand et al., 1994, references therein; von Seckendorff et al., 2004, references therein) have suggested that mantle enrichment for many lamprophyres could be coupled with subduction, and that asthenospheric mantle experience upwelling due to delamination of subcontinental lithospheric mantle, leading to orogenic collaps and magmatism, including mantle derived lamprophyres. The field setting of the above-mentioned lamprophyres mirrors to some degree the field setting of the ones in Liverpool Land. If the lamprophyres in the study area are related to the Hodal-Storefjord Monzodiorite and of the same age as the lamprophyres in the Fjord Region, this would support the proposed models for the generation of c. 420 Ma intrusives in Renland (Rehnström, written comm.). And the same process, with post-subductional, sublithospheric mantle delamination and orogenic collapse could be responsible for the Hodal-Storfjord Monzodiorite and the younger generation of plutons in Renland. The proposed tectonic setting of the Hodal-Storefjord Monzodiorite and the younger granitoids on Renland are shown in Figure 69. Further geochemical work on the intrusives on Liverpool Land and dating of the lamprophyre dikes would hopefully shed light on the tectonic setting of these granitoids, and possibly both the early (subduction-related magmatism) and the late stage development of the Caledonian orogen as a whole.

5.3 Exhumation of the Liverpool Land UHP-rocks

5.3.1 Introduction

Hartz et al. (2005) reported preliminary data indicating UHP-metamorphism occurring at c. 393-397 Ma on Liverpool Land. Therefore an eclogite from the same area has been re-dated in this study and the age reported here (399 ± 2 Ma) is slightly older, but overlapping the age reported by Hartz et al.(2005). An attempt of getting a P-T estimate was not successful, other than confirming that the rock is a true eclogite (see Chapter 3).

The data presented in the preceeding chapters indicate that the eclogites were exhumed to amphibolite facies conditions by c. 388 Ma, as constrained by anatectic pegmatites. Furthermore top-to-the-south displacement on the Gubbedalen Shear Zone occurred under amphibolite facies conditions at c. 386 Ma, constrained by the syn-tectonic granite dikes. The melts resulting in these granite dikes, might have been generated by decompressional melting of the gneisses in the high grade terrane. Exhumation of the eclogites to temperatures below c. 400 °C (corresponding to a crustal depth of c. 15 km, considering an average geotherm of c. 25 °C/km) was not achieved earlier than c. 370 Ma, constrained by a rutile cooling temperature. The top-to-the-south displacement of the high grade terrane continued under decreasing temperatures, at least down to the brittle-ductile transition for quartz, reflecting the role the southwards thrusting had in the exhumation.

5.3.2 Southern Liverpool Land – A piece of Baltica?

It is generally accepted that Baltica was subducted under Laurentia during the Caledonian continent-continent collision, leading to HP- and UHP- metamorphism in the Baltic crust (e. g., Andersen et al., 1991; Rey et al., 1997; Tucker et al., 2004). Thus the formation of the UHP-rocks of Liverpool Land, apparently seem contradictory. Furthermore, the UHP-rocks of the Western Gneiss Region in Norway occur in the parautochthonous basement (Gee et al., 1985), contrary to the eclogites in the East Greenland Caledonides that are part of the over-riding plate. A more complex tectonic development clearly must have been the case. A model for the formation and exhumation of the UHP-rocks of Liverpool Land is discussed below.

To account for the presumed > 25 kbar peak pressure for the eclogites of Liverpool Land (Hartz et al., 2005), the rocks must have been down to a depth of more than 70 km. Even far greater depths must have been reached for the UHP-rocks in NEGEP, where peak pressures of more than 35 kbar have been recorded (Gilotti et al., 2004). NEGEP and Liverpool Land are, however, separated by a large distance, and they seem to be part of a different crustal domain (Schlindwein and Jokat, 2000), so they should be treated as different terranes with different tectono-metamorphic histories.

Characteristic for the high grade terrane of Liverpool Land is the occurrence of ultramafic lenses in addition to the eclogite pods (Smith and Cheeney, 1981). Similar occurrences are also well known from the Western Gneiss Region (e. g., Brueckner, 1998), but not from NEGEP. Another interesting observation is that the protolith age of the eclogite is c. 1660 Ma, which is significantly younger than the protolith ages from NEGEP and the basement gneisses of East Greenland (Brueckner et al., 1998; Gilotti et al., 2004; McClelland et al., 2006; Thrane, 2004). Protolith ages of several eclogites, as well as basement gneisses, from the Western Gneiss Region are equal to or overlapping with the protolith age of the Liverpool Land eclogite (Root et al., 2004; Tucker et al., 2004; Walsh et al., 2007; Tucker et al., 1990). Also, ages for HP- and UHP-metamorphism in the Western Gneiss Region are similar (c. 415-395 Ma) (Carswell et al., 2003; Root et al., 2004; Tucker et al., 2004; Walsh et al., 2007) to the age obtained for the eclogite dated in this study, whereas the ages for UHP-metamorphism in NEGEP are generally younger c. 360 Ma (McClelland et al., 2006). Also, a marked difference in crustal structure north and south of 76 °N was described by Schlindwein and Jokat (2000). The above-mentioned differences between the Liverpool Land high grade terrane and NEGEP, indicates that the eclogites of the two terranes are not related and have undergone different tectono-metamorphic histories. Although these observations do not exclude a Laurentian affinity for the high grade terrane of Liverpool Land, the similarities between this high grade terrane and the Western Gneiss Region may indicate a close relationship. Accepting this, the high grade terrane of Liverpool Land could represent a "slice" of the deeply subducted Baltic crust, which later on in the collision process was emplaced in tectonic contact with rocks of Laurentian affinity (North-East Greenland). Paleogeographic reconstructions show that the Western Gneiss Region and Liverpool Land was adjacent to each other in Middle Devonian time (Dewey and Strachan, 2003).

5.3.3 Uplift and exhumation of the Liverpool Land Eclogites

Initial exhumation

A possible way of bringing a "slice" of Baltica crust onto the Laurentian plate could be by imbrication and thickening of deep Baltica crust, followed by accretion onto the lower crust of the Laurentian plate during a late stage of the Caledonian orogeny. Analogue experiments have indicated that imbrication of subducted crust can be partly buoyancy-driven, leading to extrusion of deeply subducted crust into the overriding plate in a continent-continent collision zone (Chemenda et al., 1996). Depending on the tectonic regime (i. e. highly compressional or low compressional), Chemenda et al.(1996) found that the failure point for the crust in the subducting slab will vary. As the Western Gneiss Region is considered parautochthonous (Gee et al., 1985), an imbricated "slice" of the Baltica crust could not represent a complete crustal section as in the models of Chemenda et al.(1996). Rather a crustal fragment and not the whole crustal section must have experienced failure and decoupling from the subducting slab. The point of failure must have been below the overriding plate as the peak pressures of Liverpool Land are reported to be above 25 kbar (Hartz et al., 2005). Partly following the model of Chemenda et al (1996) (but excluding the possibility of decoupling of a complete crustal section of the subducting slab), this would bring a sliver of subducted crust in contact with the overriding plate's lithosphere along an extrusion channel between the two plates, and coupling with the overriding plate could be achieved. This tectonic development is shown in a schematic way in Figure 69. It is important to note that the model of obduction of subducted crust according to Chemenda et al.(1996) considers the whole subducted crust as being structurally homogenous (i. e. with no asperities and with constant density). Natural subducted crust will, however, most likely be heterogeneous with pre-existing structures and density contrasts, the response to unevenly distributed metamorphism and various protolith lithologies. This will lead to different mechanisms of failure and decoupling, as well as probably different points of failure in the subducted crust. However, in a general sense their model can be applied as a principal mechanism of imbrication and uplift of deeply subducted crust. As a model for the origin of the Liverpool Land UHP-rocks, this does not conflict with the models for subduction and eduction of the Western Gneiss Region. A similar model of late Early Devonian imbrication of the Baltican basement, uplifting the HP- and UHP-rocks of the Western Gneiss Region was developed by Tucker et al.(2004). These authors explain exhumation with upper crustal extension contemporaneously with deeper level convergence and thrusting of part of the Baltica basement.

An alternative model is the eduction model of Andersen et al.(1991), where rapid exhumation following slab break-off (decoupling of the thermal boundary layer) could be responsible for bringing distal parts of the educted Baltica slab in contact with the overriding Laurentian plate. In their model the slab break-off leads to extension and footwall uplift and rotation on major west-dipping detachments. This could have left the subducted Baltica crust in tectonic contact with the Laurentian plate.

A likely consequence of both models is that the educted material of previously subducted Baltica crust would be placed below the overriding plate. Extensional movement on major east-dipping shear zones in the Laurentian plate (i. e. in the East Greenland Caledonides) could have isolated a sliver of the educted/exhumed, previously subducted Baltic crust. The possibility that a major west-dipping lower crustal reflector could represent an educted sliver of the previously subducted Baltica plate, was discussed by Schlindwein and Jokat (2000).

A third scenario is that the eclogites of East Greenland could have formed by some process of intracontinental subduction. The same mechanisms could have been responsible for uplift/exhumation (i. e. buoyancy-driven imbrication or loss of the thermal boundary layer).

Later stage exhumation

The data presented in the preceeding chapters indicate that c. 399 Ma eclogitisation was followed by uplift and exhumation resulting in anatexis at c. 388 Ma, represented by pegmatites in the mafic boudin-necks. As many of the pegmatites, contain abundant euhedral amphibole (although not the one dated in this study), the anatexis most likely occurred under amphibolite facies conditions. Amphibolite facies conditions associated with southwards thrusting of the high grade terrane is constrained by the syntectonic granite dikes intruding at c. 386 Ma. Thus the second stage stage of exhumation of the high grade terrane must have been initiated prior to the granite dike emplacement (i. e., considering the buoyancy driven imbrication the first stage). A viable, but unconstrained model for the later stage of uplift and exhumation of the Liverpool Land eclogites, within the time frame outlined above is presented in the following.

As the GSZ is oriented almost perpendicular to the main structural grain of the East Greenland Caledonides, thrusting and crustal thickening of the high grade terrane cannot be explained by straight forward simple shear models of orogen-perpendicular extension or

contraction. It should be stressed that no systematic and detailed strain analyses have been conducted, and that the strain pattern described in this study is based on general mapping and observations. The aim of this study was to constrain the kinematics and timing on the shear zone in a restricted area, but the observations made, give some indications to the processes responsible for the exhumation of the eclogites.

Sinistral wrench faults that were active to at least late Middle Devonian times have been described from the Fjord Region (72-76 °N) down to the Scoresby Sund (Western Fault Zone) (Figure 1)(Larsen and Bengaard, 1991). These authors speculatively linked these fault zones to the Storstrømmen Shear Zone further north. The Storestrømmen Shear Zone was first properly described from Dronning Louise Land (Figure1)(Holdsworth and Strachan, 1991), where a lateral, ductile shear zone is thought to have accommodated large displacements. Holdsworth and Strachan (1991) attributed this shear zone to the foreland thrusting in Dronning Louise Land, in an overall transpressional tectonic setting, thought to reflect the oblique convergence of Baltica and Laurentia. If their interpretations were right, this implies that sinistral transpression was active in Middle Devonian time, as thrusting in Dronning Louise Land is dated to c. 390 Ma (see Chapter 2)(Dallmeyer and Strachan, 1994). Dallmeyer and Strachan (1994) also recorded $^{40}Ar/^{39}Ar$ muscovite ages in the Storestrømmen Shear Zone down to 370 Ma, showing that the shear zone was active under lower amphibolite facies conditions at this time. These data conflicts with later postulates, claiming overall transtension in the East Greenland Caledonides from Middle Devonian times (Dewey and Strachan, 2003). Holdsworth and Strachan (1991) indicated that the Storestrømmen Shear Zone could be traced for more than 300 km, and also suggested that it originally continued further south, according to Larsen and Bengård (1991), but that it was obscured by Devonian and Mesozoic basin formation. Sartini Rideout et al.(2006) suggested that displacement on the dextral Germania Land deformation zone in the NEGEP (Figure 1)(Chapter 2), with exhumation of c. 360 Ma UHP-eclogites, occurred in a transpressional setting. The location and orientation of this deformation zone may indicate that it is linked to the Storestrømmen Shear zone. The occurrences of major strike slip faults in the northern/central part of the North-East Greenland Caledonides, the suggested overall oblique convergence between Laurentia and Baltica (Holdsworth and Strachan, 1991; Torsvik et al., 1996), and the documented strike-slip displacements in the Western Fault Zone (Larsen and Bengaard, 1991), indirectly indicate that major sinistral strike-slip motion occurred all along the North-East Greenland part of the Laurentian margin during the Caledonide orogeny.

The initial flattening of the leucosomes in the felsic gneisses of the high grade terrane could be explained by heterogeneous, transpression affecting a zone with shallowly dipping boundary walls (i. e., a thrust associated with an asymmetric flower structure)(Dewey et al., 1998)(Figure 70). This would fit with the observed shallow dip of the foliation in the high grade terrane of Liverpool Land. A consequence of such a structural setting is that some displacement of the upper plate would be extensional, opposite to the thrusting direction (Figure 70)(Dewey et al., 1998). The extensional, upper part of the GSZ displaces the upper plate northwards, i. e. opposite to the southwards directed footwall thrusting. As a consequence, what is now the footwall block would have been extruded. To fit this model into an overall sinistral tectonic regime a restraining bend must have been the active lower boundary (Figure 70). The restraining bend could either have been a pre-existing structure, or simply a shallowly dipping contractional shear zone/ fault forming at a high angle to the strike of a presumed major strike-slip zone. The latter structural development has been observed in analogue transpression experiments with modest strike slip components (Schreurs and Colletta, 1998). Similar structures also occur naturally, exemplified by the asymmetric "flower structures" of the Jargalant Range of the Western Altai, Mongolia (Cunningham et al., 1996). These possible analogues are, however, representative for the middle/upper crust, and it is not clear how such structures evolve at greater depths.

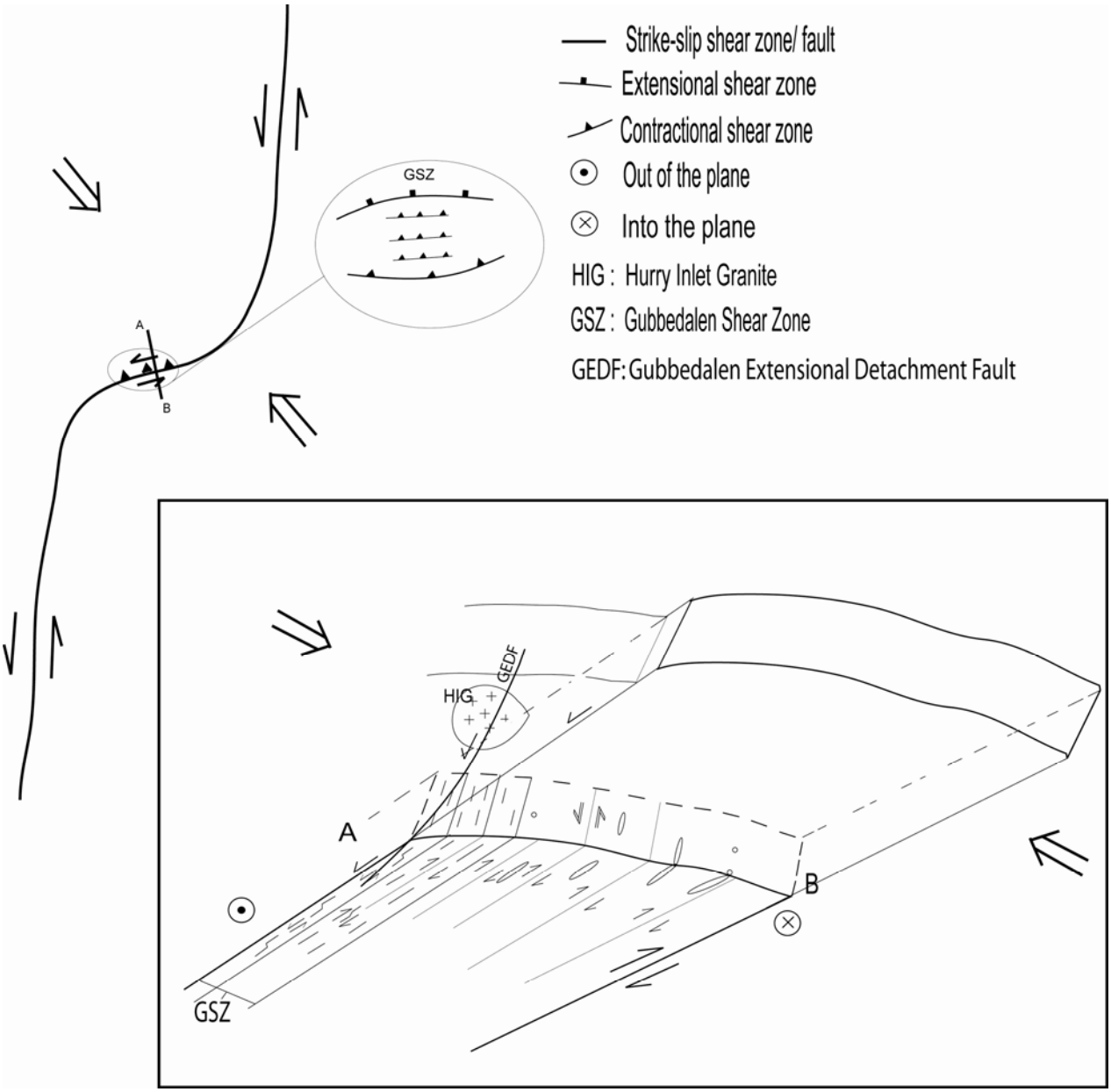

Figure 70: A schematic drawing illustrating the transpression model for the second stage of uplift and exhumation of the Liverpool Land eclogites. The lower inset is a 3D-illustration of the profile A-B. The surface represented by A-B is the surface exposed today. The drawing illustrates the proposed tectonic setting at c. 385 Ma, with material being thrust over a lower "master" thrust (not exposed/detected), and with some extension occuring in the Upper Plate, leading to extrusion of what is now the Lower Plate. The overburden at c. 385 Ma is supposed to be c. 20 km (amphibolite facies conditions). The GDEF is also shown in the picture, but it is not certain weather it was active from this stage, or only later. The GDEF brought the Hurry Inlet Granite in contact with the Lower Plate. The figure is not to scale.

Independent of the structural setting of the restraining bend, a structural setting where strain partitioning acted on an oblique surface (represented by the restraining bend) to the main strike-slip direction, is appropriate for explaining the observed structures (Figure 70).

Although the gneiss-foliation in the footwall is variable (probably due to heterogeneous strain, mainly caused by differential deformation around the mafic lenses), the westerly striking foliation of the GSZ would fit the expected strain pattern in such a sinistral transpressional regime. If the deformation zone is confined by boundary zones constituted by an east-west trending restraining bend, in an obliquely convergent stress regime, with sinistral strike slip occurring parallel to the orogen, type A transpression of Fossen and Tikoff (1998) would be expected. Type A transpression involves shortening parallel and perpendicular to the strike-slip component, and stretching perpendicular to the two shortening directions (Figur 70) Such a strain field can be obtained if the far field stresses act approximately perpendicular to the shear zone, but a component of strike slip is active due to major strike slip zones responding to the oblique convergence. Thus strain would be expected to partition into a component parallel and a component perpendicular to the strike of the shear zone. According to the model of Fossen and Tikoff (1998), the initial phase in this type of transpression can lead to flattening of structural elements. But as transpression continues, the strain will change and be progressively more constrictional. This is compatible with field observations, where flattening occurred initially, appearing to be overprinted by constrictional strain in many places. Thus the SL-tectonites of the high grade terrane could be explained by a model of increasing transpression in a zone with confined shallowly dipping (c. 30° for the upper boundary, constrained by the foliation of the extensional part of the GSZ) boundaries normal to the strike slip direction. The model of Fossen and Tikoff (1998) also predicts rotation of strain markers into the direction of stretching with continued transpression. This is consistent with the trend of the linear elements in the high grade terrane. As the strain in the high grade terrane is localised in high strain zones with obvious simple shear, top-to-the-south strain markers, simple shear in the thrust direction (i. e., perpendicular to the strike and parallel to the foliation of the shear zone) is required. According to Jones and Holdsworth (1998) a component of pure shear is expected to act perpendicular to the shear zone foliation, and simple shear to act in the foliation plane, one component parallel to the strike and one component perpendicular to the strike of the foliation if the two blocks confining the zone of transpressional deformation are moving relative to each other in both the horizontal and vertical directions.

If the model presented here is applied, according to Jones and Holdsworth (1998) simple shear is expected to act both parallel and perpendicular to the strike in the foliation plane. Furthermore, as thrusting is the main mechanism of material transport here, it is required that

the block being thrust upon the other moves vertically (upward) relatively to the lower block (south of the restraining bend). Such tectonic setting will explain the simple shear component, and the development of the penetrative foliation observed in the GSZ, and in the minor high strain zones in the high grade terrane. It is also expected that the component of simple shear will localise strain, whereas the pure shear component will distribute strain more widely (Lin et al., 1998, references therein). This is also consistent with the observations of high strain zones (GSZ) with penetrative foliation and simple shear kinematic indicators.

As the main lower thrust boundary is not detected/ exposed, the exhumation-model outlined above is difficult to test, but it does explain the structural features observed. Furthermore, the area investigated is a restricted area, and it can not be considered representative for the deformation pattern elsewhere in the East Greenland Caledonides. Neither was our mapping conducted to constrain the boundaries of the shear zone. However, local and more regional mapping (e. g., tracing of the shear zone and search for other deformation zones in the area), as well as detailed strain-analyses in the high grade terrane, would contribute towards a more constrained tectonic model for the exhumation of the high grade terrane.

The proposed model for uplift and exhumation by extrusion of the high grade terrane (the footwall block in the exposed tectonostratigraphy) implies that the topographic relief would have increased over the extruded crust. Hence, elevated erosive potential of the uplifted area would be a consequence. Erosion therefore probably played an important role in the exhumation. Much of the exhumation was, in addition to the extrusion and erosion, probably accomodated by extensional displacement on the brittle Gubbedalen Extensional Detachment and possibly other extensional structures at a high crustal level (Figure 64).

6 Conclusion

Following conclusion can be made on the basis of the discussion above (Figure 69)(Figure 70):

Late Ordovician-Early Silurian magmatism, probably in a continental arc setting, was responsible for the generation of the Hurry Inlet Granite batholith. The emplacement of this batholith occurred in at least two phases, one at c. 445 Ma, and one at c. 438 Ma. A major pluton, the Hodal-Storefjord Monzodiorite was emplaced at c. 424 Ma, possibly related to delamination of a suprasubduction mantle wedge.

The Liverpool Land eclogites were metamorphosed at c. 399 Ma, possibly as a part of the Baltic subducted slab. It is here proposed that uplift and initial exhumation took place by buoyancy-driven imbrication of the subducted crust. Amphibolite facies conditions was reached by c 388 Ma, constrained by crystallisation of amphibolite facies anatectic pegmatites. Later exhumation is proposed to have occurred in a transpressional setting, where thrusting under amphibolite facies conditions on a restraining bend was the main mechanism of uplift. This thrusting was initiated no later than c. 386 Ma, as constrained by intrusion of syntectonic granite dikes. Simultaneous extensional displacements of the Upper Plate led to extrusion. This, together with erosion, contributed to exhumation. A rutile cooling temperature from the dated eclogite show that exhumation of the high grade terrane to a crustal level with temperatures below c. 400 °C (c. 15 km if an average geotherm is considered) was not achieved earlier than c. 370 Ma. Part of the exhumation was also achieved by extensional displacement on the Gubbedalen Extensional Detachment Fault.

7 References

Andersen, T. B., Jamtveit, B. V., Dewey, J. F. and Swensson, E., 1991. Subduction and eduction of continental crust: a major mechanism during continent-continent collision and extensional collaps, a model based on the south Norwegian Caledonides. Terra Nova, 3: 303-310.

Andresen, A., Hames, W. E. and Hartz, E., 1995. New constraints on timing and nature of orogenic deformation within the East Greenland Caledonides, GSA Abstracts with Programs, 27, no.6.

Andresen, A., Hartz, E. and Vold, J., 1998. A late orogenic extensional origin for the infracrustal gneiss domes of the East Greenland Caledonides (72-74° N). Tectonophysics, 285(3-4): 353-369.

Andresen, A. and Hartz, E., 1998. Basement-cover relationships and orogenic evolution in the central East Greenland Caledonides. GFF, 120(2): 191-198.

Andresen, A., Rehnström, E. and Holte, M., 2007. Evidence for simultaneous contraction and extension at different crustal levels during the Caledonian orogeny in NE Greenland. Journal of the Geological Society, London, 164: 1-12.

Augland, L. E., Andresen, A., Myhre, P. I. and Corfu, F., 2007. The Gubbedalen Shear Zone (GSZ), East Greenland: A terrane boundary within the East Greenland Caledonides. NGF Abstracts and proceedings, 1: 3.

Brueckner, H. K., 1998. Sinking intrusion model for the emplacement of garnet-bearing peridotites into continent collision orogens. Geology, 26(7): 631-634.

Brueckner, H. K., Gilotti, J. A. and Nutman, A. P., 1998. Caledonian eclogite-facies metamorphism of early Proterozoic protoliths from the North-East Greenland eclogite province. Contributions to mineralogy and petrology, 130(2): 103-120.

Bryhni, I. and Andreasson, P. G., 1985. Metamorphism in the Scandinavian Caledonides. In: Gee, D. G. and Sturt, B. A. (eds) *The Caledonide Orogen-Scandinavia and Related Areas*. John Wiley and Sons Ltd.: 763-781.

Caby, R., 1972. Preliminary results of mapping in the Caledonian rocks of Canning Land and Wegener Halvø, East Greenland. Rapport Grønlands Geologiske Undersøgelse, 48: 7-20.

Carswell, D. A., Tucker, R. D., O'Brien, P. J. and Krogh, T. E., 2003. Coesite micro-inclusions and U/Pb age of zircons from the Hareidland Eclogite in the Western Gneiss Region of Norway. Lithos, 67(3-4): 181-190.

Chemenda, A. I., Mattauer, M. and Bokun, A. N., 1996. Continental subduction and a mechanism for exhumation of high-pressure metamorphic rocks: new modeling and field data from Oman. Earth and Planetary Science Letters, 143: 173-182.

Cherniak, D. J., 2000. Pb diffusion in rutile. Contributions to mineralogy and petrology, 139(2): 198-207.

Cherniak, D. J. and Watson, E. B., 2003. Diffusion in Zircon. In: Hanchar, J. M. and Hoskins, P. W. O. (eds) *Zircon*. Reviews in Mineralogy & Geochemistry, 53: 26.

Clemmensen, L. B. and Jepsen, H.F., 1992. Lithostratigraphy and geological setting of Upper Proterozoic shoreline-shelf deposits, Hagen Fjord Group, eastern North Greenland. Rapp. Grønlands Geol. Unders., 157: 2-26.

Coe, K., 1975. The Hurry Inlet granite and related rocks of Liverpool Land, East Greenland. Grønlands Geologiske Undersøgelse Bulletin, 115: 34.

Coe, K. and Cheeney, R. F., 1972. Preliminary results of mapping in Liverpool Land, East Greenland. Rapport Grønlands Geologiske Undersøgelse, 48: 7-20.

Collinson, J. D., 1980. Stratigraphy of the Independence Fjord Group (Proterozoic) of Eastern North Greenland. Rapport Grønlands Geologiske Undersøgelse, 99: 7-23.

Corfu, F., Hanchar, J. M., Hoskin, P. W. O. and Kinny, P. D., 2003. Atlas of zircon textures. In: Hanchar, J. M. and Hoskin, P. W. O. (eds) *Zircon*. Reviews in Mineralogy & Geochemestry, 53: 469-500.

Cunningham, D., Windley, B.F., Dorjnamjaa, D., Badamgarov, G. and Saandar, M., 1996. A structural transect across the Mongolian Western Altai: Active transpressional mountain building in central Asia. Tectonics, 15(1): 142-156.

Dallmeyer, R. D. and Strachan, R. A., 1994. $^{40}Ar/^{39}Ar$ mineral age constraints on the timing of deformation and metamorphism, North-East Greenland Caledonides. Rapport Grønlands Geologiske Undersøgelse, 162: 153-162.

Dewey, J. F., Holdsworth, R. E. and Strachan, R. A., 1998. Transpression and transtension zones. In: Holdsworth, R. E., Strachan, R. A. and Dewey, J. F. (eds) *Continental Transpressional and Transtensional Tectonics*. Geological Society, London, Special Publications, 135: 1-14.

Dewey, J. F. and Strachan, R. A., 2003. Changing Silurian-Devonian relative plate motion in the Caledonides: sinistral transpression to sinistral transtension. Journal of the Geological Society, 160: 219-229.

Dhuime, B., Bosch, D., Bruguier, O., Caby, R. and Pourtales, S., 2007. Age, provenance and post-deposition metamorphic overprint of detrital zircons from the Nathorst Land group (NE Greenland)-A LA-ICP-MS and SIMS study. Precambrian Research, 155: 24-46.

Elvevold, S. and Gilotti, J. A., 2000. Pressure-temperature evolution of retrogressed kyanite eclogites, Weinschenk Island, North-East Greenland Caledonides. Lithos, 53(2): 127-147.

Elvevold, S., Thrane, K. and Gilotti, J. A., 2003. Metamorphic history of high-pressure granulites in Payer Land, Greenland Caledonides. Journal of metamorphic geology, 21(1): 49-63.

Fossen, H. and Tikoff, B., 1998. Extended models of transpression and transtension, and application to tectonic settings. In: Holdsworth, R. E., Strachan, R. A. and Dewey, J. F. (eds) *Continental Transpressional and Transtensional Tectonics*. Geological Society, London, Special Publications, 135: 15-33.

Friedrichsen, J. D. and Surlyk, F., 1976. Geologisk Kort over Grønland: Hurry Inlet 70 Ø. 1 Nord.

Friderichsen, J. D., Gilotti, J. A., Henriksen, N., Higgins, A. K., Hull, J. M., Jepsen, H. F. and Kalsbeek, F., 1991. The crystalline rocks of Germania Land, Nordmarken and adjacent areas, North-east Greenland. Rapport Grønlands Geologiske Undersøgelse, 152: 85-94.

Friderichsen, J. D., Holdsworth, R. E., Jepsen, H. F. and Strachan, R. A., 1990. Caledonian and pre-Caledonian geology of Dronning Louise Land, North-East Greenland. Rapport Grønlands Geologiske Undersøgelse, 148: 133-141.

Friedrichsen, J. D., Henriksen, N. and Strachan, R. A., 1994. Basement-cover relationships and regional structure in the Grandjean Fjord- Bessel Fjord region (75-76N), North-East Greenland. Rapport Grønlands Geologiske Undersøgelse, 162: 17-33.

Gee, D. G., Kumpulainen, R., Roberts, D., Stephens, M. B., Thon, A., Zachrisson, E., 1985. Scandinavian Caledonides: Tectonostratigraphic Map. In: Gee, D. G. and Sturt, B.A. (eds) *The Caledonide Orogen-Scandinavia and Related Areas*. John Wiley and Sons Ltd.

Gilotti, J. A., 1993. Discovery of a medium temperature eclogite province in the Caledonides of North-East Greenland. Geology, 21: 523-526.

Gilotti, J. A. and Krogh Ravna, E. J., 2002. First evidence for ultrahigh-pressure metamorphism in the north-east Greenland Caledonides. Geology, 30(6): 551-554.

Gilotti, J. A., Nutman, A. P. and Brueckner, H. K., 2004. Devonian to Carboniferous collision in the Greenland Caledonides; U-Pb zircon and Sm-Nd ages of high-pressure and ultrahigh-pressure metamorphism. Contributions to mineralogy and petrology, 148(2): 216-235.

Gleadow, A. J. W. and Brooks, C. K., 1979. Fission track dating, thermal histories and tectonics of igneous intrusions in East Greenland. Journal Contributions to Mineralogy and Petrology, 71(1): 45-60.

Haller, J., 1971. Geology of the East Greenland Caledonides. John Wiley and Sons Ltd.: 411 pp.

Haller, J., 1985. The East Greenland Caledonides-reviewed. In: Gee, D. G. and Sturt, B.A. (eds) *The Caledonide Orogen-Scandinavia and Related Areas.* John Wiley and Sons Ltd.

Hambrey, M. J., Peel, J. S. and Smith, M. P., 1989. Upper Proterozoic and Lower Palaeozoic strata in northern East Greenland. Rapport Grønlands Geologiske Undersøgels, 145: 103-108.

Hansen, B. T. and Steiger, R. H., 1971. The Geochronology of the Scoresby Sund area. Rapport Grønlands Geologiske Undersøgelse, 37: 55-57.

Harrison, T. M., Catlos, E. J. and Montel, J. M., 2002. U-Th-Pb dating of phosphate minerals. In: Kohn, J. M., Rakovan, J. and Hughes, J. M. (eds) *Phosphates* Reviews in Mineralogy and Geochemistry, 48: 523-558.

Hartz, E., Andresen, A., Hodges, K. V. and Martin, M. W., 2001. Syncontractional extension and exhumation of deep crustal rocks in the East Greenland Caledonides. Tectonics, 20(1): 58-77.

Hartz, E., Andresen, A., Martin, M. W. and Hodges, K. V., 2000. U-Pb and $^{40}Ar/^{39}Ar$ constraints on the Fjord region detachment zone; a long-lived extensional fault in the central East Greenland Caledonides. Journal of the Geological Society, 157(4): 795-809.

Hartz, E., Condon, D., Austrheim, H. and Erambert, M., 2005. Rediscovery of the Liverpool Land Eclogites (Central East Greenland): A post supra-subduction UHP province. Mitt. Osterr. Miner. Ges., 150.

Henriksen, N., 1981. The Charcot Land tillite, Scoresby Sund, East Greenland. In: Hambrey, M. J. and Harland, W. B. (eds) *Earth's pre-Pleistocene glacial record*. Cambridge University Press: 776-777.

Henriksen, N. and Higgins, A. K., 1969. Preliminary results of mapping in the crystalline complex around Nordvestfjord, Scoresby Sund, East Greenland. Rapport Grønlands Geologiske Undersøgelse, 21: 5-20.

Higgins, A. K., 1974. The Krummedal supracrustal sequence around inner Nordvestfjord, Scoresby Sund, East Greenland. Rapport Grønlands Geologiske Undersøgelse, 67: 5-34.

Higgins, A. K., 1988. The Krummedal Supracrustal sequence in East Greenland. In: Winchester, J. A. (eds) *Later Proterozoic stratigraphy of the northern Atlantic regions*. Blackie, Glascow.: 86-96.

Higgins, A. K., Elvevold, S., Escher, J. C., Frederiksen, K. S., Gilotti, J. A., Henriksen, N., Jepsen, H. F., Jones, K. A., Kalsbeek, F., Kinny, P. D., Leslie, A. G., Smith, M. P., Thrane, K. and Watt, G. R., 2004. The foreland-propagating thrust architecture of the East Greenland Caledonides 72 °-75 ° N. Journal of the Geological Society, London, 161(6): 1009-1026.

Higgins, A. K., Friderichsen, J. D. and Thyrsted, T., 1981. Precambrian metamorphic complexes in the East Greenland Caledonides (72-74 ° N) - their relationships to the Eleonore Bay Group, and Caledonian orogenesis. Rapport Grønlands Geologiske Undersøgelse, 104: 5-46.

Higgins, A. K. and Leslie, A. G., 2000. Restoring thrusting in the East Greenland Caledonides. Geology, 28(11): 1019-1022.

Higgins, A. K., Leslie, A. G. and Smith, M. P., 2001. Neoproterozoic-lower Palaeozoic stratigraphical relationships in the marginal thin-skinned thrust belt of the East Greenland Caledonides; comparisons with the foreland in Scotland. Geological magazine, 138(2): 143-160.

Holdsworth, R. E. and Strachan, R. A., 1991. Interlinked system of ductile strike slip and thrusting formed by Caledonian sinistral transpression in northeastern Greenland. Geology, 19: 510-513.

Hoskin, P. W. O. and Schaltegger, U., 2003. The Composition of Zircon and Igneous and Metamorphic Petrogenesis. In: Hanchar, J. M. and Hoskins, P. O. W. (eds) *Zircon*. Reviews in Mineralogy and Geochemistry, 53(1): 27-62.

Jarvik, E., 1961. Devonian Vertebrates (East Greenland). In: Raasch, G. O. (eds) *Geology of the Arctic,* 1: 197-294.

Jepsen, H. F., Kalsbeek, F. N. and Suthren, R. J., 1980. The Zig-Zag Dal Basalt Formation, North Greenland. Rapport Grønlands Geolologiske Undersøgelse, 99: 25-32.

Jones, K. A. and Strachan, R. A., 2000. Crustal thickening and ductile extension in the NE Greenland Caledonides: a metamorphic record from anatectic pelites. Journal of metamorphic geology, 18(6): 719.

Jones, R. R. and Holdsworth, R. E., 1998. Oblique simple shear in transpression zones. In: Holdsworth, R. E., Strachan, R. A. and Dewey, J. F. (eds) *Continental Transpressional and Transtensional Tectonics*. Geological Society, London, Special Publications, 135: 35-40.

Kalsbeek, F., Jepsen, H. F. and Jones, K. A., 2001a. Geochemistry and petrogenesis of S-type granites in the East Greenland Caledonides. Lithos, 57(2-3): 91-109.

Kalsbeek, F., Jepsen, H. F. and Nutman, A. P., 2001b. From source migmatites to plutons; tracking the origin of ca. 435 Ma S-type granites in the East Greenland Caledonian Orogen. Lithos, 57(1): 1-21.

Kalsbeek, F., Nutman, A. P. and Taylor, P. N., 1993. Paleoproterozoic basement province in the Caledonian fold belt of North-East Greenland. Precambrian Research, 63: 163-178.

Kalsbeek, F., Thrane, K., Nutman, A. P. and Jepsen, H. F., 2000. Late Mesoproterozoic to early Neoproterozoic history of the East Greenland Caledonides; evidence for Grenvillian orogenesis? Journal of the Geological Society, 157(Part 6): 1215-1225.

Kranck, E. H., 1935. On the crystalline complex of Liverpool Land. Meddelelser om Grønland, 95(7): 1-122.

Krogh, T. E., 1973. A low-contamination method for hydrothermal decomposition of zircon and extraction of U and Pb for isotopic age determination. Geochimica et cosmochimica acta, 37: 485-494.

Krogh, T. E., 1982. Improved accuracy of U-Pb zircon ages by the creation of more concordant systems using an air abrasion technique. Geochimica et cosmochimica acta, 46: 637-649.

Larsen, P. H. and Bengaard, H. J., 1991. Devonian basin initiation in East Greenland: a result of sinistral wrench faulting and Caledonian extensional collapse. Journal of the Geological Society, London, 148: 355-368.

Larsen, P. H., Olsen, H., Rasmussen, J. A. and Wilken, U. G., 1989. Sedimentological and structural investigations of the Devonian basin, East Greenland. Rapport Grønlands Geologiske Undersøgelser, 145: 108-113.

Leslie, A. G. and Higgins, A. K., 1999. Granitic signposts to Grenvillian deformation in the Caledonian fold and thrust belt of eastern Greenland. Irish journal of earth sciences, 17: 131.

Leslie, A. G. and Nutman, A. P., 2003. Evidence for Neoproterozoic orogenesis and early high temperature Scandian deformation events in the southern East Greenland Caledonides. Geological magazine, 140(3): 309-333.

Lin, S., Jiang, D. and Williams, P. F., 1998. Transpression (or transtension) zones of triclinic symmetry: natural example and theoretical modeling. In: Holdsworth, R. E., Strachan, R. A. and Dewey, J. F. (eds) *Continental Transpressional and Transtensional Tectonics*. Geological Society, London, Special Publications, 135: 41-57.

Ludwig, K. R., 2003. ISOPLOT/Ex, A geochronological toolkit for Microsoft Excel. Berkeley Geochronology Center Special, Publication 4: 70 p.

McClelland, W. C. and Gilotti, J. A., 2003. Late-stage extensional exhumation of high-pressure granulites in the Greenland Caledonides. Geology, 31(3): 259-262.

McClelland, W. C., Gilotti, J. A. and Stemmerik, L., 2007. Correlation of basement deformation and basin development in the carboniferous, North East Greenland. NGF Abstracts and proceedings, 1: 59.

McClelland, W. C., Power, S. E., Gilotti, J. A., Mazdab, F. K. and Wopenka, B., 2006. U-Pb SHRIMP geochronology and trace-element geochemistry of coesite-bearing zircons, north-east Greenland Caledonides. In: Hacker, B. R., McClelland, W. C. and Liou, J. G. (eds) *Ultrahigh-pressure: Deep Continental Subduction. Special papers*, Geological Society of America, 403: 23-43.

McKerrow, W. S., Mac Niocaill, C. and Dewey, J. F., 2000. The Caledonian Orogeny redefined. Journal of the Geological Society, 157(Part 6): 1149-1154.

Moncreiff, A. C. M., 1989. The tillite Group and related rocks of East Greenland: implications for Late Proterozoic Paleogeography. In: R. A. Gayer (eds) The Caledonide Geology of Scandinavia, Graham & Trotman, London: 285-297.

Nordgulen, Ø., Bickford, M. E., Nissen, A. L. and Wortman, G. L., 1993. U-Pb zircon ages from the Bindal Batholith, and the tectonic history of the Helgeland Nappe Complex, Scandinavian Caledonides. Journal of the Geological Society, 150: 771-783.

Oberli, F., Meier, M., Berger, A., Rosenberg, C. L. and Gier, E. R., 2004. U-Th-Pb and 230Th/238U disequilibrium isotope systematics: Precise accessory mineral chronology and melt evolution tracing in the Alpine Bergell intrusion. Geochimica et Cosmochimica Acta, 68(11): 2543-2560.

Pearce, J. A., Harris, N. B. W. and Tindle, A. G., 1984. Trace element discrimination diagrams for the tectonic interpretation of granitic rocks. Journal of Petrology, 25: 956-983.

Phillips, W. E. A. and Friderichsen, J. D., 1981. The Late Precambrian Gåseland tillite, Scoresby Sund, East Greenland. In: J. Hambrey and W. B. Harland (eds) *Earth's pre-Pleistocene glacial record,* Cambridge University Press: 773-775.

Phillips, W. E. A., Stillman, J. D., Friderichsen, D. H. and Jemelin, L., 1973. Preliminary results of mapping in the western gneiss and schist zone around Vestfjord and inner Gåsefjord, South-West Scoresby Sund. Rapport Grønlands Geologiske Undersøgelser, 58: 17-32.

Pupin, J. P., 1980. Zircon and granite petrology. Contributions to mineralogy and petrology, 73(3): 207-220.

Rasmussen, J. A. and Smith, M. P., 2001. Conodont geothermometry and tectonic overburden in the northernmost East Greenland Caledonides. Geological Magazine, 138: 687–698.

Rey, P., Burg, J. P. and Casey, M., 1997. The Scandinavian Caledonides and their relationship to the Variscan Belt. In: Burg, J. P. and Ford, M. (eds) *Orogeny Through Time.* Special Publication, Geological Society, London, 121: 179-200.

Roberts, D. and Gee, D. G., 1985. An introduction to the structures of the Scandinavian Caledonides. In: Gee, D. G. and Sturt, B.A. (eds) *The Caledonide Orogen-Scandinavia and Related Areas*. John Wiley and Sons Ltd.: 55-68.

Roberts, D., Melezhik, V. M. and Heldal, T., 2002. Carbonate formations and early NW-directed thrusting in the highest allochthons of the Norwegian Caledonides: evidence of a Laurentian ancestry. Journal of the Geological Society, London, 159: 117-120.

Rock, N. M. S., Gaskarth, J. W., Henney, P. J. and Shand, P., 1988. Late Caledonian dyke-swarms of northern Britain; some preliminary petrogenetic and tectonic implications of their province-wide distribution and chemical variation. The Canadian mineralogist, 26(Part 1): 3-22.

Root, D. B., Hacker, B. R., Mattinson, J. M. and Wooden, J. L., 2004. Zircon geochronology and ca. 400 Ma exhumation of Norwegian ultrahigh pressure rocks; an ion microprobe and chemical abrasion study. Earth and planetary science letters, 228(3-4): 325-341.

Sahlstein, T. G., 1935. Petrographie der Eklogiteinshclusse in den Gneisen des sudvwestlichen Liverpool-Landes in Ost-Grønland. Meddelelser om Grønland, 95(5): 1-43.

Sartini Rideout, C., Gilotti, J. A. and McClelland, W. C., 2006. Geology and timing of dextral strike-slip shear zones in Danmarkshavn, north-east Greenland Caledonides. Geological magazine, 143(4): 431-446.

Schlindwein, V. and Jokat, W., 2000. Post-collisional extension of the East Greenland Caledonides: a geophysical perspective. Geophysical journal international, 140(3): 559-567.

Schmitz, M. D. and Bowring, S. A., 2003. Constraints on the thermal evolution of continental lithosphere from U-Pb accessory mineral thermochronometry of lower crustal xenoliths, southern Africa. Contributions to mineralogy and petrology, 144: 592-618.

Schreurs, G. and Colletta, B., 1998. Analogue modelling of faulting in zones of continental transpression and transtension. In: Holdsworth, R. E., Strachan, R. A. and Dewey, J. F. (eds) *Continental Transpressional and Transtensional Tectonics*. Geological Society, London, Special Publications, 135, 59-79 pp.

Shand, P., Gaskarth, J. W., Thirwall, M. F. and Rock, N. M. S., 1994. Late caledonian dike swarms of South-Eastern Scotland. Mineralogy and Petrology, 51: 277-298.

Simpson, C. and Wintsch, R. P., 1989. Evidence for deformation-induced K-feldspar replacement by myrmekite. Journal of metamorphic geology, 7: 261-275.

Smith, D. C. and Cheeney, R. F., 1981. A new occurrence of garnet-ultrabasite in the Caledonides; a Cr-rich chromite-garnet-lherzolite from Tvaerdalen, Liverpool Land, East Greenland. Terra cognita, 1(1): 74.

Smith, M. P., Rasmussen, J. A., Robertson, S., Higgins, A. K. and Leslie, A. G., 2004. Lower Palaeozoic stratigraphy of the East Greenland Caledonides. Geological Survey of Denmark and Greenland Bulletin, 6: 5-28.

Stacey, J. S. and Kramers, J. D., 1975. Approximation of terrestrial lead isotope evolution by a two-stage model. Earth and planetary science letters, 26(2): 207-221.

Steltenpohl, M., Hames, W., Andresen, A. and Markl, G., 2003. New Caledonian eclogite province in Norway and potential Laurentian (Taconic) and Baltic links. Geology, 31(11): 985-988.

Stephens, M. B. and Gee, D. G., 1985. A tectonic model for the eugeoclinal terranes in the central Scandinavian Caledonides. In: Gee, D. G. and Sturt, B.A. (eds) *The Caledonide Orogen-Scandinavia and Related Areas.* John Wiley and Sons Ltd.: 953-978.

Stipp, M., 2002. The eastern Tonale fault zone: a'natural laboratory'for crystal plastic deformation of quartz over a temperature range from 250 to 700oC. Journal of structural geology, 24(12): 1861.

Stipp, M., Heilbronner, R. and Stunitz, H., 1999. Dislocation creep microstructures as indicators of deformation conditions; microstructural analysis of field examples. Abstracts with programs - Geological Society of America, 31(7): 109.

Strachan, R. A., Friderichsen, D. H., Holdsworth, R. E. and Jepsen, H. F., 1994. Regional geology and Caledonian structure, Dronning Louise Land, North-East Greenland. Rapport Grønlands Geologiske Undersøgelser, 162: 71-76.

Thompson, R. N., 1982. Magmatism of the British Tertiary volcanic province. Scottish Journal of Geology, 18(1): 49-107.

Thrane, K., 2002. Relationships between Archaean and Palaeoproterozoic crystalline basement complexes in the southern part of the East Greenland Caledonides; an ion microprobe study. Precambrian research, 113(1-2): 19-42.

Thrane, K., 2004. Palaeoproterozoic age of a basement gneiss complex in the Charcot Land tectonic window, East Greenland Caledonides Geological Survey of Denmark and Greenland Bulletin, 6: 57-66.

Tirsgaard, H. and Sønderholm, M., 1997. Lithostratigraphy, sedimentary evolution and sequence stratigraphy of the Upper Proterozoic Lyell Land Group (Eleonore Bay Supergroup) of East and North-East Greenland. Geology of Greenland Survey Bulletin, 178: 1-60.

Torsvik, T. H., Smethurst, M. A., Meert, J. G., Van der Voo, R., Mckerrow, W. S., Brasier, M. D., Sturt, B. and Walderhaug, H. J. 1996. Continental break-up and collision in the Neoproterozoic and Palaeozoic; a tale of Baltica and Laurentia. Earth-science reviews, 40(3-4): 229-258.

Tucker, R. D., Krogh, T. E., and Råheim, A., 1990, Proterozoic evolution and age-province boundaries in the central part of the Western Gneiss Region, Norway: Results of U-Pb dating of accessory minerals from Trondheimsfjord to Geiranger. In: Gower, C. F., Ryan, B., and Rivers, T., (eds) *Middle Proterozoic Geology of the Southern Margin of Proto Laurentia-Baltica*. Geological Association of Canada Special Paper 38: 149–173.

Tucker, R. D., Robinson, P., Solli, A., Gee, D. G., Thorsnes, T., Krogh, T. E., Nordgulen, Ø. and Bickford, M. E., 2004. Thrusting and extension in the Scandian hinterland, Norway; new U-Pb ages and tectonostratigraphic evidence. The American journal of science, 304(6): 477-532.

Upton, B. G. J., Rämö, O. T., Heaman, L. M., Blichert-Toft, J., Kalsbeek, F., Barry, T. L. and Jepsen, H. F., 2005. The Mesoproterozoic Zig-Zag Dal basalts and associated intrusions of eastern North Greenland; mantle plume-lithosphere interaction. Contributions to mineralogy and petrology, 149(1): 40-56.

Vidal, J. L., Kubin, L., Debat, P. and Soula, J. C., 1980. Deformation and dynamic recrystallization of K- feldspar augen in orthogneiss from Montagne Noir, Occitania, Southern France. Lithos, 13: 247-255.

Vold, J., 1997. Et studie av den tectonometamorfe utvikling av gneisene i liggblokken til 'the Fjord Region Detachment Zone' på Kap Hedlund, Sentrale Øst Grønland. . Cand. Scient. University of Oslo.

von Seckendorff, V., Timmerman, M. J., Kramer, W. and Wrobel, P., 2004. New ^{40}Ar/^{39}Ar ages and geochemistry of Late Carboniferous-Early Permian lamprophyres and related volcanic rocks in the Saxothuringian Zone of the Variscan Orogen, Germany. In: Wilson, M., Neumann, E. -R., Davies, G. R., Timmerman, M. J., Heeremans, M. and Larsen, B. T. (eds) *Permo-Carboniferous Magmatism and Rifting in Europe.* Geological Society Special Publications, 223: 335-359.

Walsh, E. O., Hacker, B. R., Gans, P. B., Grove, M. and Gehrels, G., 2007. Protolith ages and exhumation histories of (ultra)high-pressure rocks across the Western Gneiss Region, Norway. Geological Society of America Bulletin, 119: 289-301.

Watt, G. R., Kinny, P. D. and Friderichsen, J. D., 2000. U-Pb geochronology of Neoproterozoic and Caledonian tectonothermal events in the East Greenland Caledonides. Journal of the Geological Society, 157: 1031-1048.

White, A. P. and Hodges, K. V., 2002. Multi-stage extensional evolution of the central East Greenland Caledonides. Tectonics, 21: 1211-1228.

White, A. P. and Hodges, K. V., 2003. Pressure-temperature-time evolution of the central East Greenland Caledonides; quantitative constraints on crustal thickening and synorogenic extension. Journal of metamorphic geology, 21(9): 875-897.

White, A. P., Hodges, K. V., Martin, M. W. and Andresen, A., 2002. Geologic constraints on middle-crustal behavior during broadly synorogenic extension in the central East Greenland Caledonides. International journal of earth sciences, 91(2): 187-208.

Yoshinobu, A. S., Barnes, C. G., Nordgulen, Ø., Prestvik, T., Fanning, M., Pedersen, R. B., 2002. Ordovician magmatism, deformation, and exhumation in the Caledonides of central Norway: An orphan of the Taconic orogeny? Geology, 30(10): 883-886.